AD

AD623129

USAAVLABS TECHNICAL REPORT 65-63

DESIGN AND WIND TUNNEL TEST OF A MODEL HELICOPTER ROTOR HAVING AN INDEPENDENTLY MOVABLE INBOARD BLADE PANEL R-420

By

D. G. Ekquist

October 1965

U. S. ARMY AVIATION MATERIEL LABORATORIES

FORT EUSTIS, VIRGINIA

CONTRACT DA 44-177-AMC-129(T)

VERTOL DIVISION
THE BOEING COMPANY

BLANK PAGES
IN THIS
DOCUMENT
WERE NOT
FILMED

DEPARTMENT OF THE ARMY
U S ARMY AVIATION MATERIEL LABORATORIES
FORT EUSTIS VIRGINIA 23604

This report has been reviewed by the U. S. Army Aviation Materiel Laboratories, and the data contained herein are considered to be valid. The report is published for the dissemination of information.

Task 1P125901A13903
Contract DA 44-177-AMC-129(T)
USAAVLABS Technical Report 65-63
October 1965

DESIGN AND WIND TUNNEL TEST OF A MODEL HELICOPTER ROTOR HAVING AN INDEPENDENTLY MOVABLE INBOARD BLADE PANEL

R-420

by

D. G. Ekquist

Prepared by

VERTOL DIVISION
THE BOEING COMPANY
Morton, Pennsylvania

for

U.S. ARMY AVIATION MATERIEL LABORATORIES
FORT EUSTIS, VIRGINIA

SUMMARY

A model segmented rotor was tested by The Boeing Company on a powered model Rotor Test Stand (RTS) in the University of Maryland Wind Tunnel. The objective of the test was to determine the propulsive capability at high advance ratio of a rotor having the panel inboard of 50-percent radius on each blade following a prescribed nonsinusoidal pitch schedule while the outboard panel followed a "conventional" swashplate control motion. Theory indicates that the loss in propulsive force capability with increasing advance ratio that has been noted for conventional rotors could thus be reduced.

Rotor performance data was obtained at an advance ratio of 0.60 and an advancing blade tip Mach number of 0.36. Data were taken for a collective pitch range from 16 degrees to 32 degrees and for a control axis angle of attack range from -57 degrees to -12 degrees.

Two nonsinusoidal pitch schedules and a "conventional" rotor (inboard panel locked to outboard) were tested. The maximum propulsive force measured for the segmented rotor was more than nine times that for the conventional rotor(drag of hubs and shanks included, in both cases). The segmented rotor was able to absorb power efficiently up to a level of P/qd^2V of 0.024, and showed no sign of faltering there. The limit was due to cyclic pitch limits associated with model geometry. The conventional rotor, on the other hand, showed a breakdown in its aerodynamic behavior which limited its efficient range of power absorption to $P/qd^2V = 0.016$.

The segmented rotor's ability to produce propulsive force at high advance ratio has significant implications with regard to helicopter performance potential. For example, flight at 230 knots without auxiliary lift or propulsion would be well within the performance envelope of a segmented rotor of reasonable solidity, assuming a ratio of equivalent drag area to weight (f_e/W) of 0.001 square feet per pound, and advancing tip mach number of 0.94.

CONTENTS

	Page
SUMMARY	iii
LIST OF ILLUSTRATIONS	vi
LIST OF SYMBOLS	xiv
INTRODUCTION	1
CONCLUSIONS AND RECOMMENDATIONS	2
DESCRIPTION OF TEST EQUIPMENT	3
EXPERIMENTAL PROCEDURE	7
EXPERIMENTAL RESULTS	11
BIBLIOGRAPHY	80
DISTRIBUTION	81
APPENDIX: Nondimensional Parameters for V/STOL Aircraft Performance Analysis	83

ILLUSTRATIONS

Figure		Page
1.	Segmented-Rotor Wind-Tunnel Model. . .	4
2.	Definition of Axis System and Sign Convention	16
3.	Segmented Rotor Pitch Schedules 3 and 4	17
4.	Rotor Drag Polar Comparing Conventional and Segmented Rotors Where $\Delta\theta_{INBD} = 0°$, $\Delta\psi = 0°$, $P/qd^2V = 0.018$, $\mu' = 0.60$, $M_{(1)(90)} = 0.36$	19
5.	Rotor Drag Polar Comparing Conventional and Segmented Rotors With Hub and Shank Tares Removed Where $\Delta\theta_{INBD} = 0°$, $\Delta\psi = 0°$, $P/qd^2V = 0.018$, $\mu' = 0.60$, $M_{(1)(90)} = 0.36$	20
6.	Rotor Drag Polar for Pitch Schedule 3 Showing the Effect of Azimuth Phasing Where $\Delta\theta_{INBD} = 0°$, $P/qd^2V = 0.018$, $\mu' = 0.60$, $M_{(1)(90)} = 0.36$	21
7.	Rotor Drag Polar for Pitch Schedule 3 Showing the Effect of Collective Pitch on Inboard Segment Where $\Delta\psi = 0°$, $P/qd^2V = 0.018$, $\mu' = 0.60$, $M_{(1)(90)} = 0.36$	22
8.	Rotor Drag Polar for Pitch Schedule 3 Showing the Effect of Collective Pitch on Inboard Segment Where $\Delta\psi = 20°$, $P/qd^2V = 0.018$, $\mu' = 0.60$, $M_{(1)(90)} = 0.36$	23

Figure		Page
9.	Comparison of Conventional and Segmented Rotor Propulsive-Force Limits for Pitch Schedule 3 Where $\Delta\theta_{INBD} = 0°$, $\Delta\psi = 0°$, $\mu' = 0.60$, $M_{(1)(90)} = 0.36$	24
10.	Polar Map Comparison of Conventional and Segmented Rotor Where $\Delta\theta_{INBD} = 0°$, $\Delta\psi = 0°$, $\mu' = 0.60$, $M_{(1)(90)} = 0.36$ . .	25
11.	Polar Map of Conventional Rotor Where $\mu' = 0.60$, $M_{(1)(90)} = 0.36$	26
12.	Polar Map of Segmented Rotor Pitch Schedule 3 Where $\Delta\theta_{INBD} = 0°$, $\Delta\psi = 0°$, $\mu' = 0.60$, $M_{(1)(90)} = 0.36$	27
13.	Polar Map of Segmented Rotor With Hub and Shank Tares Removed Where $\Delta\theta_{INBD} = 0°$, $\Delta\psi = 0°$, $\mu' = 0.60$, $M_{(1)(90)} = 0.36$ Compared With Conventional Rotor .	28
14.	Polar Map of Segmented Rotor Pitch Schedule 4 Where $\Delta\theta_{INBD} = 0°$, $\Delta\psi = 0°$, $\mu' = 0.60$, $M_{(1)(90)} = 0.36$	29
15.	Polar Map of Segmented Rotor Pitch Schedule 3 Where $\Delta\theta_{INBD} = 4°$, $\Delta\psi = 0°$, $\mu' = 0.60$, $M_{(1)(90)} = 0.36$	30
16.	Polar Map of Segmented Rotor Pitch Schedule 3 Where $\Delta\theta_{INBD} = 8°$, $\Delta\psi = 0°$, $\mu' = 0.60$, $M_{(1)(90)} = 0.36$	31
17.	Polar Map of Segmented Rotor Pitch Schedule 3 Where $\Delta\theta_{INBD} = -10°$, $\Delta\psi = 0°$, $\mu' = 0.60$, $M_{(1)(90)} = 0.36$ . .	32
18.	Polar Map of Segmented Rotor Pitch Schedule 3 Where $\Delta\theta_{INBD} = 0°$, $\Delta\psi = 20°$, $\mu' = 0.60$, $M_{(1)(90)} = 0.36$.	33

Figure		Page
19.	Polar Map of Segmented Rotor Pitch Schedule 3 Where $\Delta\theta_{INBD}$ = -10°, $\Delta\psi$ = 20°, μ' = 0.60, $M_{(1)(90)}$ = 0.36 . .	34
20.	Polar Map of Segmented Rotor Pitch Schedule 3 Where $\Delta\theta_{INBD}$ = -15.9°, $\Delta\psi$ = 20°, μ' = 0.60, $M_{(1)(90)}$ = 0.36 . .	35
21.	Polar Map of Segmented Rotor Pitch Schedule 3 Where $\Delta\theta_{INBD}$ = 0°, $\Delta\psi$ = -20°, μ' = 0.60, $M_{(1)(90)}$ = 0.36 .	36
22.	Propulsive Efficiency of Conventional and Segmented Rotors Where $\Delta\theta_{INBD}$ = 0°, $\Delta\psi$ = 0°, L/qd^2 = 0.04, μ' = 0.60, $M_{(1)(90)}$ = 0.36	37
23.	Effect on Propulsive Efficiency of Azimuth Phasing of Segmented Rotor Pitch Schedule 3 Where $\Delta\theta_{INBD}$ = 0°, L/qd^2 = 0.04, μ' = 0.60, $M_{(1)(90)}$ = 0.36	38
24.	Effect on Propulsive Efficiency of Collective Pitch on Inboard Segment of Segmented Rotor Pitch Schedule 3 Where $\Delta\psi$ = 0°, L/qd^2 = 0.04, μ' = 0.60, $M_{(1)(90)}$ = 0.36	39
25.	Effect on Propulsive Efficiency of Collective Pitch on Inboard Segment of Segmented Rotor Pitch Schedule 3 Where $\Delta\psi$= 20°, L/qd^2 = 0.04, μ' = 0.60, $M_{(1)(90)}$ = 0.36	40
26.	Hub and Shank Tares for Segmented Rotor Where μ' = 0.60, $M_{(1)(90)}$ = 0.36 .	41

Figure		Page
27.	Segmented Rotor Nondimensionalized Lift for Pitch Schedule 3 Where $\Delta\theta_{INBD}=0°$, $\Delta\psi=0°$, $\mu'=0.60$, $M_{(1)(90)}=0.36$, Hub and Shank Tares Removed	42
28.	Segmented Rotor Nondimensionalized Propulsive Force for Pitch Schedule 3 Where $\Delta\theta_{INBD}=0°$, $\Delta\psi=0°$, $\mu'=0.60$, $M_{(1)(90)}=0.36$, Hub and Shank Tares Removed	43
29.	Segmented Rotor Nondimensionalized Power for Pitch Schedule 3 Where $\Delta\theta_{INBD}=0°$, $\Delta\psi=0°$, $\mu'=0.60$, $M_{(1)(90)}=0.36$, Hub and Shank Tares Removed . . .	44
30.	Conventional Rotor Nondimensionalized Lift ($\mu'=0.60$, $M_{(1)(90)}=0.36$, Hub and Shank Tares Removed.)	45
31.	Conventional Rotor Nondimensionalized Propulsive Force ($\mu'=0.60$, $M_{(1)(90)}=0.36$, Hub and Shank Tares Removed)	46
32.	Conventional Rotor Nondimensionalized Power ($\mu'=0.60$, $M_{(1)(90)}=0.36$, Hub and Shank Tares Removed)	47
33.	Conventional Rotor Nondimensionalized Lift ($\mu'=0.60$, $M_{(1)(90)}=0.36$)	48
34.	Conventional Rotor Nondimensionalized Propulsive Force ($\mu'=0.60$, $M_{(1)(90)}=0.36$)	49
35.	Conventional Rotor Nondimensionalized Power ($\mu'=0.60$, $M_{(1)(90)}=0.36$)	50
36.	Segmented Rotor Nondimensionalized Lift for Pitch Schedule 4 Where $\Delta\theta_{INBD}=0°$, $\Delta\psi=0°$, $\mu'=0.60$, $M_{(1)(90)}=0.36$	51

Figure		Page
37.	Segmented Rotor Nondimensionalized Propulsive Force for Pitch Schedule 4 Where $\Delta\theta_{INBD}=0°, \Delta\psi=0°, \mu'=0.60, M_{(1)(90)}=0.36$	52
38.	Segmented Rotor Nondimensionalized Power for Pitch Schedule 4 Where $\Delta\theta_{INBD}=0°, \Delta\psi=0°, \mu'=0.60, M_{(1)(90)}=0.36$	53
39.	Segmented Rotor Nondimensionalized Lift for Pitch Schedule 3 Where $\Delta\theta_{INBD}=4°, \Delta\psi=0°, \mu'=0.60, M_{(1)(90)}=0.36$	54
40.	Segmented Rotor Nondimensionalized Propulsive Force for Pitch Schedule 3 Where $\Delta\theta_{INBD}=4°, \Delta\psi=0°, \mu'=0.60, M_{(1)(90)}=0.36$	55
41.	Segmented Rotor Nondimensionalized Power for Pitch Schedule 3 Where $\Delta\theta_{INBD}=4°, \Delta\psi=0°, \mu'=0.60, M_{(1)(90)}=0.36$	56
42.	Segmented Rotor Nondimensionalized Lift for Pitch Schedule 3 Where $\Delta\theta_{INBD}=8°, \Delta\psi=0°, \mu'=0.60, M_{(1)(90)}=0.36$	57
43.	Segmented Rotor Nondimensionalized Propulsive Force for Pitch Schedule 3 Where $\Delta\theta_{INBD}=8°, \Delta\psi=0°, \mu'=0.60, M_{(1)(90)}=0.36$	58
44.	Segmented Rotor Nondimensionalized Power for Pitch Schedule 3 Where $\Delta\theta_{INBD}=8°, \Delta\psi=0°, \mu'=0.60, M_{(1)(90)}=0.36$	59

Figure		Page
45.	Segmented Rotor Nondimensionalized Lift for Pitch Schedule 3 Where $\Delta\theta_{INBD}=0°$, $\Delta\psi=-20°$, $\mu'=0.60$, $M_{(1)(90)}=0.36$	60
46.	Segmented Rotor Nondimensionalized Propulsive Force for Pitch Schedule 3 Where $\Delta\theta_{INBD}=0°$, $\Delta\psi=-20°$, $\mu'=0.60$, $M_{(1)(90)}=0.36$	61
47.	Segmented Rotor Nondimensionalized Power for Pitch Schedule 3 Where $\Delta\theta_{INBD}=0°$, $\Delta\psi=-20°$, $\mu'=0.60$, $M_{(1)(90)}=0.36$	62
48.	Segmented Rotor Nondimensionalized Lift for Pitch Schedule 3 Where $\Delta\theta_{INBD}=-15.9°$, $\Delta\psi=20°$, $\mu'=0.60$, $M_{(1)(90)}=0.36$	63
49.	Segmented Rotor Nondimensionalized Propulsive Force for Pitch Schedule 3 Where $\Delta\theta_{INBD}=-15.9°$, $\Delta\psi=20°$, $\mu'=0.60$, $M_{(1)(90)}=0.36$	64
50.	Segmented Rotor Nondimensionalized Power for Pitch Schedule 3 Where $\Delta\theta_{INBD}=-15.9°$, $\Delta\psi=20°$, $\mu'=0.60$, $M_{(1)(90)}=0.36$	65
51.	Segmented Rotor Nondimensionalized Lift for Pitch Schedule 3 Where $\Delta\theta_{INBD}=-10°$, $\Delta\psi=20°$, $\mu'=0.60$, $M_{(1)(90)}=0.36$	66
52.	Segmented Rotor Nondimensionalized Propulsive Force for Pitch Schedule 3 Where $\Delta\theta_{INBD}=-10°$, $\Delta\psi=20°$, $\mu'=0.60$, $M_{(1)(90)}=0.36$	67

Figure		Page
53.	Segmented Rotor Nondimensionalized Power for Pitch Schedule 3 Where $\Delta\theta_{INBD}$=-10°, $\Delta\psi$=20°, μ'=0.60, $M_{(1)(90)}$=0.36	68
54.	Segmented Rotor Nondimensionalized Lift for Pitch Schedule 3 Where $\Delta\theta_{INBD}$=0°, $\Delta\psi$=20°, μ'=0.60, $M_{(1)(90)}$=0.36	69
55.	Segmented Rotor Nondimensionalized Propulsive Force for Pitch Schedule 3 Where $\Delta\theta_{INBD}$=0°, $\Delta\psi$=20°, μ'=0.60, $M_{(1)(90)}$=0.36	70
56.	Segmented Rotor Nondimensionalized Power for Pitch Schedule 3 Where $\Delta\theta_{INBD}$=0°, $\Delta\psi$=20°, μ' =0.60, $M_{(1)(90)}$=0.36	71
57.	Segmented Rotor Nondimensionalized Lift for Pitch Schedule 3 Where $\Delta\theta_{INBD}$=0°, $\Delta\psi$=7.5°, μ'=0.60, $M_{(1)(90)}$=0.36	72
58.	Segmented Rotor Nondimensionalized Propulsive Force for Pitch Schedule 3 Where $\Delta\theta_{INBD}$=0°, $\Delta\psi$ =-7.5°, μ'=0.60, $M_{(1)(90)}$=0.36	73
59.	Segmented Rotor Nondimensionalized Power for Pitch Schedule 3 Where $\Delta\theta_{INBD}$=0°, $\Delta\psi$=-7.5°, μ' =0.60, $M_{(1)(90)}$=0.36	73
60.	Segmented Rotor Nondimensionalized Lift for Pitch Schedule 3 Where $\Delta\theta_{INBD}$=0°, $\Delta\psi$=0°, μ'=0.60, $M_{(1)(90)}$= 0.36	74

Figure		Page
61.	Segmented Rotor Nondimensionalized Propulsive Force for Pitch Schedule 3 Where $\Delta\theta_{INBD}=0°$, $\Delta\psi=0°$, $\mu'=0.60$, $M_{(1)(90)}=0.36$	75
62.	Segmented Rotor Nondimensionalized Power for Pitch Schedule 3 Where $\Delta\theta_{INBD}=0°$, $\Delta\psi=0°$, $\mu'=0.60$, $M_{(1)(90)}=0.36$	76
63.	Segmented Rotor Nondimensionalized Lift for Pitch Schedule 3 Where $\Delta\theta_{INBD}=-10°$, $\Delta\psi=0°$, $\mu'=0.60$, $M_{(1)(90)}=0.36$	77
64.	Segmented Rotor Nondimensionalized Propulsive Force for Pitch Schedule 3 Where $\Delta\theta_{INBD}=-10°$, $\Delta\psi=0°$, $\mu'=0.60$, $M_{(1)(90)}=0.36$	78
65.	Segmented Rotor Nondimensionalized Power for Pitch Schedules Where $\Delta\theta_{INBD}=-10°$, $\Delta\psi=0°$, $\mu'=0.60$, $M_{(1)(90)}=0.36$	78
66.	Comparison of Test and Theory Where $\Delta\theta_{INBD}=0°$, $\Delta\psi=0°$, $P/qd^2V=0.008$, $\mu'=0.60$, $M_{(1)(90)}=0.36$, Hub and Shank Tares Removed	79
67.	Determination of Aircraft Maneuver Capability	84
68.	Universal Induced-Drag Relationship	85
69.	Construction of Force Polar Envelope for Powered Lift/Propulsion Systems	86

SYMBOLS

A_M	Model reference area (πR^2) in square feet
A_T	Wind tunnel cross sectional area in square feet
c	Model rotor blade chord in feet
d	Model rotor diameter in feet
D_E	Effective drag ($D_E = P/V - X$) in pounds
D_E/qd^2	Nondimensionalized effective drag
D_i	Wind axis drag ($D_i = -X = H\cos\alpha_s + T\sin\alpha_s$) in pounds
L/qd^2	Nondimensionalized Lift
n	Ratio of initial-to-final induced velocity
P	Power ($P = Q\Omega$) in foot-pounds per second
P/qd^2V	Nondimensionalized power
Q	Model rotor torque in foot-pounds
q	Free stream dynamic pressure ($q = 1/2\ \rho V^2$) in pounds per square foot
R	Model rotor radius in feet
T	Model rotor thrust in pound
t	Maximum thickness of airfoil section in feet
V	Free stream velocity, corrected for tunnel wall interference, in feet per second
V_∞	Free-stream velocity in feet per second
X	Propulsive force ($X = -T\sin\alpha_s - H\cos\alpha_s$) in pounds
X/qd^2	Nondimensionalized propulsive force

$(\alpha_s)_c$	Shaft angle of attack, corrected for tunnel wall interference, in degrees
α_{CA}	Control axis angle-of-attack, corrected for tunnel wall interference, ($\alpha_{CA} = (\alpha_s)_c - B_l$) in degrees
θ_{OBD}	Collective pitch on outboard segment in degrees
$\Delta\theta_{INBD}$	Collective pitch on inboard segment in degrees
ψ	Azimuth angle, measured counter-clockwise from the downwind position, in degrees
$\Delta\psi$	Change in the azimuth phasing of a pitch schedule in degrees
θ	Inboard-segment pitch angle in degrees
B_l	Longitudinal cyclic pitch in degrees
$\Delta\alpha$	Wind tunnel wall interference correction to shaft angle in degrees
W	Weight of the aircraft in pounds
W_o	Vertical induced velocity at the rotor, positive upward, in feet per second
W_h	Hover induced velocity in feet per second
U_o	Horizontal induced velocity at rotor, positive rearward, in feet per second
ΔW	Wall-induced upwash in feet per second
ΔU	Wall-induced horizontal velocity in feet per second
δ_{UL}	Horizontal velocity factor due to lift
δ_{UD}	Horizontal velocity factor due to drag
δ_{WL}	Vertical velocity factor due to lift
δ_{WD}	Vertical velocity factor due to drag

μ'	Advance ratio = $V/\Omega R$
Ω	Rotor tip speed in radians per second
$M_{(1)(90)}$	Advancing blade tip Mach no. $M_{(1)(90)} = \frac{V + \Omega R}{a}$
σ	Rotor solidity $\sigma = \frac{3C}{\pi R}$
ρ	Air density in slugs per cubic foot
f_e	Equivalent parasite drag area in square feet
H	Hub shaft axis normal force in pounds

INTRODUCTION

The maximum forward speed of a helicopter is limited by stall of the retreating rotor blades. Use of increased rotor tip speed to relieve this condition becomes an uneconomical solution when the mach number of the advancing tip approaches unity. The power required to overcome the compressibility drag-rise is then too great. Even if the blade is designed with a thin airfoil (for high critical mach number) at the tip, speeds much greater than 200 knots are difficult to attain.

Another approach to increased speed is the use of greater blade area, permitting operation at higher advance ratio without stall. A different problem arises in this case: the inboard portion of the blade, following the same cyclic pitch variation as the tip, operates with an unfavorable angle of attack schedule if the tip path plane is inclined forward for propulsion. The result is that, above approximately 0.55 advance ratio, the propulsive capability of an ordinary rotor is very limited.

The compound helicopter solves this difficulty by using a separate propulsion system, together with some degree of unloading of the rotor by means of wings.

The additional weight and complexity of the auxiliary propulsion system might be eliminated if the inboard portion of the rotor blades were permitted to operate with an independent pitch schedule. Theoretical studies carried out by The Vertol Division of Boeing indicated that a blade having a cyclically twistable segment inboard of the 50-percent radial station would be capable of producing propulsive force efficiently at an advance ratio of 0.60.

Construction and wind tunnel tests of a model embodying this concept were to be undertaken by Boeing under the original contract under which this report is written. Design studies indicated that the twistable segment was difficult to build. Also, further theoretical work showed that nearly equivalent performance could be attained with an inboard segment moving as a unit.

The approach was accordingly revised, and a movable segment with a cam-controlled pitch schedule, independent of that of outboard blade panel, was designed, built, and tested.

The philosophy of the test program was to establish the aerodynamic possibilities of the movable segment concept, using a design involving minimum risk of mechanical difficulty. Refinement in terms of weight reduction, choice of blade profile, planform, and twist distribution was considered to be of secondary importance. The following section discusses the design in detail.

CONCLUSIONS AND RECOMMENDATIONS

The results of the wind tunnel tests of the model segmented rotor blade demonstrate clearly that the segmented rotor concept is aerodynamically successful. That is, it is possible to develop a high level of propulsive force at an advance ratio of 0.60 by use of the segment, while the so-called conventional rotor is unable profitably to absorb power in the propulsive flight regime.

Furthermore, manipulation of the pitch schedule of the inboard segment by phase shifting and by changes in its collective pitch resulted in comparatively small changes in performance. This implies that a refined pitch schedule for the inboard segment would offer only slight further improvement.

Another meaningful result is the insensitivity of performance to pitch schedule in the reverse flow region. Indeed, a complete removal of pitch variation on the retreating side produced only a small degradation in propulsive capability. This implies the possibility of significant simplification in pitch schedule design.

The above conclusions can be summarized in one statement:

> The aerodynamic principle of the segment rotor is established, and only relatively small improvements can be expected by refining the schedule of the inner segment.

Therefore, the following course of action is recommended:

1. Application of the segmented rotor principle to more realistic blade and hub designs should be studied from the points of view of stress, dynamics, design complexity, and cost. Particular attention should be given to comparisons of the segmented rotor with other advanced systems designed for the same objective, such as compound configurations or the lead-lag (Derschmidt) rotor.

2. If the segmented rotor appears both practical and competitive in the light of the above study, tests of a dynamically realistic segmented model rotor should be carried out. These tests should serve the dual purposes of evaluating design simplifications (such as sinusoidal motion of the inboard segment, or restriction of the motion to a large-chord trailing edge flap) and establishing the dynamic and structural feasibility of the segmented rotor.

DESCRIPTION OF TEST EQUIPMENT

Figure 1 shows the segmented-rotor model on the wind tunnel test stand, and in various stages of assembly.

ROTOR TEST STAND

The test stand is powered by a 120-horsepower induction motor which is coupled to the rotor through a two-speed gearbox. Rotor rpm is controlled by varying motor frequency and voltage.

The motor, gearbox, rotor and hub are isolated from the supporting structure by six separate flexures. Mounted on the flexures are electric strain gages for monitoring six component forces and moments. This assembly is mounted to a streamlined tunnel floor mount through a trunnion. The trunnion allows the changing of shaft angle of attack by means of remotely operated hydraulic actuators.

SEGMENTED ROTOR

The segmented rotor (a fully articulated rotor) is constructed in two parts. The outboard segment is controlled by a conventional swashplate and the inboard segment is controlled by a cam. The cam may input any arbitrary cyclic schedule to the inner segment. By removing the inner segment pitch links and attaching the inner segment to the outer segment, the conventional swashplate then controls both inner and outer segment. This provides a method by which the segmented rotor can be operated as a conventional rotor. The following is a list of the physical characteristics of the segmented rotor.

Radius	4 feet
Chord	6 inches
Number of Blades	3
Root Cutout	18.9%
Solidity	.119
Twist	0 degree

Thickness Distribution:

	Radial Station	Thickness Ratio (t/c)
	18.9%	21%
	50 %	21%
Linear Distribution From	50 %	21%
To	100 %	15%

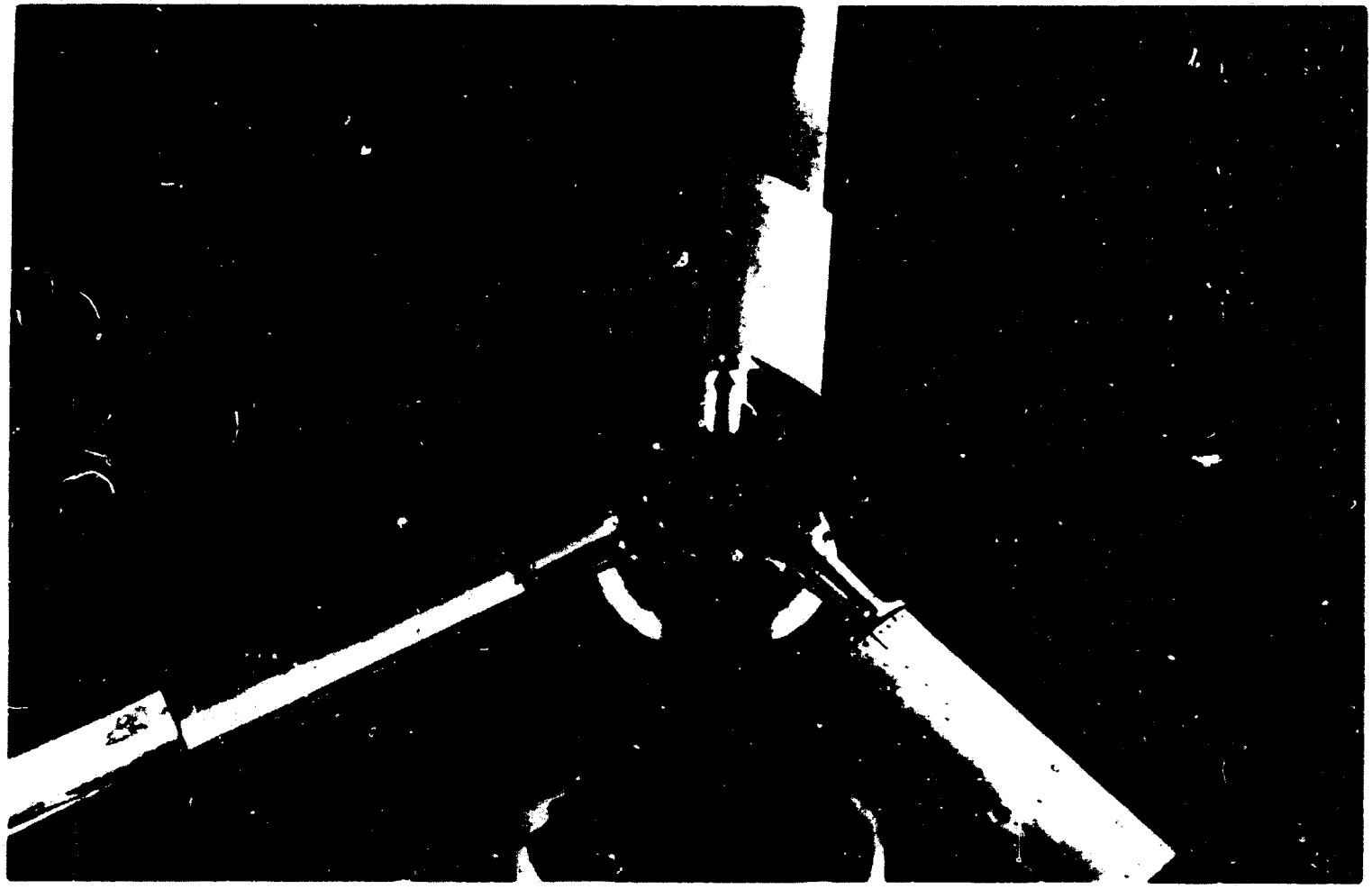

Figure 1. Segmented-Rotor Wind-Tunnel Model.
(Sheet 1 of 2)

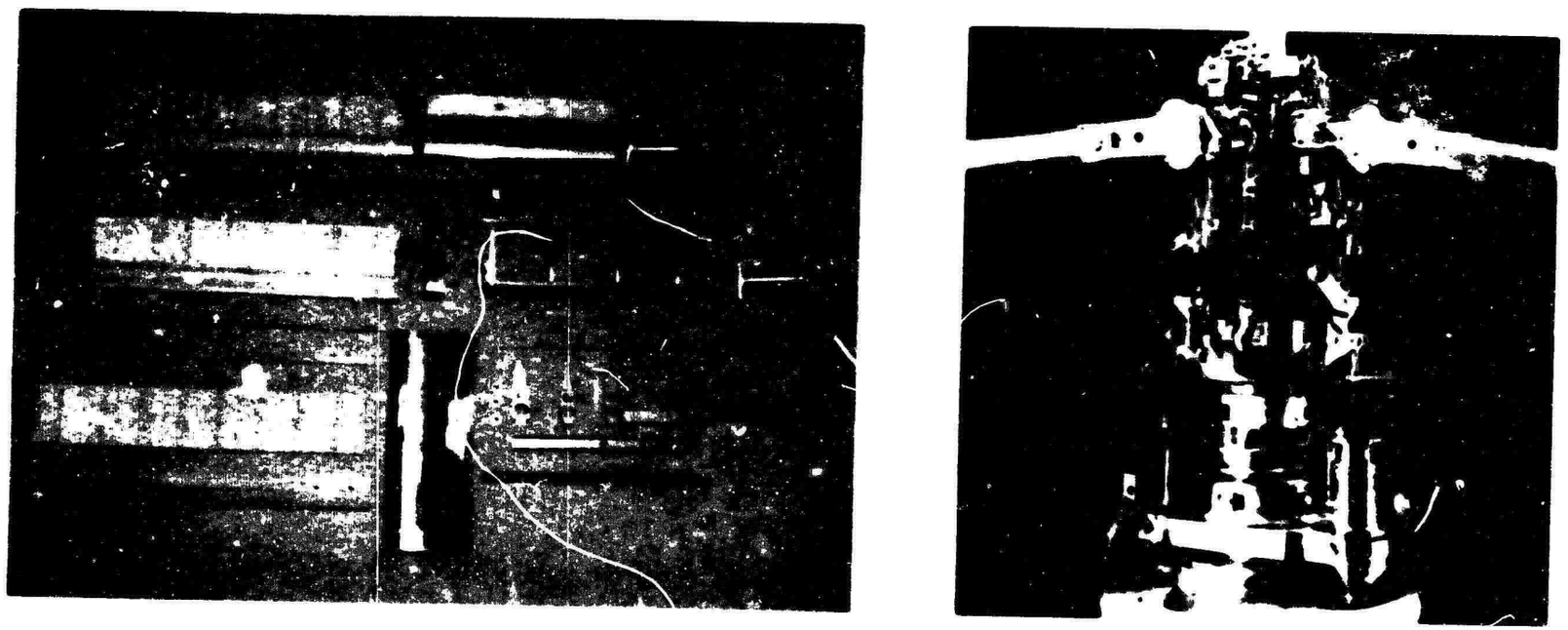

Figure 1. Segmented-Rotor Wind-Tunnel Model.
(Sheet 2 of 2)

INSTRUMENTATION

The average steady aerodynamic forces and moments are monitored by a bank of Speedomax recorders. The signals from the Speedomax recorders are digitized and used by the summary card punch for data storage. In addition, the signals from the Speedomax units are directed through sine and cosine resolvers and summing amplifiers to "on line" x-y plotters. The plotters provide "on line" plots of lift, propulsive force, and power as a function of control axis angle of attack.

Control system loads, blade loads, blade motions and test stand flexure fatigue loads are monitored and recorded on oscillograph recorders. These data are used for on line safety to ensure that test limits are maintained within the structural limitations of the model.

Scientific Advances subminiature absolute pressure transducers were installed in an attempt to obtain exploratory pressure data. The signal from these transducers was recorded on oscillograph recorder tape.

EXPERIMENTAL PROCEDURE

CALIBRATION

Pre-test and post-test calibrations were performed on the strain-gaged balance system installed in the rotor test stand. These calibrations were performed with the test stand installed in the test section of the wind tunnel. The calibration loads were applied to the model through a network of friction free pulleys and cables. The pre-test and post-test calibration agreed within one-half of one percent. The calibration data were recorded on punch cards for use in the data reduction program.

ROTOR DYNAMIC BALANCE AND BLADE TRACKING

The strain gage signals from the in-plane flexures were recorded on an oscillograph tape recorder. At the same time the rotor rpm was increased gradually until the operating speed was reached. The one-per-revolution response of the in-plane flexures was determined from the oscillograph tape. Appropriate balance weights were then inserted in the blade tip to correct for the unbalance.

Concurrent with the balancing procedure the rotor blades were visually monitored with a Strobotac. Based on this visual reference the length of individual pitch links were changed to bring the blades into track.

DATA ACQUISITION

The rotor shaft was initially set at the angle of attack corresponding to zero thrust. The rotor and wind tunnel speeds were simultaneously increased until the operating conditions were reached. When the air temperatures in the wind tunnel stabilized, adjustments were made to dynamic pressure and rotor rpm to obtain a constant advance ratio and advancing blade tip mach number. From this initial point, shaft angle sweeps were made at constant collective and cyclic pitch, data being recorded at incremental shaft positions.

Blade loads, blade motions, pitch link loads, and flexure loads were continuously monitored throughout each shaft sweep to ensure that structural or mechanical limitations were not exceeded. This procedure was repeated until the range of collective for the various configurations was completed.

Subsequent to obtaining the rotor data, the blades were

removed from the hub and replaced by aerodynamically similar blade shanks. Hub and shank tares were then obtained throughout the range of shaft angle of attack at the advance ratio and advancing blade tip mach number previously tested.

DATA REDUCTION

The calibration data cards are used as input for the data reduction program. From the calibration data a six-by-six first order linear interaction matrix is formed. The program then applies this interaction matrix to the test data cards to determine model, shaft axis, forces, and moments. In addition, wind tunnel wall corrections are applied as shown in the next section. The model shaft axes thrust and drag are then resolved into wind-axis lift and propulsive force. The positive sign convention and the resolution of thrust and drag into lift and propulsive force are illustrated on Figure 2. Lift, propulsive force, and torque power are then nondimensionalized by free stream velocity and the square of the rotor diameter.

WIND TUNNEL WALL CORRECTION PROCEDURE

Wind tunnel wall corrections are applied to the data; the procedures used are basically those of Heyson*. The following modifications were incorporated to provide compatibility with Boeing's test techniques.

Equation 36, page 18, Heyson*:

$$\left(\frac{W_o}{W_h}\right)^4 = \frac{1}{1 + \left(\frac{V}{W_o} + \frac{D_i}{L}\right)^2} \qquad (1)$$

Rearranging and expanding

$$\left(\frac{W_o}{W_h}\right)^4 + \left(\frac{W_o}{W_h}\right)^4 \left(\frac{V}{W_o}\right) + 2 \left(\frac{W_o}{W_h}\right)^4 \left(\frac{V}{W_o}\right)\left(\frac{D_i}{L}\right) + \left(\frac{W_o}{W_h}\right)^4 \left(\frac{D_i}{L}\right)^2 = 1 \qquad (2)$$

*H.H. Heyson, Linearized Theory of Wind-Tunnel Jet-Boundary Corrections and Ground Effect for VTOL-STOL Aircraft, Technical Report R-124, National Aeronautics and Space Administration.

Making the following substitutions

$$D_i = H\cos\alpha_s + T\sin\alpha_s$$

$$L = -H\sin\alpha_s + T\cos\alpha_s$$

gives the momentum theory quartic as a function of the basic forces measured on the rotor test stand. The quartic is then solved for the ratio W_o/W_h.

$$\left[\frac{W_o}{W_h}\right]^4\left[1+\left(\frac{T\sin\alpha_s + H\cos\alpha_s}{T\cos\alpha_s - H\sin\alpha_s}\right)^2\right]+2\left[\frac{T\sin\alpha_s + H\cos\alpha_s}{T\cos\alpha_s - H\sin\alpha_s}\right]\left[\frac{V}{W_h}\right]\left[\frac{W_o}{W_h}\right]^3 + \left[\frac{W_o}{W_h}\right]^2\left[\frac{V}{W_h}\right]^2 = 1 \qquad (3)$$

and the wake skew angle is calculated from

$$\chi = \arccos\,(W_o/W_h)^2 \qquad (4)$$

Then, using Equation 8, page 4, Heyson*

$$W_h = \pm\left[\frac{L}{n\rho A_M}\right]^{1/2} \qquad (5)$$

and making the following substitutions

$$n = 2.0$$

$$L = T\cos\alpha_s - H\sin\alpha_s$$

$$A_M = \pi R^2$$

gives the hover state induced velocity

$$W_h = \pm\left[\frac{T\cos\alpha_s - H\sin\alpha_s}{\pi\ 2\ \rho\ R^2}\right]^{1/2} \qquad (6)$$

The vertical and horizontal components of induced velocities are then calculated from the following expressions

*H.H. Heyson, op.cit.

$$W_o = \left[\frac{W_o}{W_h}\right] W_h \tag{7}$$

$$U_o = \left[\frac{T\sin\alpha_s + H\cos\alpha_s}{T\cos\alpha_s - H\sin\alpha_s}\right] W_o \tag{8}$$

Finally the tunnel wall induced upwash and horizontal velocities are calculated from the expressions

$$\Delta W = \frac{\pi R^2}{A_T}\left[\delta_{WL}W_o + \delta_{WD}U_o\right] \tag{9}$$

$$\Delta U = \frac{\pi R^2}{A_T}\left[\delta_{UL}W_o + \delta_{UD}U_o\right] \tag{10}$$

The values of δ_{WL}, δ_{WD}, δ_{UL}, and δ_{UD} from Heyson* are a function of the type of wind tunnel, the wake skew angle, and the location of the model in the test section.

Using ΔW and ΔU the tunnel wall induced upwash angle is calculated from the expression

$$\Delta\alpha = \arctan\left[\frac{\Delta W}{V+\Delta U}\right] \tag{11}$$

The wind tunnel wall corrections are then applied to rotor shaft angle of attack and free stream tunnel velocity as follows:

$$(\alpha_s)_c = \alpha_s + \Delta\alpha \tag{12}$$

$$V = V_\infty + \Delta U \tag{13}$$

*H.H. Heyson, op. cit.

EXPERIMENTAL RESULTS

Data were obtained on three rotor configurations for an advance ratio of 0.60 and for an advancing blade tip Mach number of 0.36. The basic rotor data (or conventional rotor), with the outboard and inboard segments locked together, provide a reference for judging the performance capabilities of the segmented rotor. The two segmented pitch schedules that were tested are identified as Schedule 3 and Schedule 4 and are shown in Figure 3. Pitch Schedule 4 is identical, in the area of the advancing blade, to pitch Schedule 3. In the region of reverse flow, Schedule 4 maintains zero pitch. The purpose of this schedule was to investigate the importance to the overall performance level of the reverse flow region.

The primary pitch schedule for the segmented rotor, Schedule 3, was designed to operate most effectively at a shaft angle of attack of -15 degrees and advance ratio of 0.60. Variations in the azimuth phasing of $\pm$20 degrees was tested, as well as variations in the pitch level by changing the collective pitch of the inboard segment.

NONDIMENSIONAL PARAMETERS

The lift, propulsive force, and effective-drag data in this report are presented in nondimensional form, by dividing the quantity in question by the free-stream dynamic pressure times the square of the rotor diameter. This form has been in use at the Vertol Division since 1962. It was adopted because of its usefulness in analysis and comparison of V/STOL lifting systems, as pointed out by Schairer* in 1961. Briefly, its advantage lies in reducing the ideal theoretical relation between lift and induced drag to a single curve, independent of planform area. (For a conventional wing, this curve would be C_D/Aspect Ratio vs. C_L/Aspect Ratio.) A more detailed discussion of this point is given in the Appendix.

ROTOR DRAG POLARS

Comparison of lift-to-effective-drag ratio for the conventional rotor, pitch Schedules 3 and 4, is shown in Figure 4. These schedules show an increase in L/D_E of 22.5 percent for Schedule 3 and 18 percent for Schedule 4, at $L/qd^2 = .04$. Figure 5 shows the same data but with hub and shank tares removed. The effect of varying the azimuth phasing

*G.S. Schairer, Looking Ahead in V/STOL, presented at the joint IAS-RAES Meeting, London, September 1961.

of Schedule 3 is shown in Figure 6. This schedule shows, within the limits of the test, that the zero phase-angle provides the optimum lift-to-effective-drag ratio.

The rotor drag polars shown in Figures 7 and 8 illustrate the effect of varying the level of collective pitch on the inboard segment of Schedule 3. Negative collective, at least up to 10 degrees, is beneficial in increasing lift-to-effective-drag ratio and decreasing minimum effective drag. A cross-plot of the minimum effective drag and the maximum lift-to-effective-drag ratio versus collective pitch on the inboard segment ($\Delta\theta_{INBD}$), would show the optimum $\Delta\theta_{INBD}$ to be approximately -6 degrees. When compared to $\Delta\theta_{INBD} = 0$, -6 degrees of $\Delta\theta_{INBD}$ increases the lift-to-effective-drag ratio by 5 percent and reduces the minimum effective drag by 7.5 percent.

ROTOR POLAR MAPS

The rotor polar maps for all of the configurations tested are presented in Figures 11 through 21. These maps are the result of cross-plotting the basic data at constant P/qd^2V. The negative X/qd^2 values represent net drag force. The positive X/qd^2 values show that the rotor system has the capability of overcoming its own drag and pulling a fuselage in addition. The limit of propulsive force obtained with the conventional rotor and the maximum measured for the segmented rotor are shown in Figures 9 and 10. These data show that a segmented rotor has the capability of propelling an aircraft at 230 knots without auxiliary lift. The calculations behind this statement are as follows:

1. Assume:

   $fe/W = 0.001$

   Gross weight (lift) per rotor = 18,000 pounds

   Rotor diameter = 60 feet

   Altitude = 5000 feet

   Forward velocity = 230 knots

   Advance ratio = 0.60

2. Since $fe = X/q$ and $L = W$, the required propulsive force is:

$$X = (fe/W)\ Lq = (0.001)\ (18{,}000)\ (155)$$
$$= 2790 \text{ pounds} \qquad (14)$$

and

$$X/qd^2 = 2790/(155)(3600) = 0.005 \quad (15)$$

3. A rotor solidity of 0.0715 would require an $X/qd^2\sigma$ of 0.0700, which is well within the capability of the segmented rotor. The tip Mach number on the advancing blade at an advance ratio of 0.6 would be:

$$M_{(1)(90)} = V(1 + 1/\mu)/1097 = (388)(2.666)/1097$$
$$= 0.94 \quad (16)$$

The spacing of the constant power lines is related to propulsive efficiency. Note for instance in Figure 11 that the spacing of the power curves for the conventional rotor rapidly decreases as power increases, thus showing a rapid decrease in propulsive efficiency. This trend is not apparent for the segmented rotor, Schedule 3, shown in Figure 12. Figure 13 presents the rotor polar map for Schedule 3 (compared with the conventional rotor) but with hub and shank tares removed.

PROPULSIVE EFFICIENCY

Propulsive force plotted against power for each of the configurations tested is shown in Figures 22 through 25. The slope of these curves represents propulsive efficiency (the ratio of incremental useful work to energy expended). Figure 22 illustrates the ability of the segmented rotor, particularly Schedule 3, to efficiently produce propulsive force well beyond the capability of conventional rotors. The effect on propulsive efficiency of varying azimuth phasing and of the level of the pitch schedule, $\Delta\theta_{INBD}$, is illustrated in Figures 23, 24, and 25.

HUB AND SHANK TARES

The data in Figure 26 were obtained with the hub, plus aerodynamically similar blade shanks. (The blade shank is defined as that part of the blade retention between the root cutout and the vertical and horizontal hinge.) The dynamic pressure and rotor tip speed were set so that an advance ratio of 0.60 and an advancing blade tip Mach number of 0.36 would have resulted if the blades were installed.

Removal of the hub and shank tares from the data provides

performance data for an isolated rotor. The procedure for removing hub tares is detailed by Ekquist*. Note that the major hub and shank tares involve a correction to propulsive force and will increase the propulsive-force level.

BASIC ROTOR DATA

The basic rotor data are presented in Figures 27 through 65 in the form in which they were acquired. Ekquist* describes the computer program which was used to reduce the raw test data. Rotor nondimensionalized lift, propulsive force, and power are shown as functions of control axis angle at constant collective pitch settings.

Note that wind tunnel wall corrections have been applied to the data.

Hub and shank tares have been removed for the conventional rotor and the basis pitch-Schedule 3 cases (Figures 27 through 32).

PRESSURE DATA

Seven pressure transducers were installed on one blade to measure oscillatory pressures. During the test it was discovered that a low-frequency galvometer had inadvertently been installed to record the pressure data. At this point, it was too late to obtain amplifying equipment required to excite the higher frequency galvometer in time to obtain useful data in this test.

COMPARISON WITH THEORY

The pitch schedules for the inboard segment were established analytically using the Vertol Division's rotor-analysis computer program. The schedules were tailored for operation at moderate power and thrust levels, below the theoretical stall of the retreating blade.

The nominal superiority of the segmented rotor under those conditions was not, in fact, borne out by the test results. Figure 66 shows rotor polars at $P/qd^2V = 0.008$ for the conventional and for the segmented rotor with pitch schedule 3, both theoretical and as tested. The reversal of the theoretical relationship is probably due to drag penalties incurred by the discontinuity in blade element pitch angle at 50-percent radius, which would cause increases in both profile and induced power. Since the analysis method used

*D. Ekquist, Generalized Data-Reduction Program for Powered Rotor and Propeller Wind-Tunnel Whirl Test, Aeronautical Investigation III-224, The Vertol Division of Boeing.

uniform induced inflow* and strip theory, neither of these effects was included.

The segmented rotor showed its superiority in the region beyond the theoretical stall line, where the analysis method is known to give unrealistic results. (For example, at the nominal stall, the lift-vs-α_{CA} line shows a sharp break in slope at that point. The test data show no such break.) Therefore, no theoretical results are shown for these high lift and power levels.

The explanation for this behavior lies in the high advance ratio ($\mu' = 0.60$) of the flight condition. Here, radial flow effects play a major role in determining the blade element stall behavior. Harris** discusses this point in detail. Incorporation of radial-flow effects into Vertol Division's rotor-analysis methods is currently underway.

---

*This restriction no longer applies to the standard rotor analysis method in use at Vertol Division, although adaptation to the problem of segmented rotors was not yet complete at the time of writing.

**F.D. Harris, Preliminary Study of Radial-Flow Effects on Rotor Blades, Technical Report R-382, The Vertol Division of Boeing, 19 January 1965.

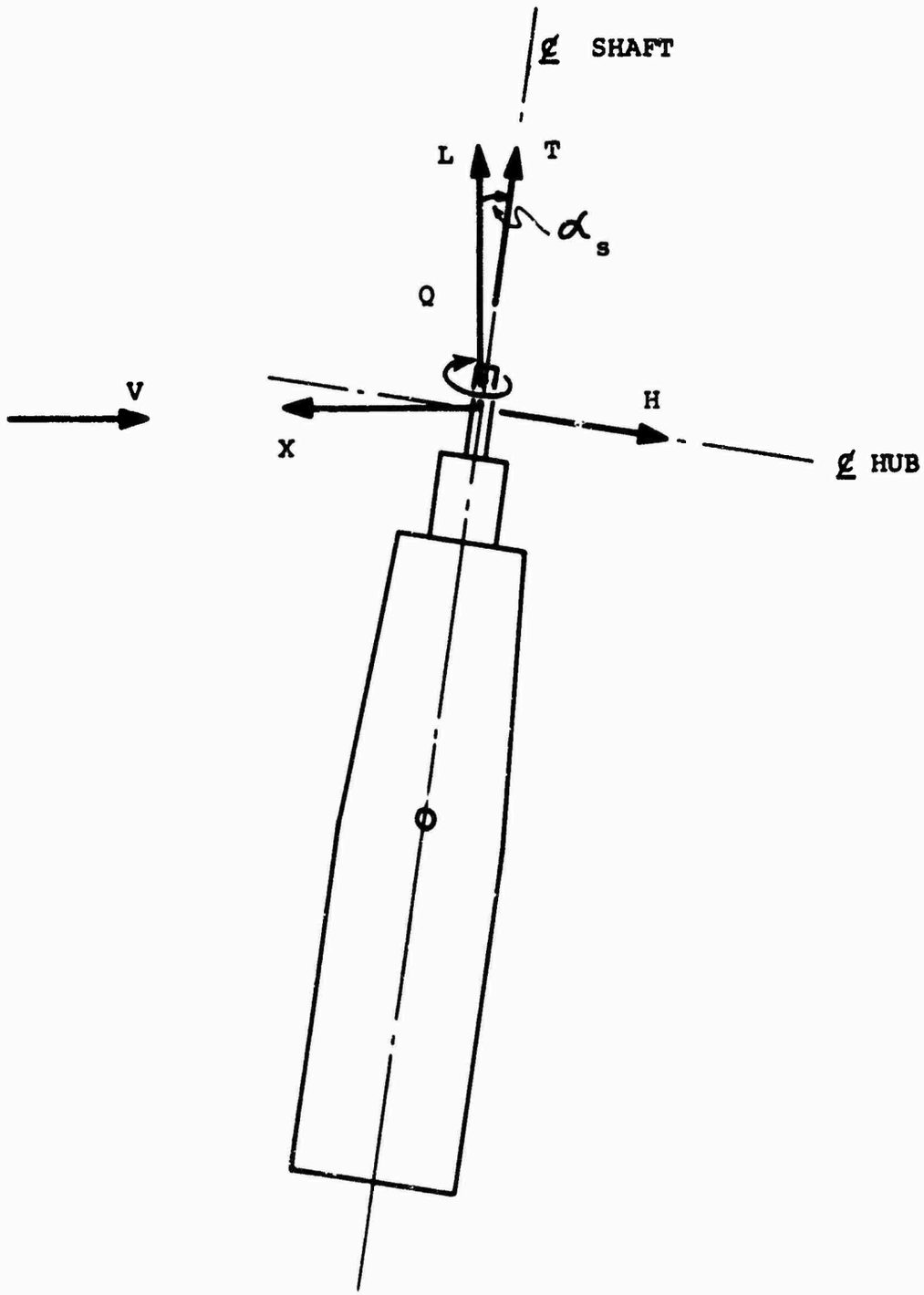

Figure 2. Definition of Axis System and Sign Convention.

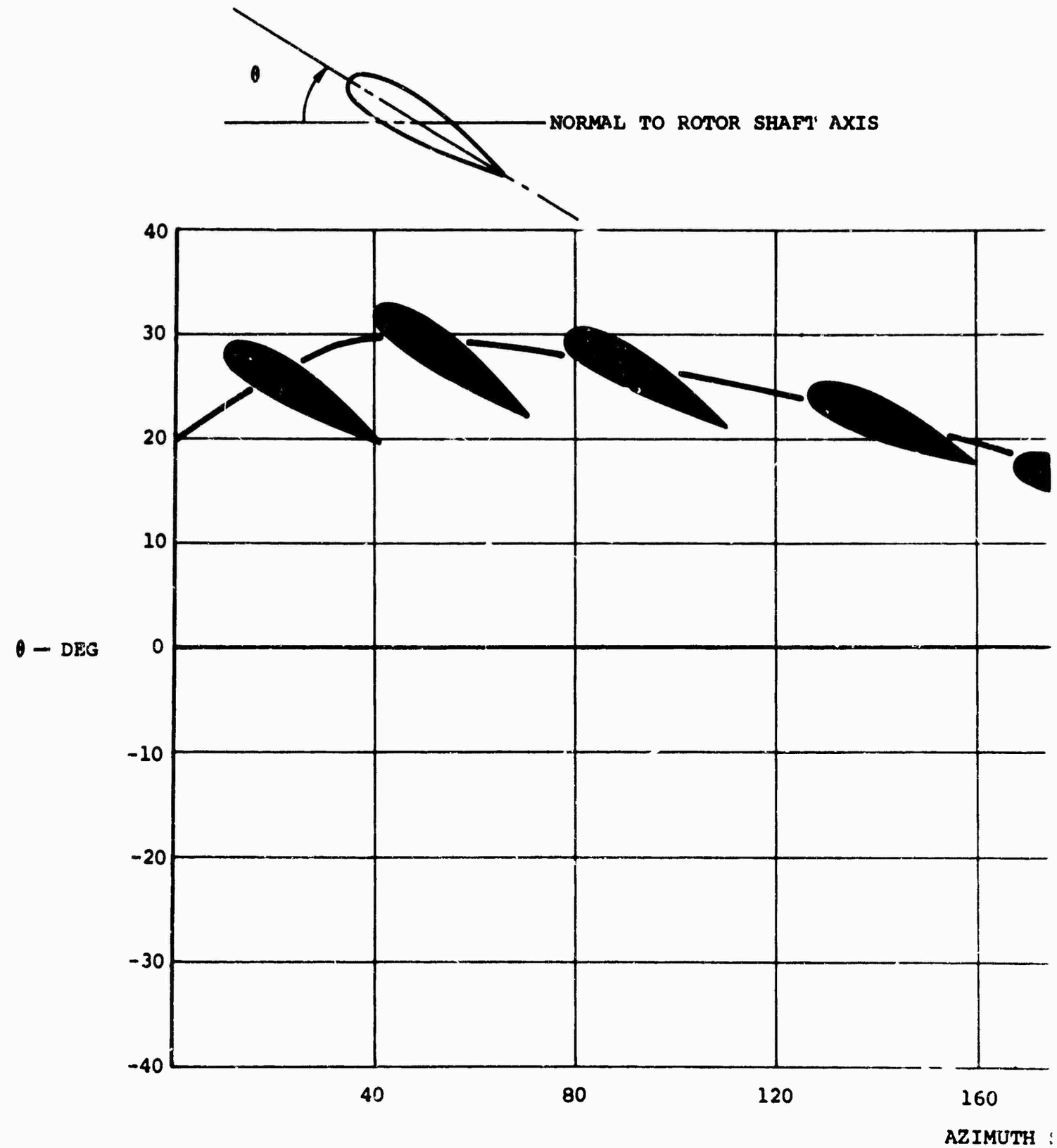

Figure 3. Segmented Rotor Pitch Schedules 3 and 4.

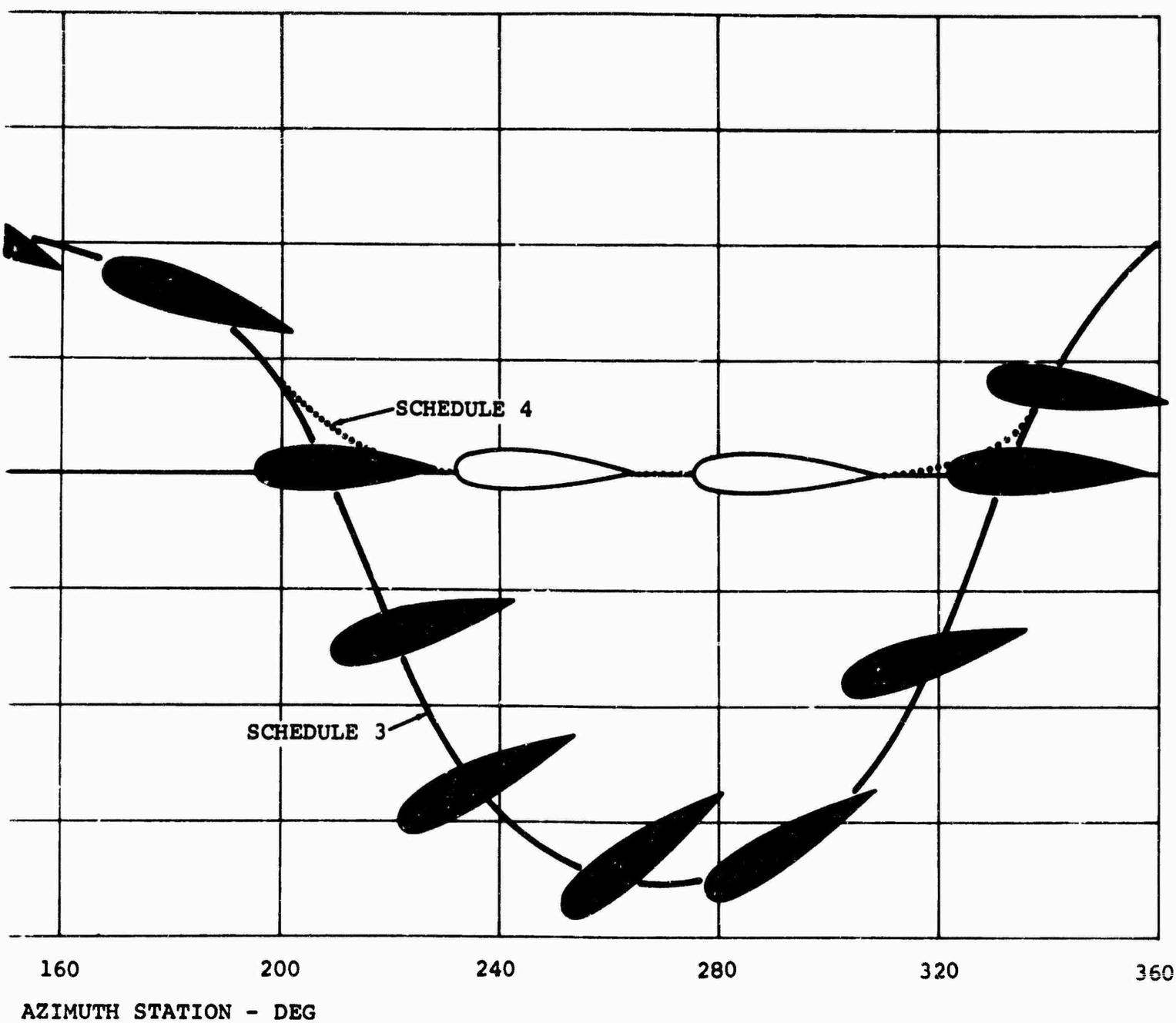
SCHEDULE 4
SCHEDULE 3
160
200
240
280
320
360
AZIMUTH STATION - DEG

B

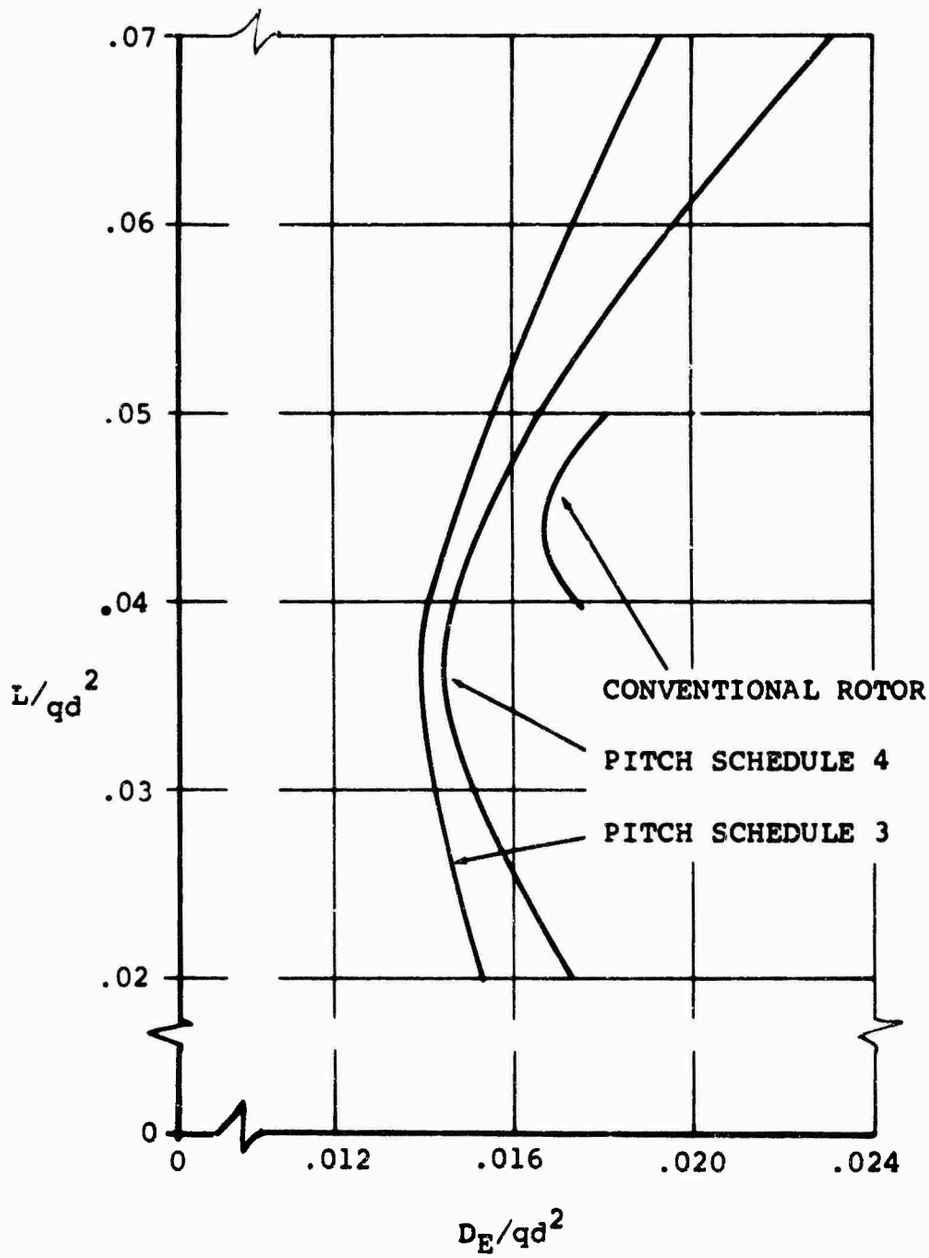

Figure 4. Rotor Drag Polar Comparing Conventional and Segmented Rotors Where $\Delta\Theta_{INBD} = 0°$, $\Delta\psi = 0°$, $P/qd^2V = 0.018$, $\mu' = 0.60$, $M(1)(90) = 0.36$.

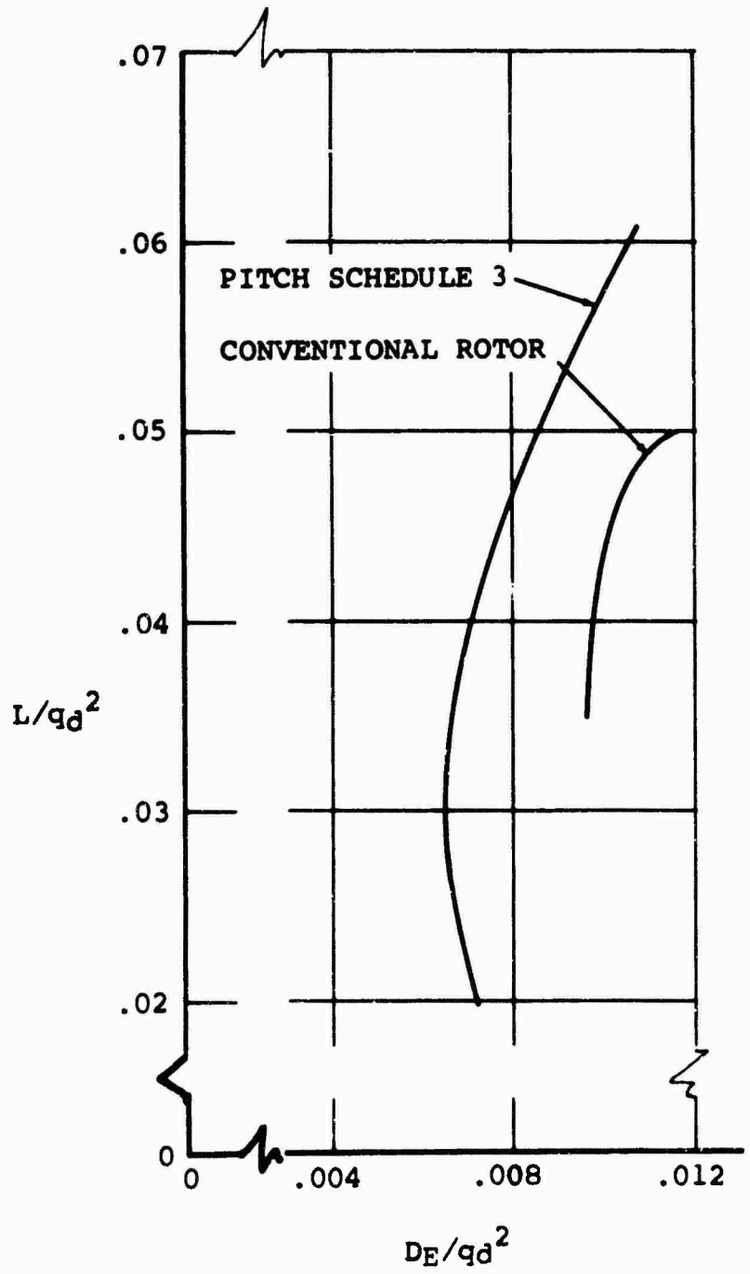

Figure 5. Rotor Drag Polar Comparing Conventional and Segmented Rotors With Hub and Shank Tares Removed Where $\Delta\theta_{INBD} = 0°$, $\Delta\psi = 0°$, $P/qd^2V = 0.018$, $\mu' = 0.60$, $M_{(1)(90)} = 0.36$.

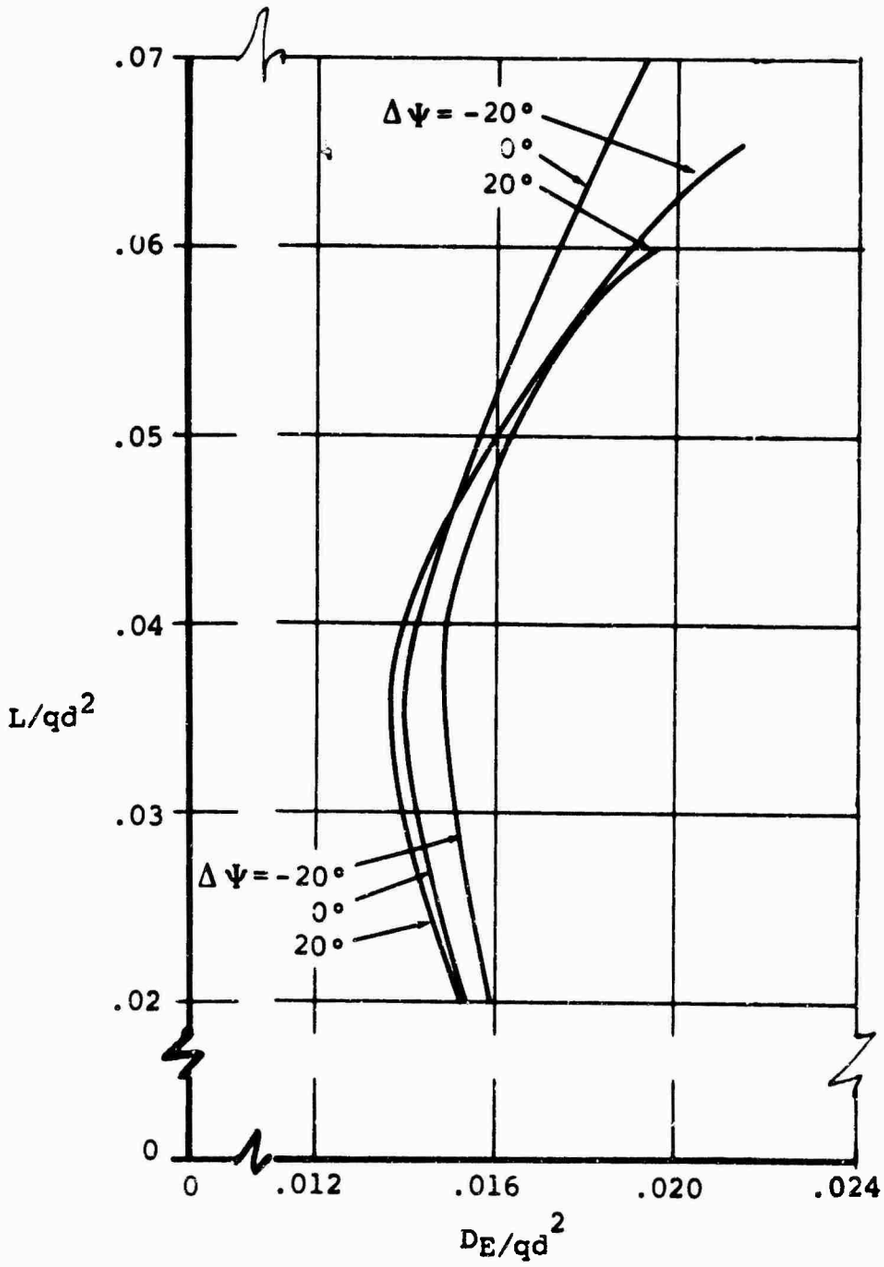

Figure 6. Rotor Drag Polar for Pitch Schedule 3 Showing the Effect of Azimuth Phasing Where $\Delta\Theta_{INBD} = 0°$, $P/qd^2V = 0.018$, $\mu' = 0.60$, $M(1)(90) = 0.36$.

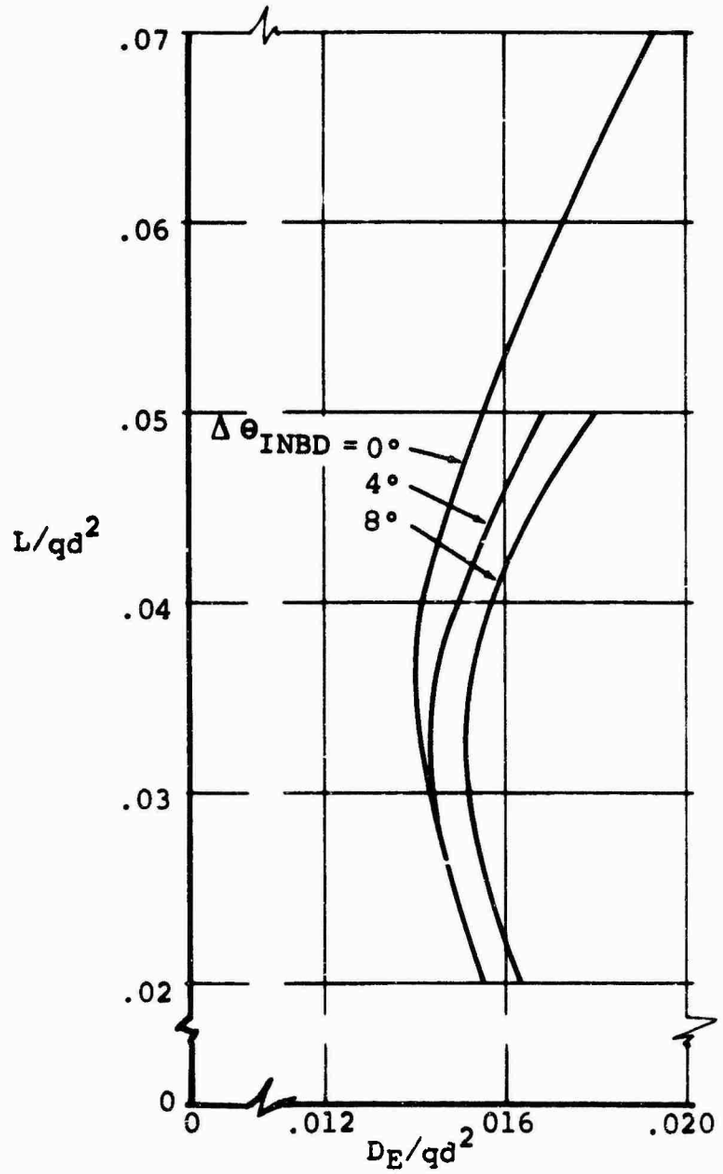

Figure 7. Rotor Drag Polar for Pitch Schedule 3 Showing the Effect of Collective Pitch on Inboard Segment Where $\Delta\psi = 0°$, $P/qd^2V = 0.018$, $\mu' = 0.60$, $M(1)(90) = 0.36$.

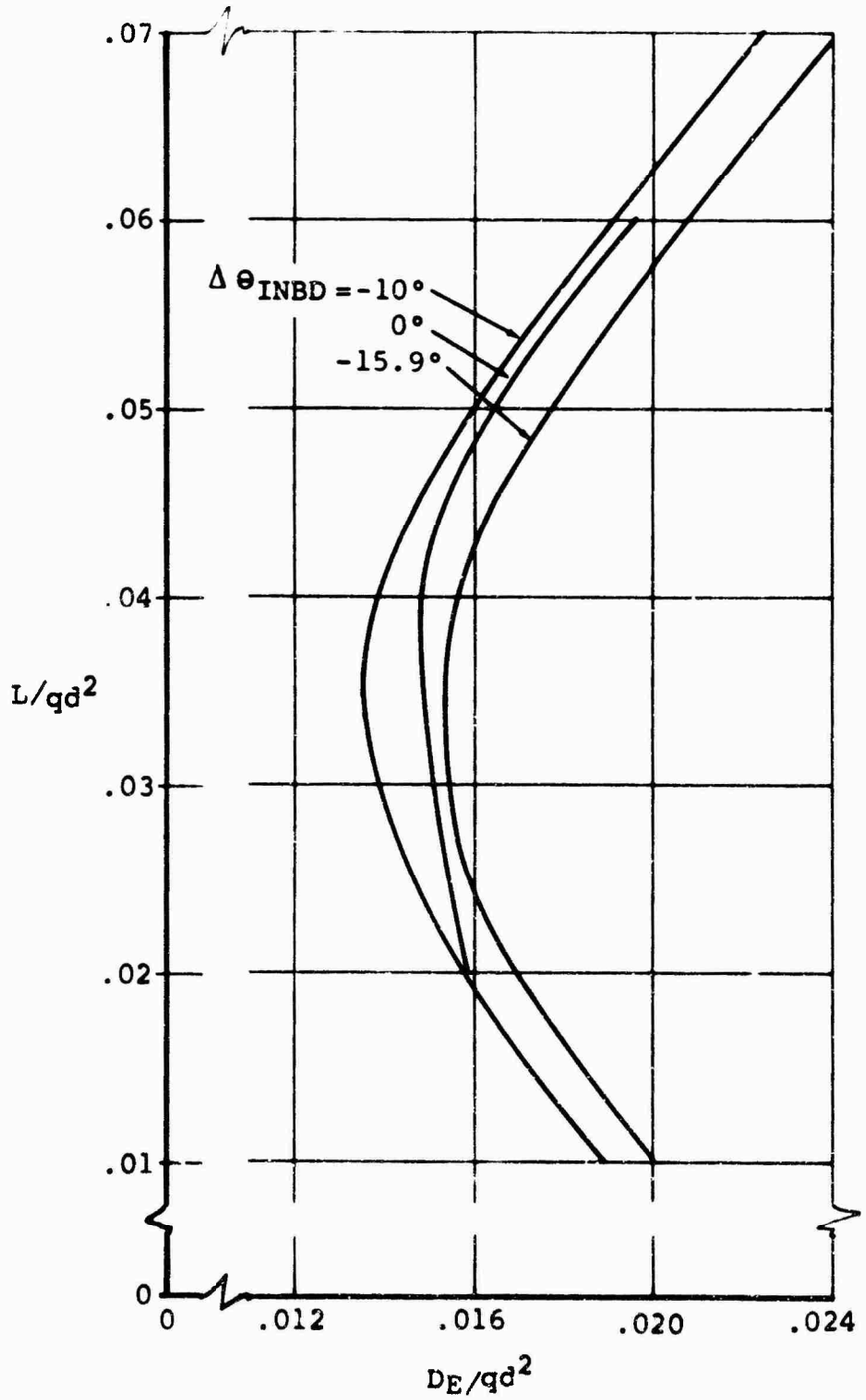

Figure 8. Rotor Drag Polar for Pitch Schedule 3 Showing the Effect of Collective Pitch on Inboard Segment Where $\Delta\psi$ = 20°, P/qd^2V = 0.018, μ' = 0.60, $M(1)(90)$ = 0.36.

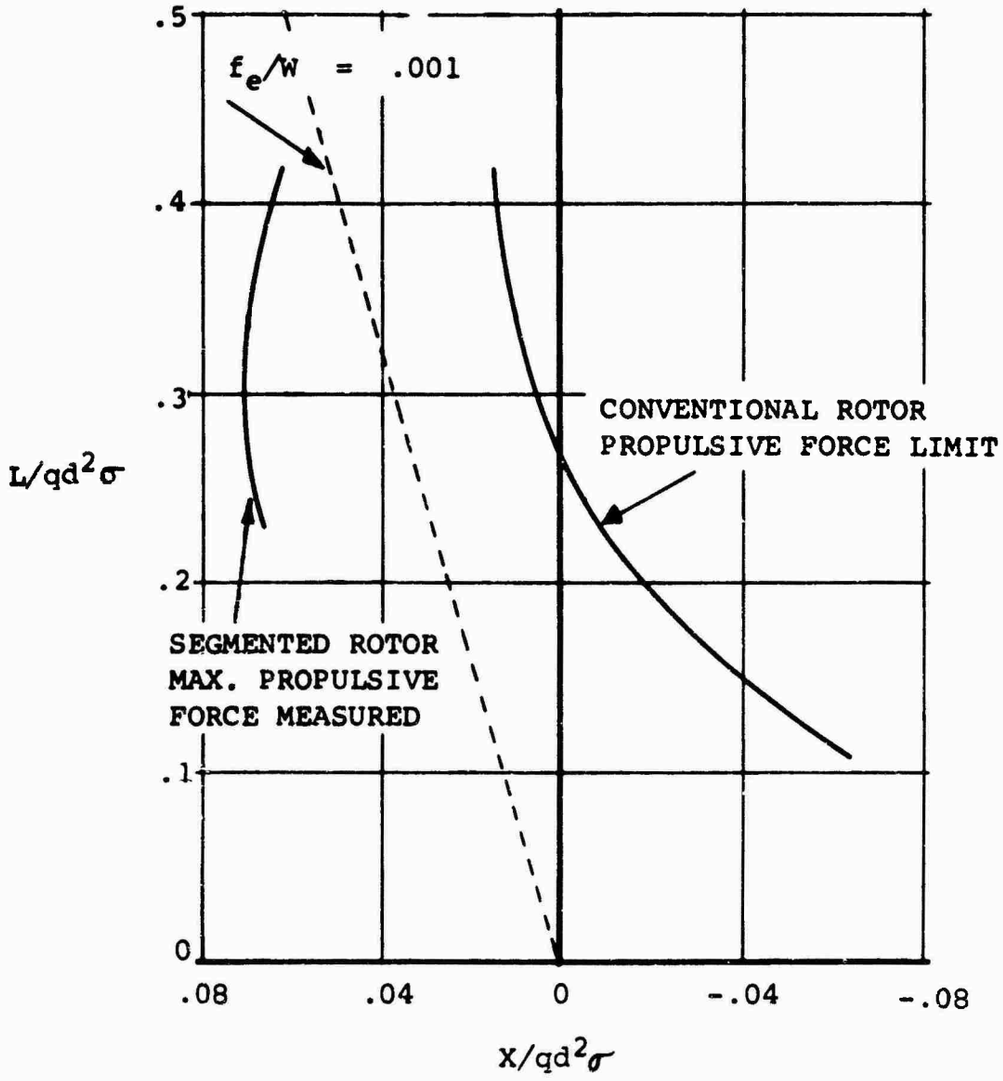

Figure 9. Comparison of Conventional and Segmented Rotor Propulsive-Force Limits for Pitch Schedule 3 Where $\Delta\theta_{INBD} = 0°$, $\Delta\psi = 0°$, $\mu' = 0.60$, $M(1)(90) = 0.36$.

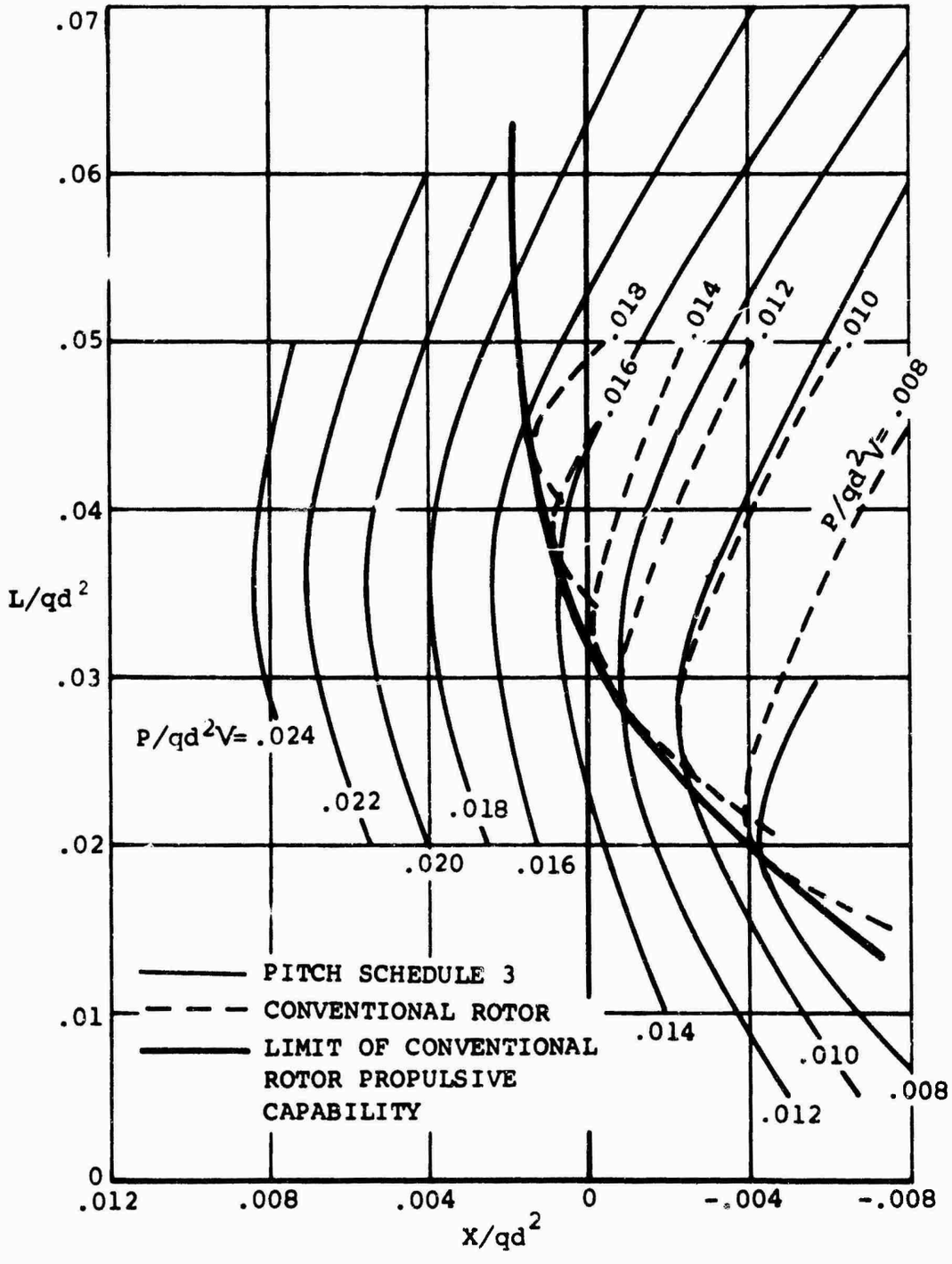

Figure 10. Polar Map Comparison of Conventional and Segmented Rotor Where $\Delta\Theta_{INBD} = 0°$, $\Delta\psi = 0°$, $\mu' = 0.60$, $M(1)(90) = 0.36$.

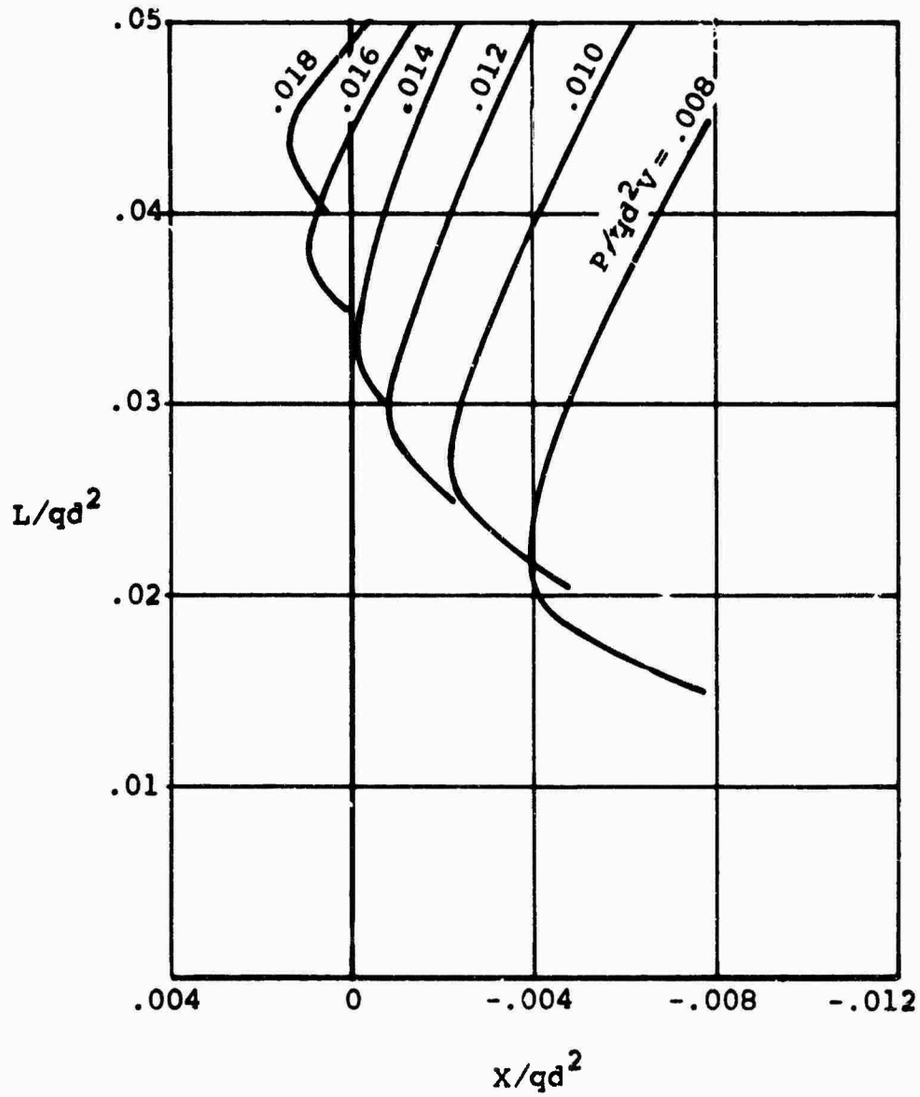

Figure 11. Polar Map of Conventional Rotor Where $\mu' = 0.60$, $M_{(1)(90)} = 0.36$.

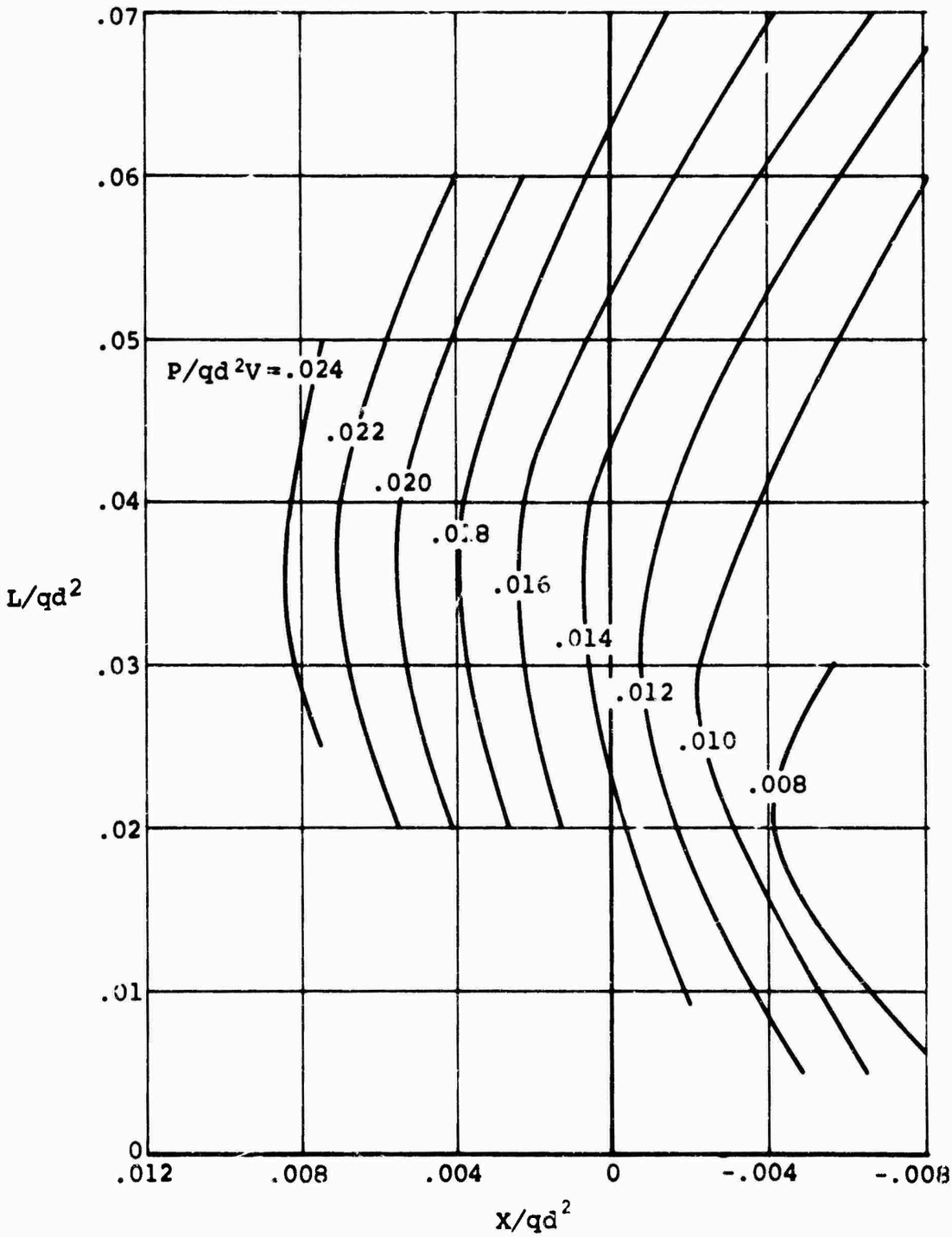

Figure 12. Polar Map of Segmented Rotor Pitch Schedule 3 Where $\Delta\theta_{INBD} = 0°$, $\Delta\psi = 0°$, $\mu' = 0.60$, $M(1)(90) = 0.36$.

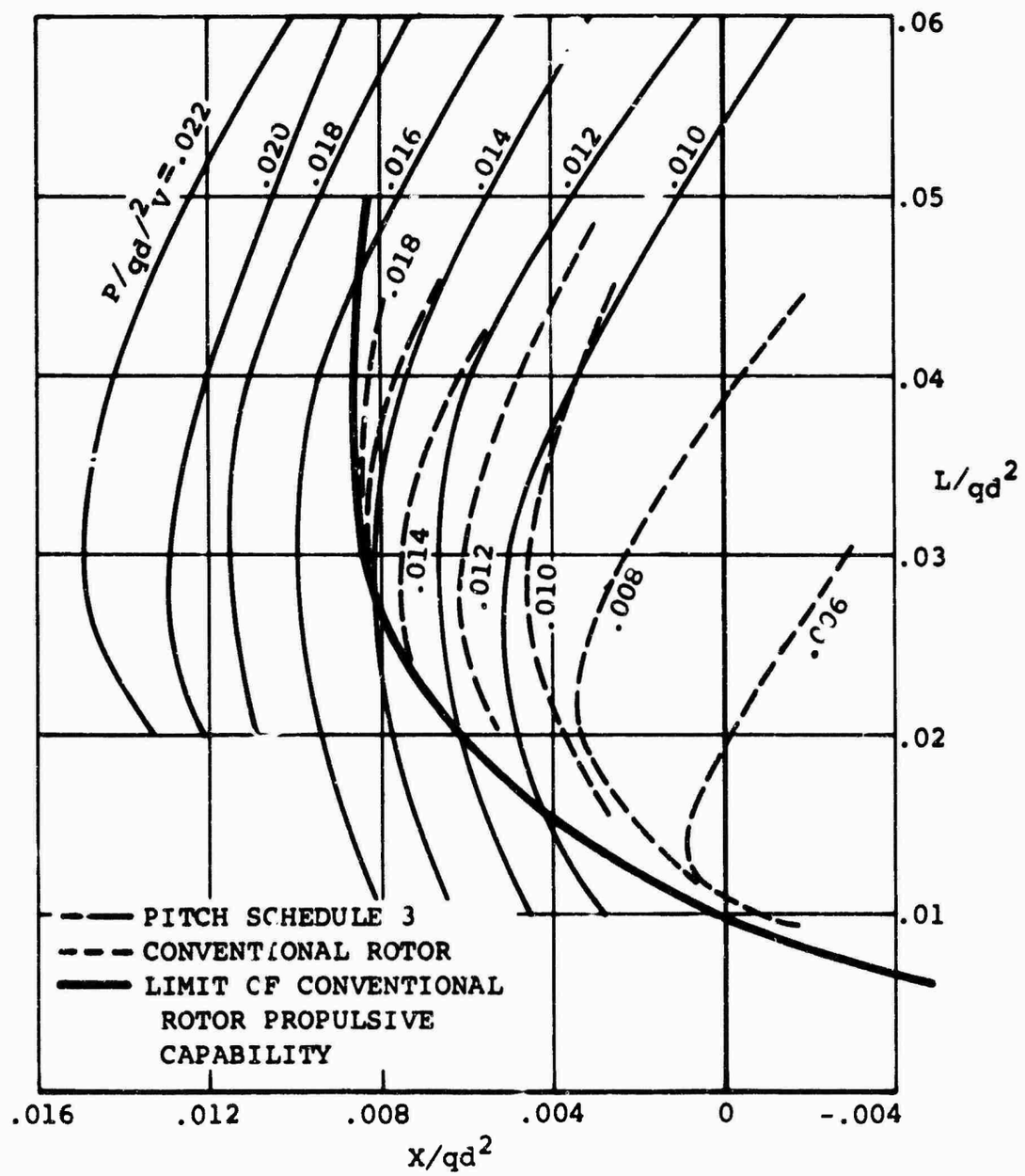

Figure 13. Polar Map of Segmented Rotor With Hub and Shank Tares Removed Where $\Delta\Theta_{INBD} = 0°$, $\Delta\psi = 0°$, $\mu' = 0.60$, $M(1)(90) = 0.36$ Compared With Conventional Rotor.

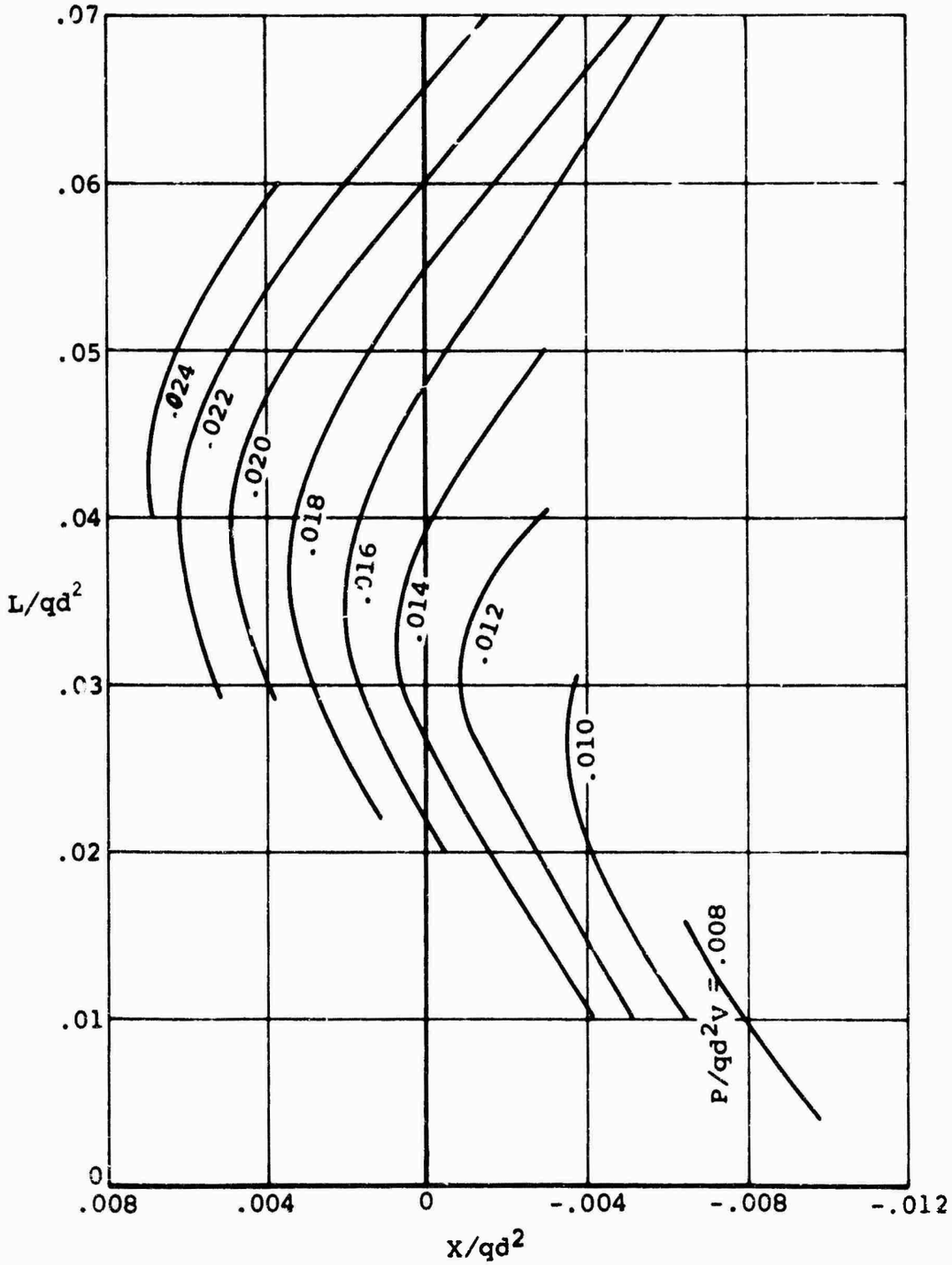

Figure 14. Polar Map of Segmented Rotor Pitch Schedule 4 Where $\Delta\Theta_{INBD} = 0°$, $\Delta\psi = 0°$, $\mu' = 0.60$, $M(1)(90) = 0.36$.

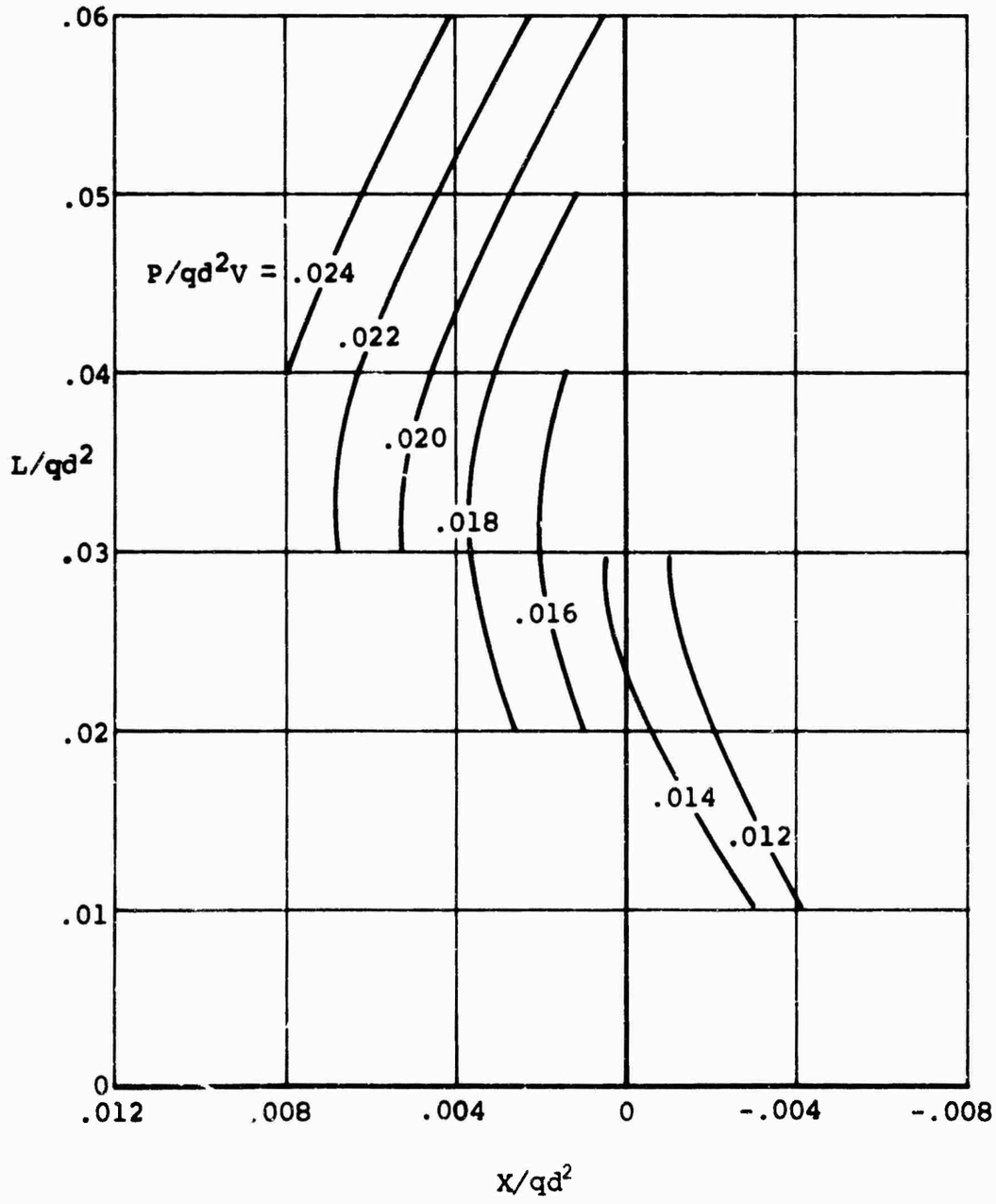

Figure 15. Polar Map of Segmented Rotor Pitch Schedule 3 Where $\Delta\theta_{INBD} = 4°$, $\Delta\psi = 0°$, $\mu' = 0.60$, $M_{(1)(90)} = 0.36$.

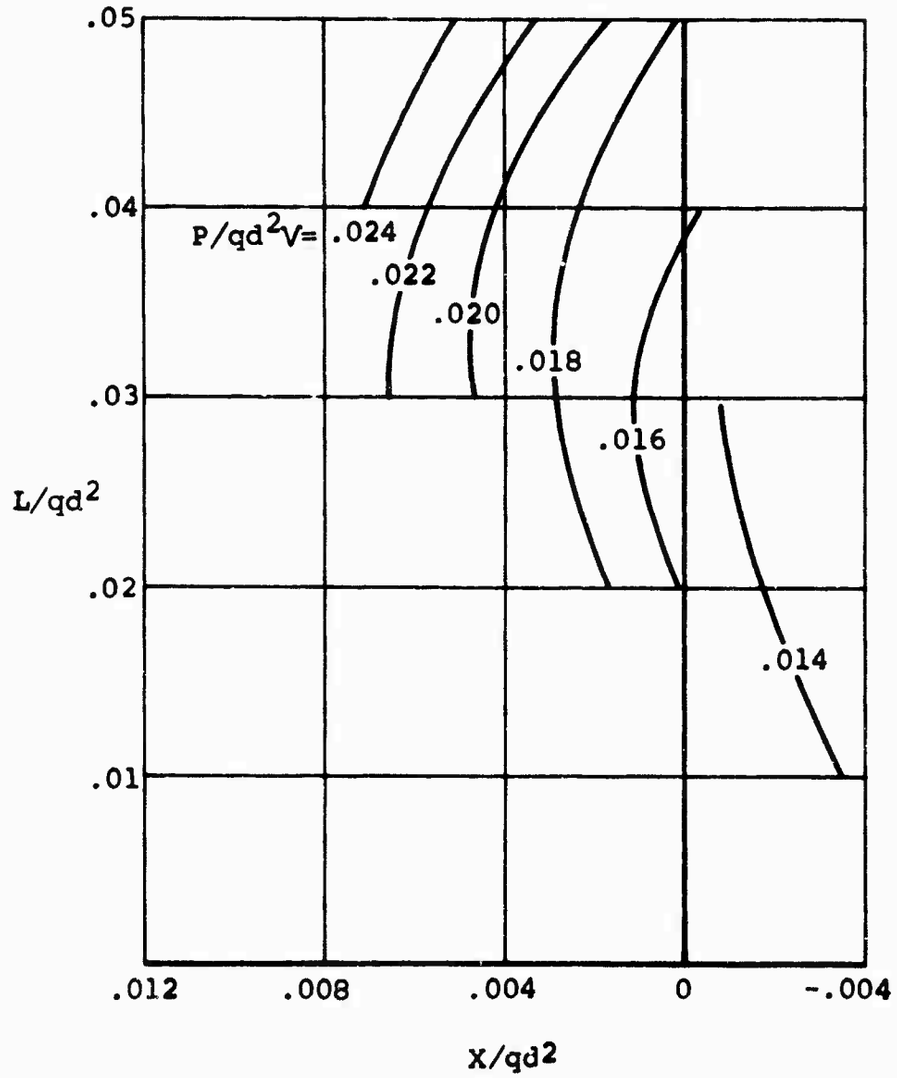

Figure 16. Polar Map of Segmented Rotor Pitch Schedule 3 Where $\Delta\Theta_{INBD} = 8°$, $\Delta\psi = 0°$, $\mu' = 0.60$, $M_{(1)(90)} = 0.36$.

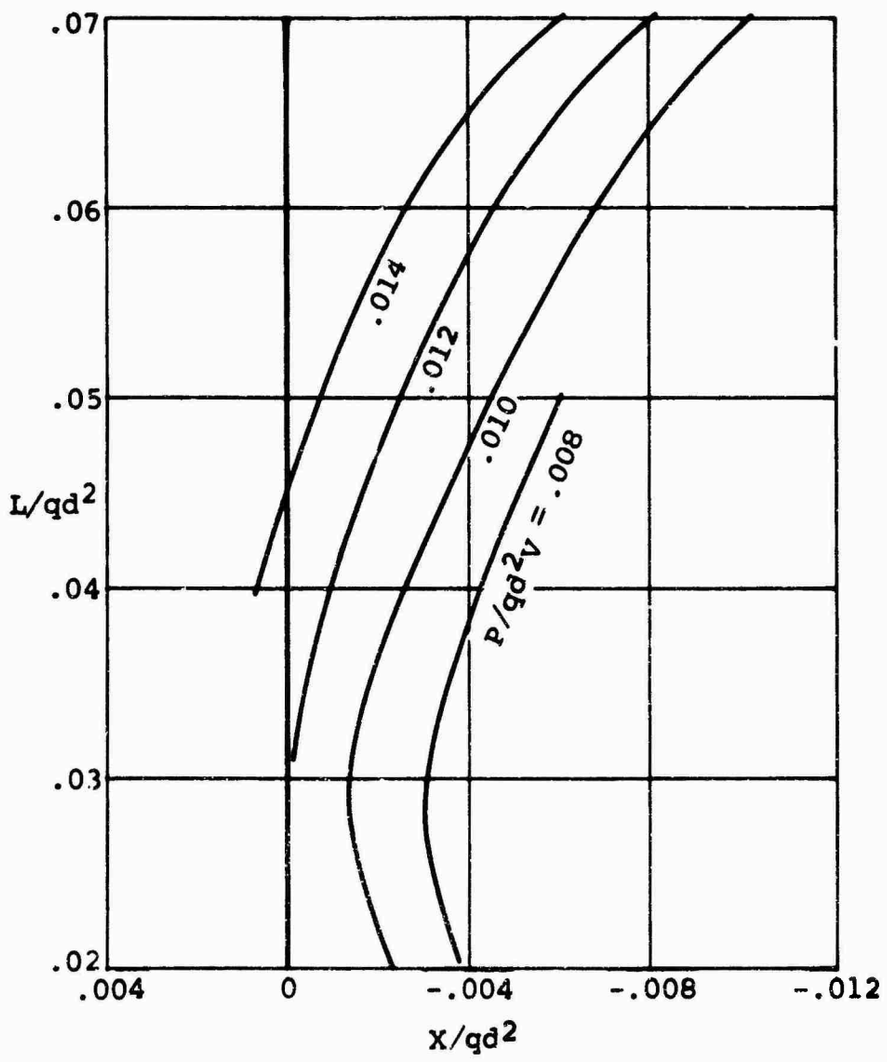

Figure 17. Polar Map of Segmented Rotor Pitch Schedule 3 Where $\Delta\Theta_{INBD} = -10°$, $\Delta\psi = 0°$, $\mu' = 0.60$, $M(1)(90) = 0.36$.

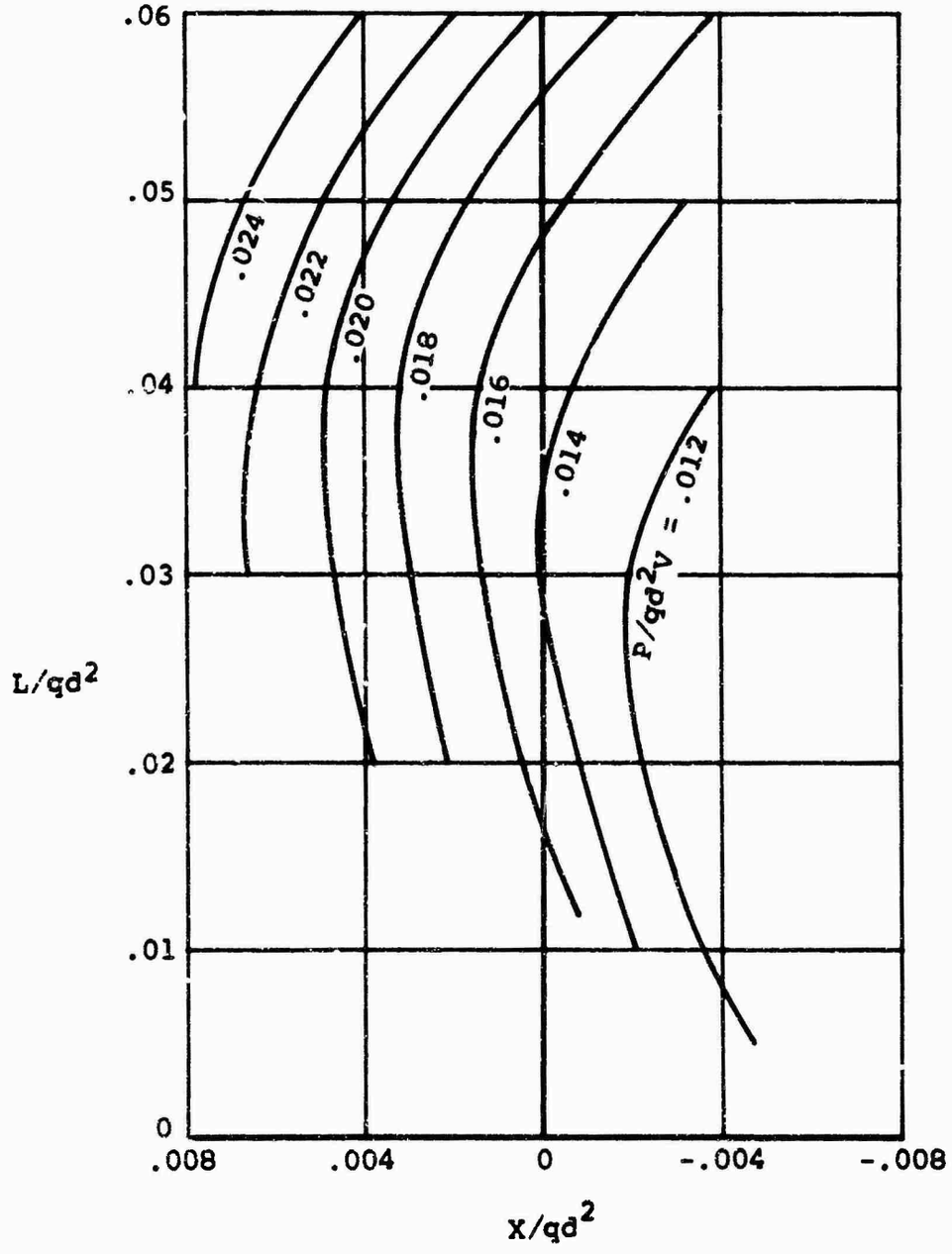

Figure 18. Polar Map of Segmented Rotor Pitch Schedule 3 Where $\Delta\Theta_{INBD} = 0°$, $\Delta\psi = 20°$, $\mu' = 0.60$, $M(1)(90) = 0.36$.

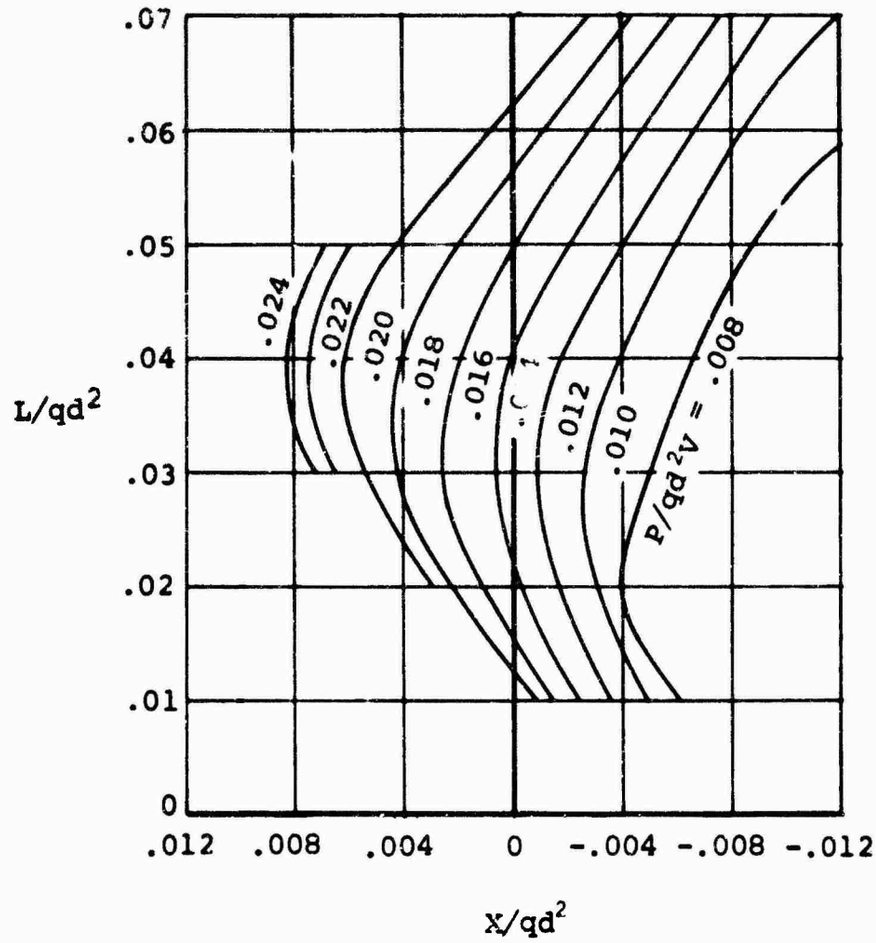

Figure 19. Polar Map of Segmented Rotor Pitch Schedule 3 Where $\Delta\theta_{INBD} = -10°$, $\Delta\psi = 20°$, $\mu' = 0.60$, $M_{(1)(90)} = 0.36$.

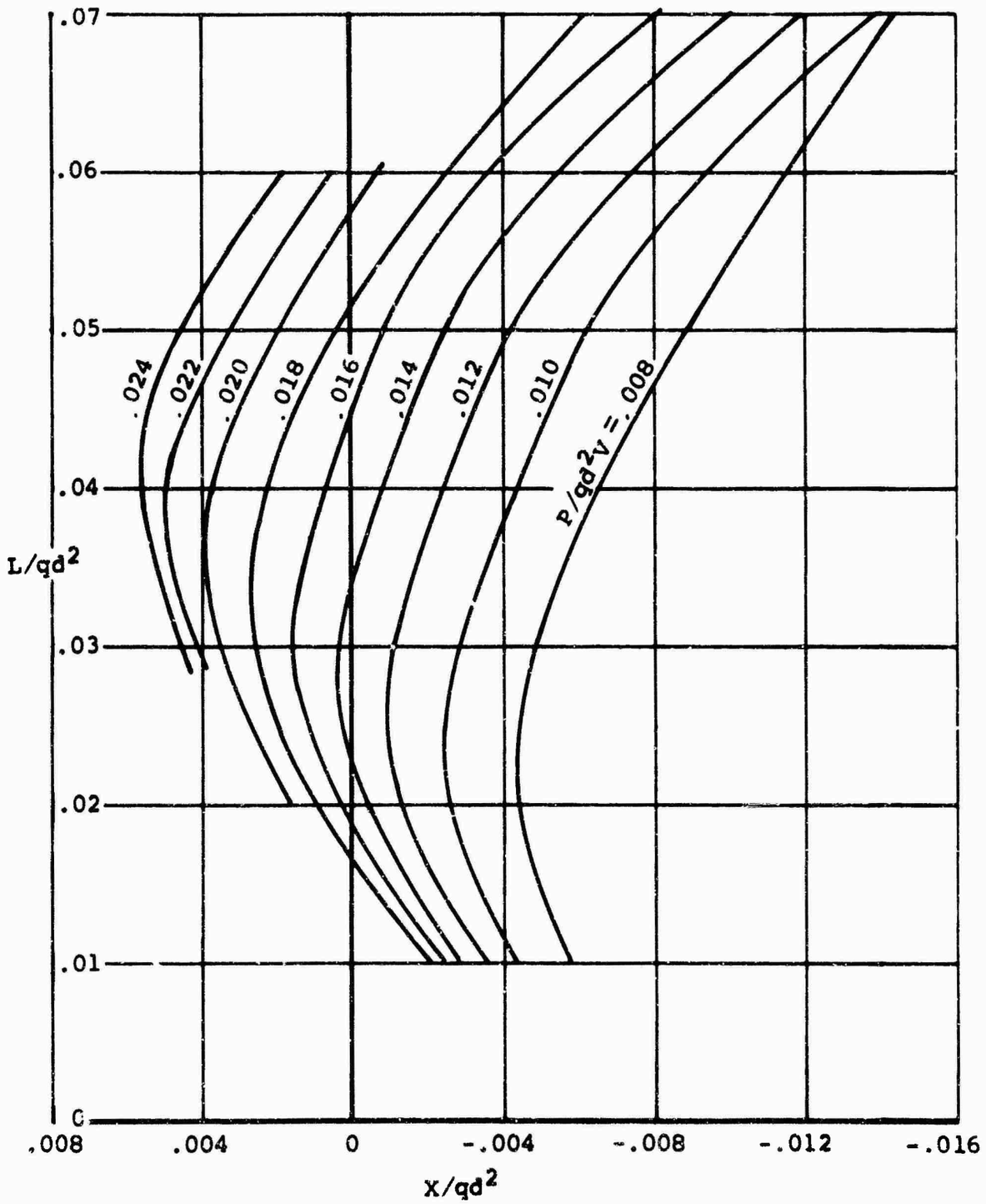

Figure 20 Polar Map of Segmented Rotor Pitch Schedule 3 Where $\Delta\theta_{INBD} = -15.9°$, $\Delta\psi = 20°$, $\mu' = 0.60$, (1) (90° = 0.36.

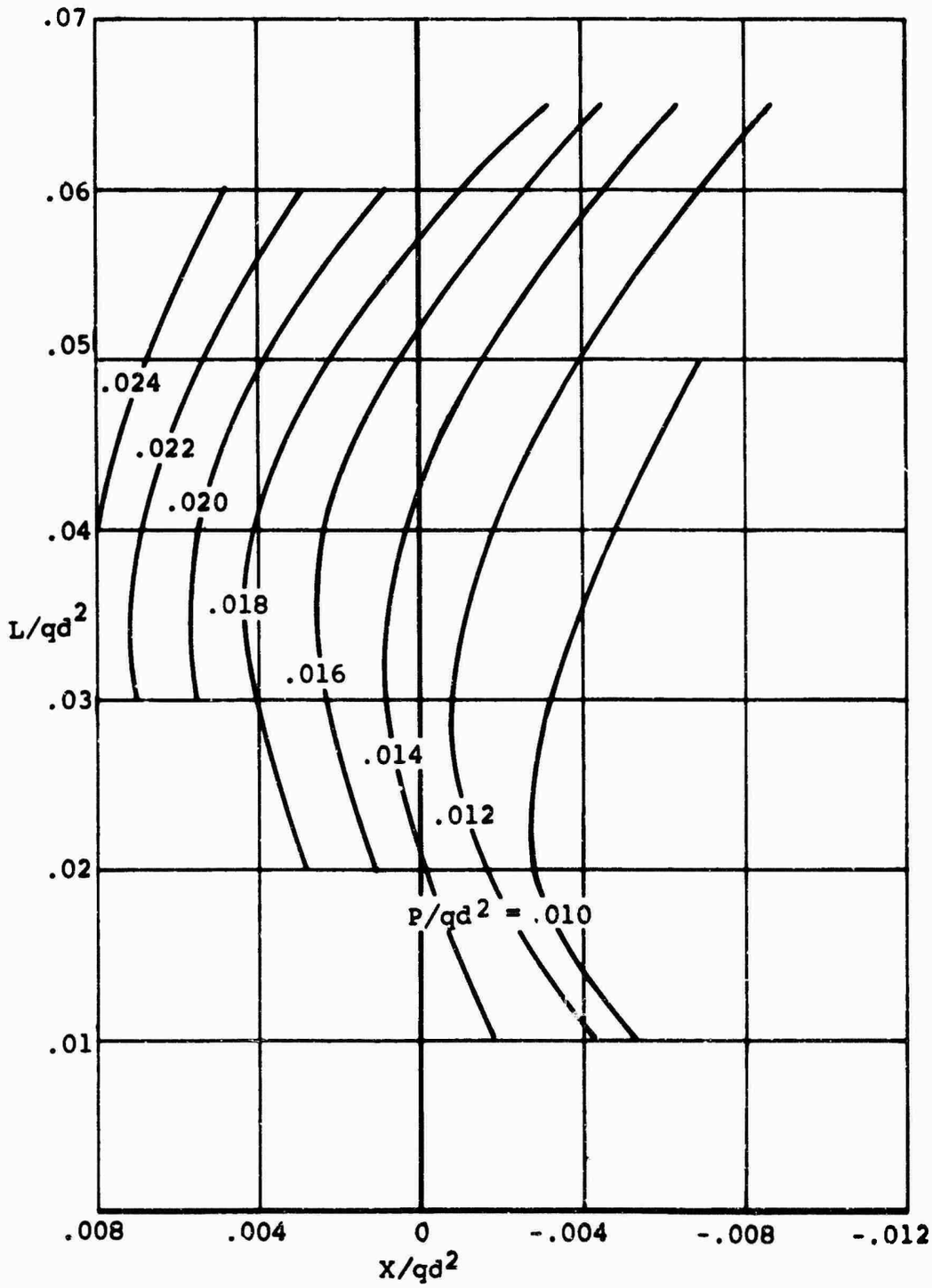

Figure 21. Polar Map of Segmented Rotor Pitch Schedule 3 Where $\Delta\theta_{INBD} = 0°$, $\Delta\psi = -20°$, $\mu' = 0.60$, $M_{(1)(90)} = 0.36$.

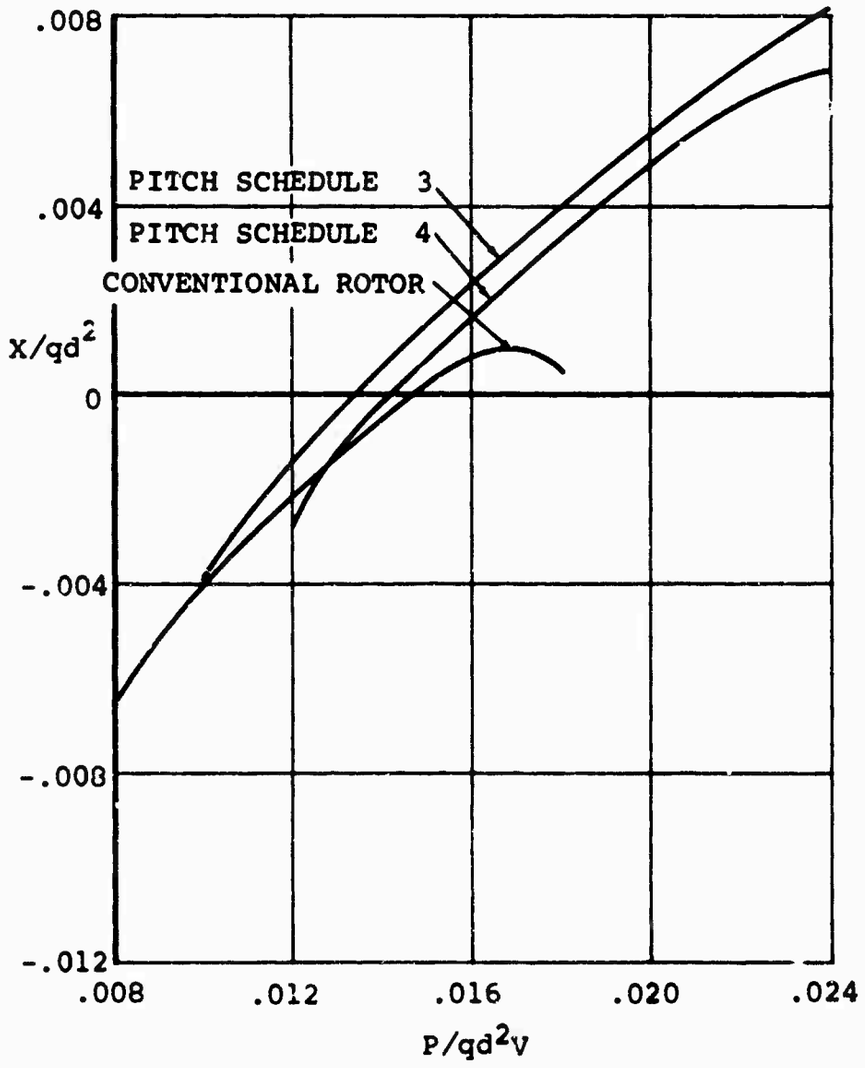

Figure 22. Propulsive Efficiency of Conventional and Segmented Rotors Where $\Delta\theta_{INBD} = 0°$, $\Delta\psi = 0°$, $L/qd^2 = 0.04$, $\mu' = 0.60$, $M(1)(90) = 0.36$.

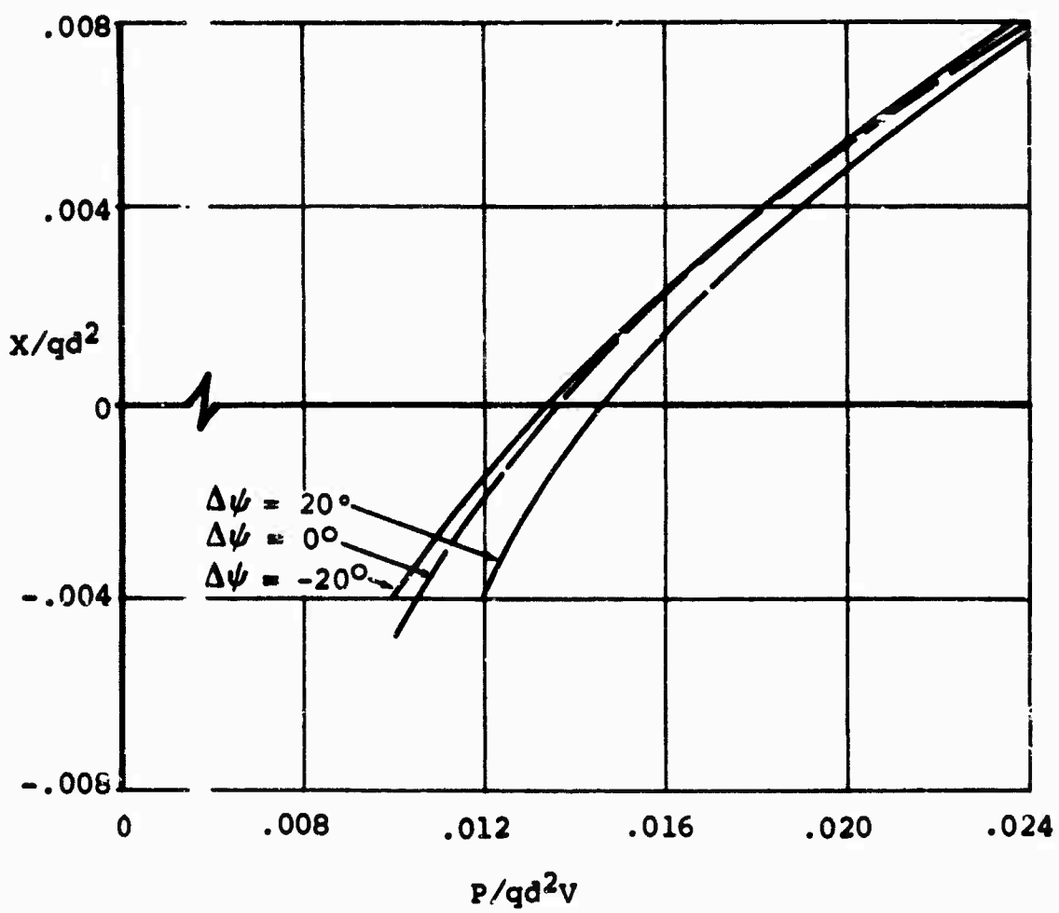

Figure 23. Effect on Propul ive Efficiency of Azimuth Phasing of Segmented Rotor Pitch Schedule 3 Where $\Delta\Theta_{INBD} = 0°$, $L/qd^2 = 0.04$, $\mu' = 0.60$, $M(1)(90) = 0.36$.

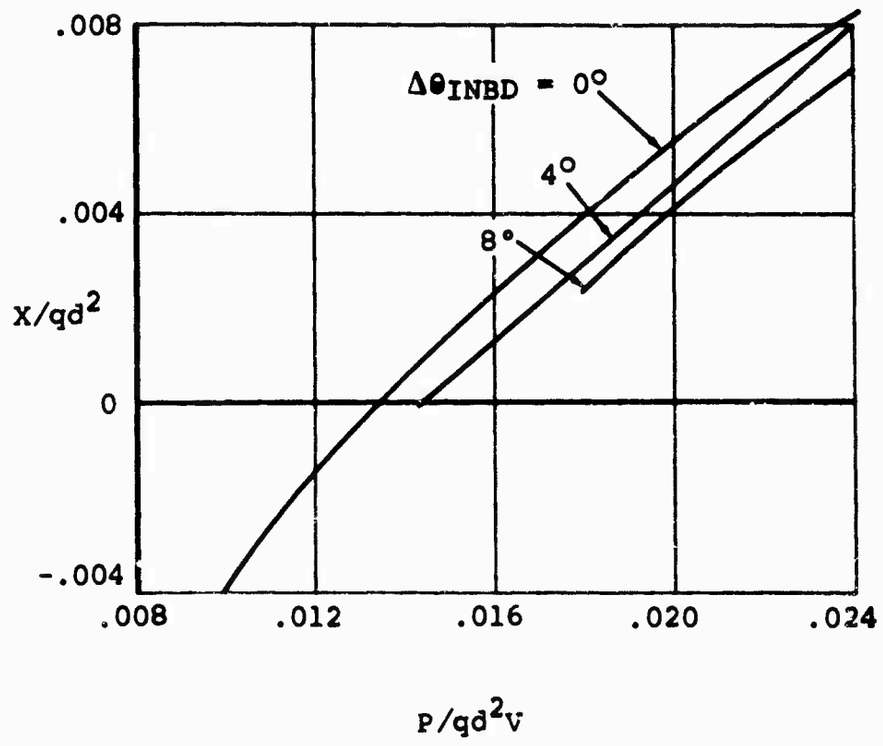

Figure 24. Effect on Propulsive Efficiency of Collective Pitch on Inboard Segment of Segmented Rotor Pitch Schedule 3 Where $\Delta\psi = 0°$, $L/qd^2 = 0.04$, $\mu' = 0.60$, $M_{(1)(90)} = 0.36$.

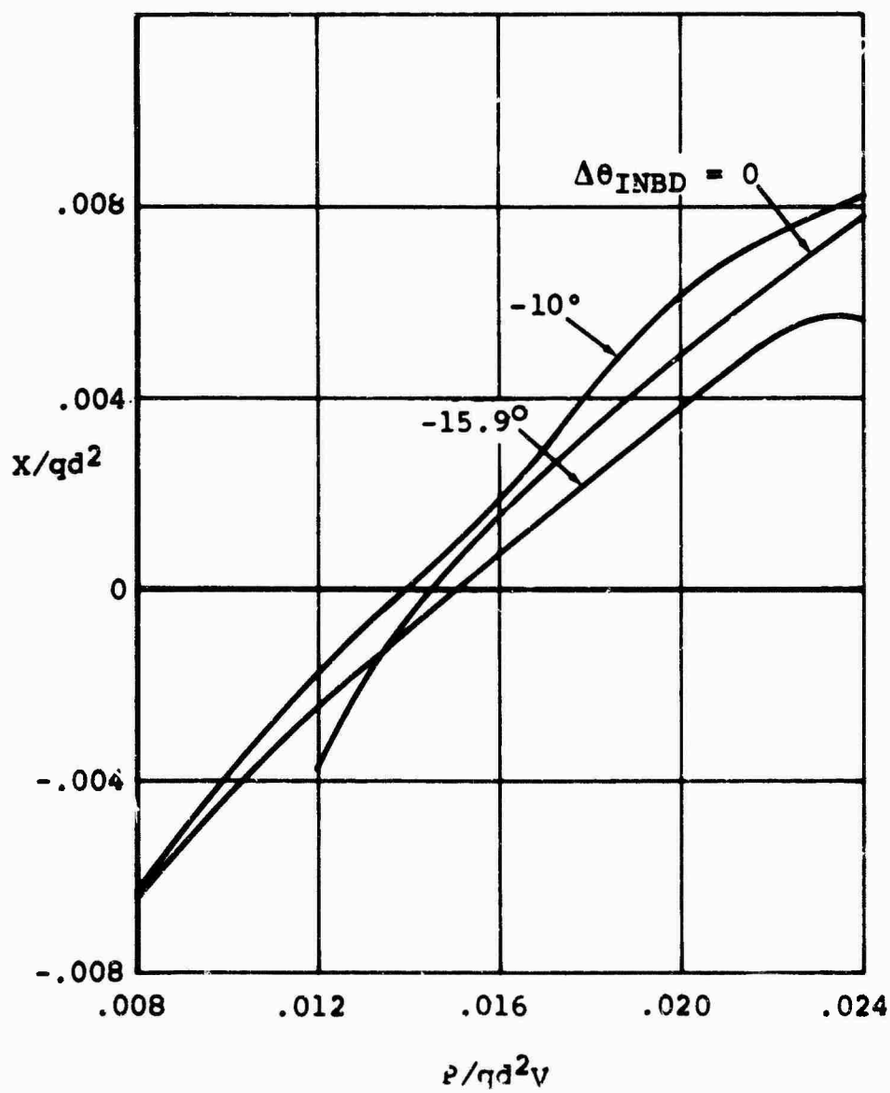

Figure 25. Effect on Propulsive Efficiency of Collective Pitch on Inboard Segment of Segmented Rotor Pitch Schedule 3 Where $\Delta\psi$ = 20°, L/qd^2 = 0.04, μ' = 0.60, M(1)(90) = 0.36.

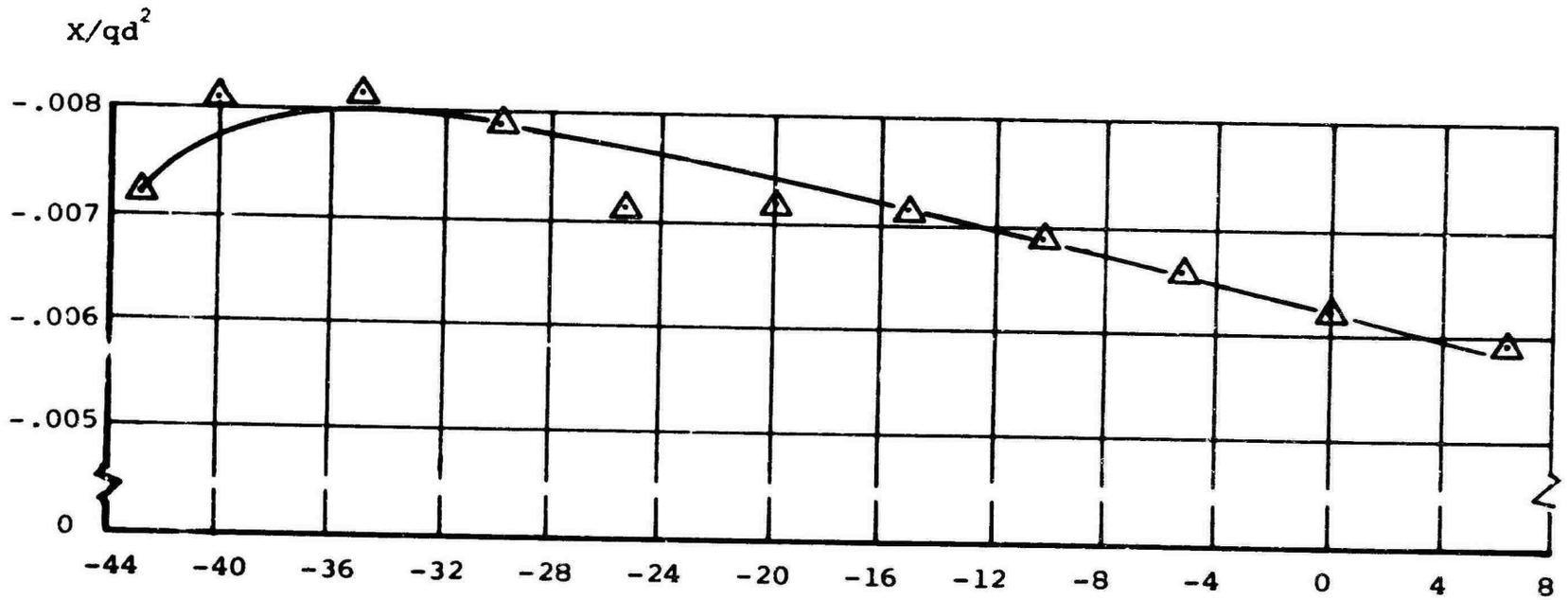

NOTE: L/qd^2 TARE = 0.002
P/qd^2V TARE = NEGLIGIBLE

Figure 26. Hub and Shank Tares for Segmented Rotor Where $\mu' = 0.60$, $M_{(1)(90)} = 0.36$.

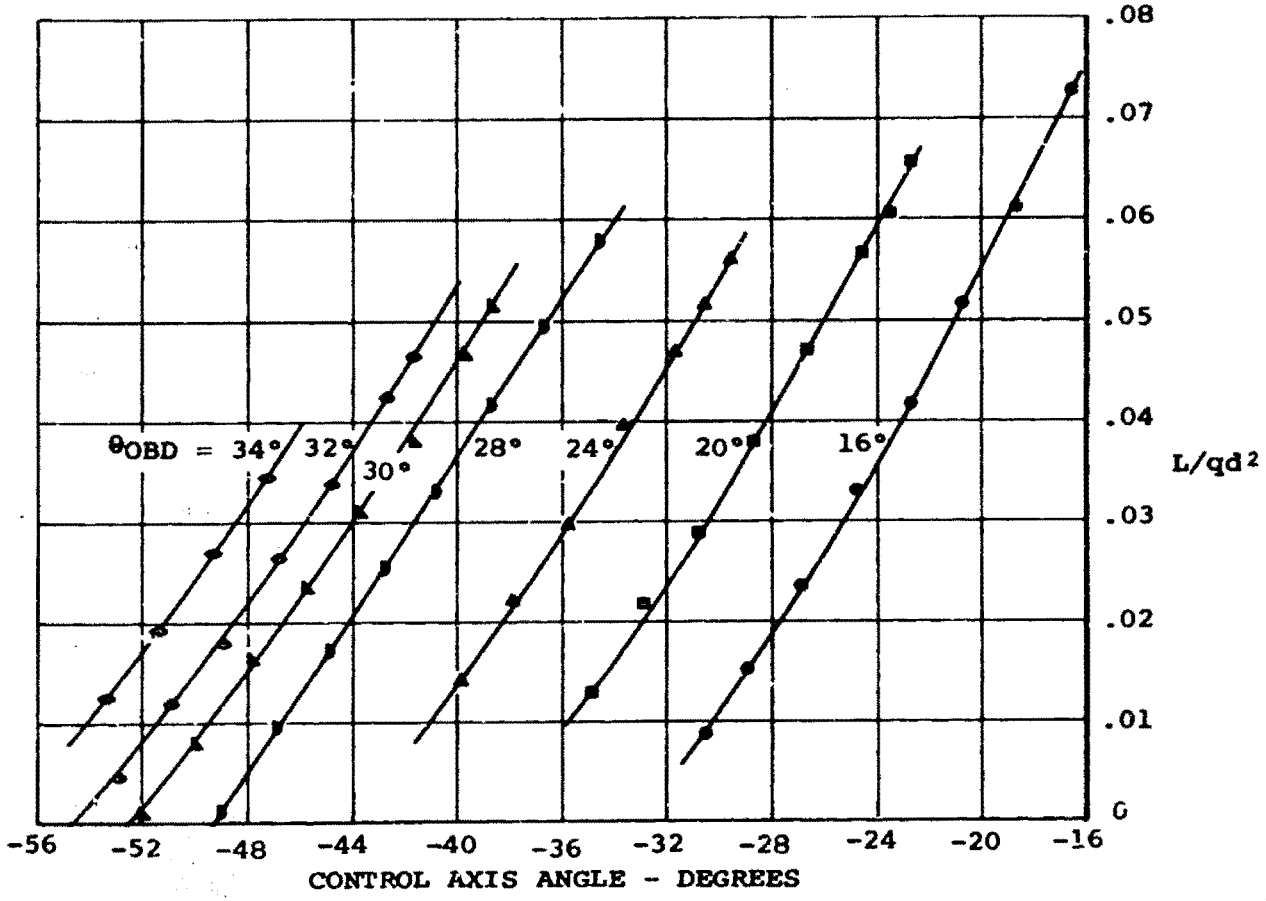

Figure 27. Segmented Rotor Nondimensionalized Lift for Pitch Schedule 3 Where $\Delta\theta_{INBD} = 0°$, $\Delta\psi = 0°$, $\mu' = 0.60$, $M(1)(90) = 0.36$, Hub and Shank Tares Removed.

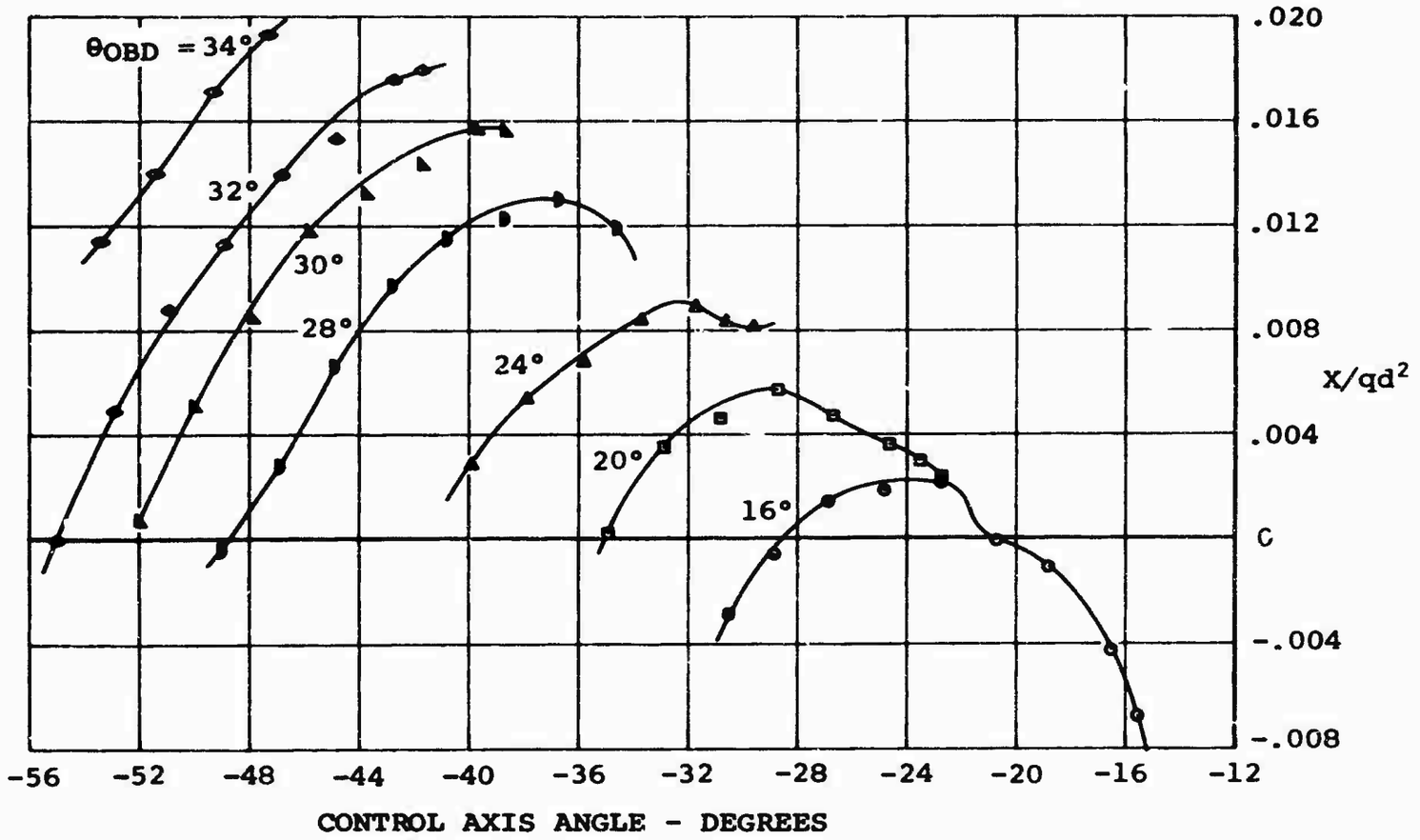

Figure 28. Segmented Rotor Nondimensionalized Propulsive Force for Pitch Schedule 3 Where $\Delta\theta_{INBD} = 0°$, $\Delta\psi = 0°$, $\mu' = 0.60$, $M_{(1)(90)} = 0.36$, Hub and Shank Tares Removed.

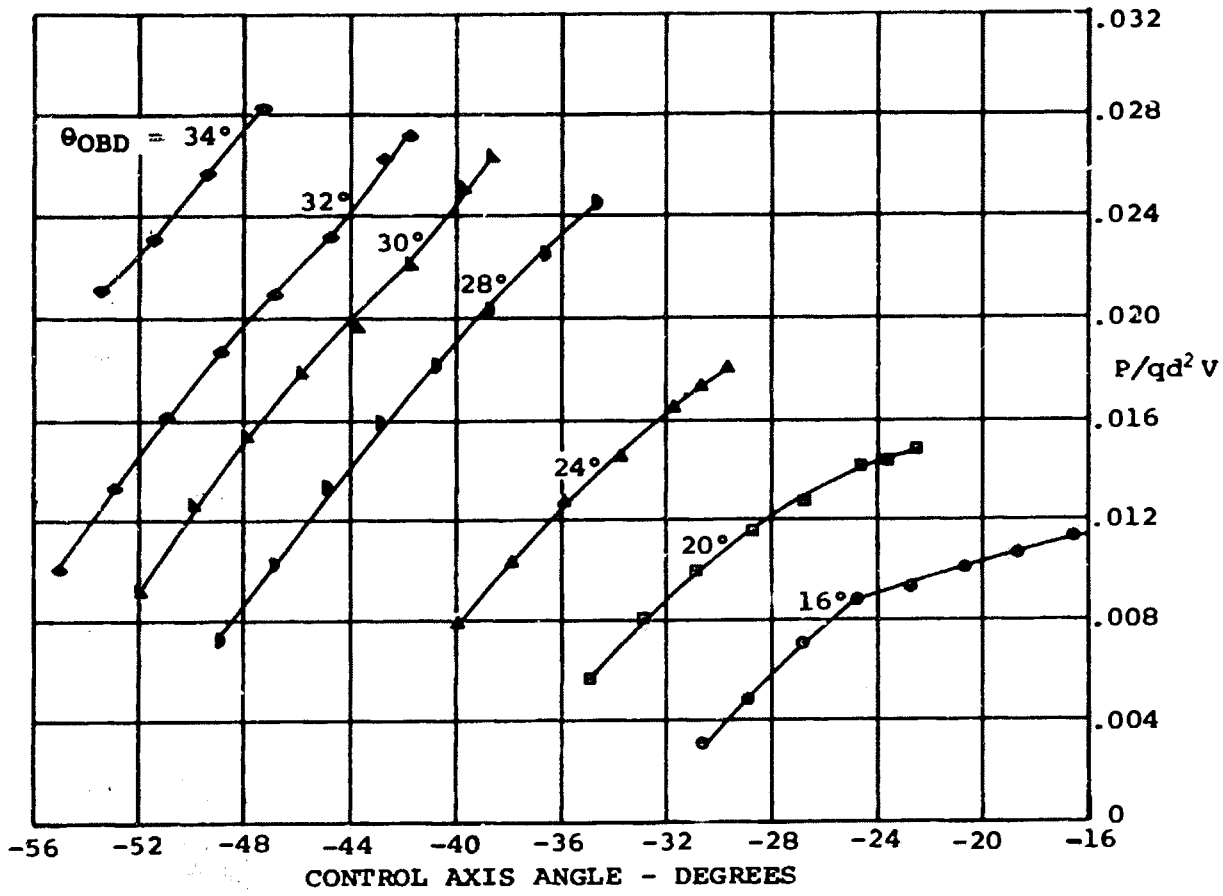

Figure 29. Segmented Rotor Nondimensionalized Power for Pitch Schedule 3 Where $\Delta\theta_{INBD} = 0°$, $\Delta\psi = 0°$, $\mu' = 0.60$, $M(1)(90) = 0.36$, Hub and Shank Tares Removed.

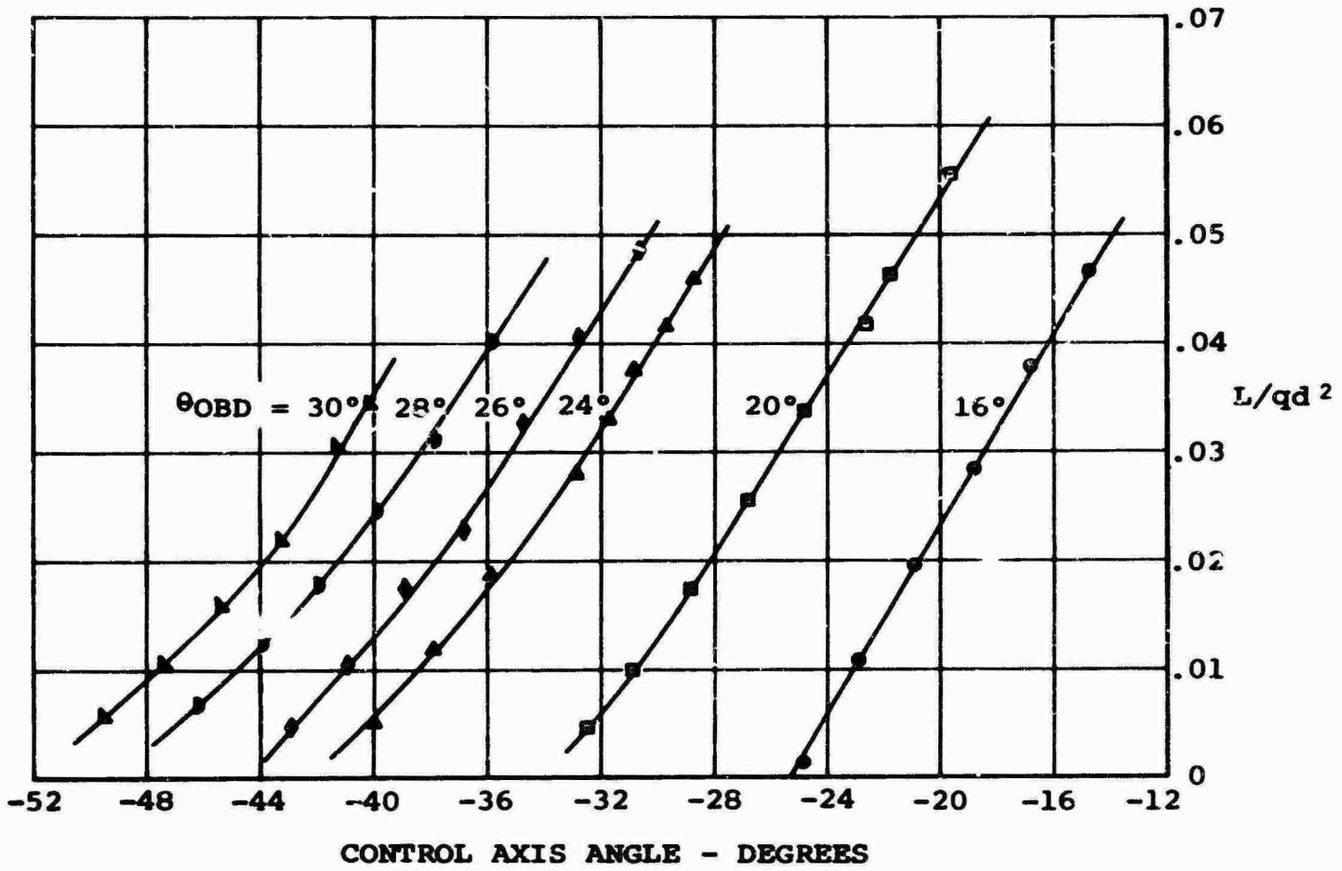

Figure 30. Conventional Rotor Nondimensionalized Lift ($\mu' = 0.60$, $M_{(1)(90)} = 0.36$, Hub and Shank Tares Removed).

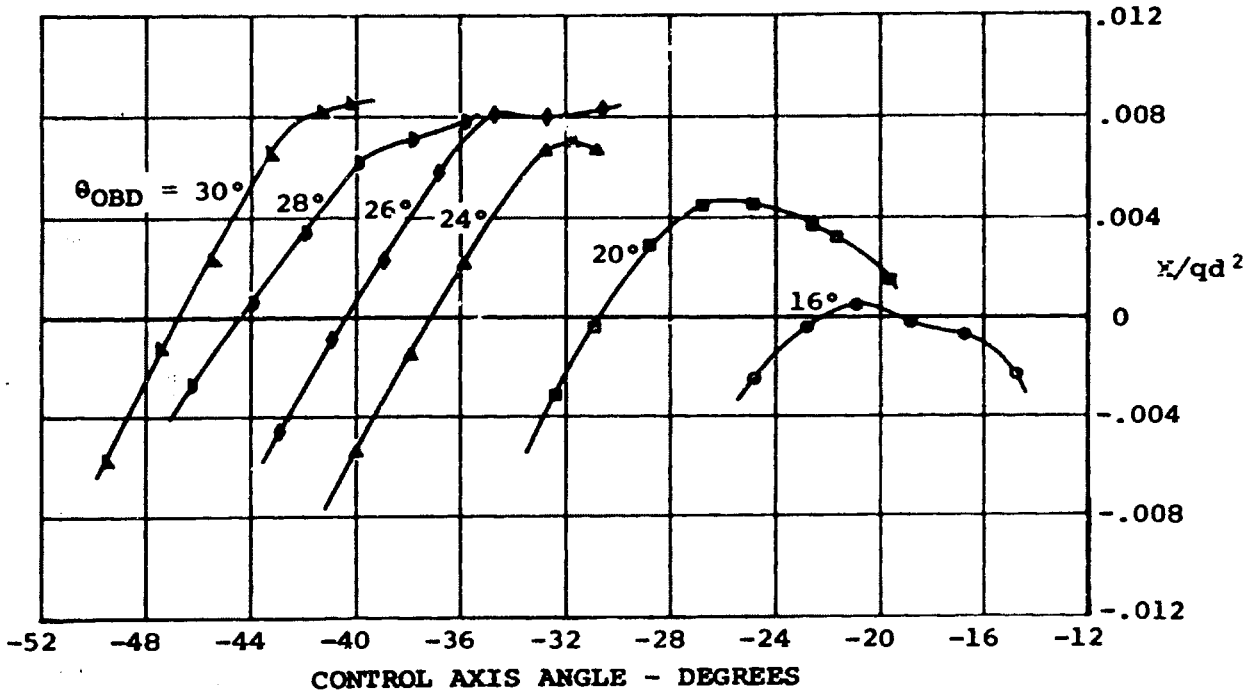

Figure 31. Conventional Rotor Nondimensionalized Propulsive Force ($\mu' = 0.60$, $M(1)(90) = 0.36$, Hub and Shank Tares Removed).

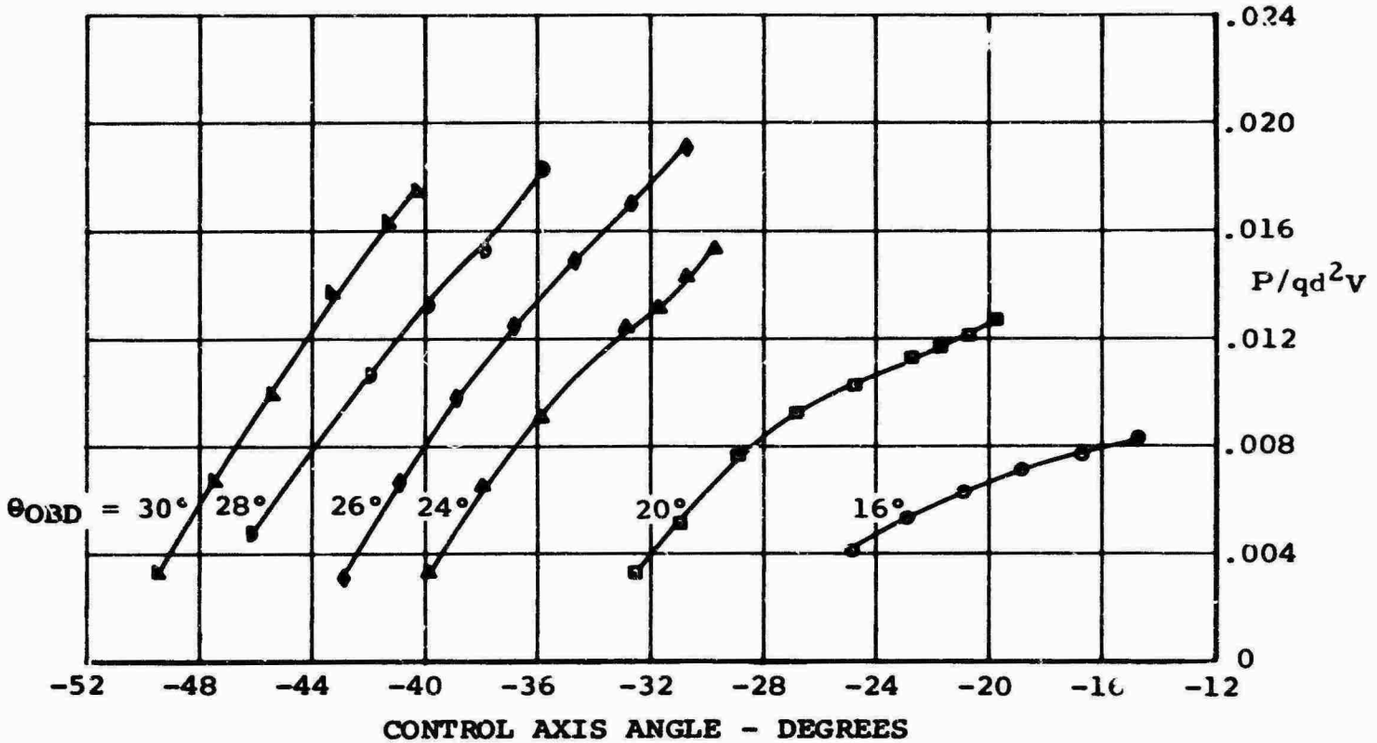

Figure 32. Conventional Rotor Nondimensionalized Power ($\mu' = 0.60$, $M_{(1)(90)} = 0.36$, Hub and Shank Tares Removed).

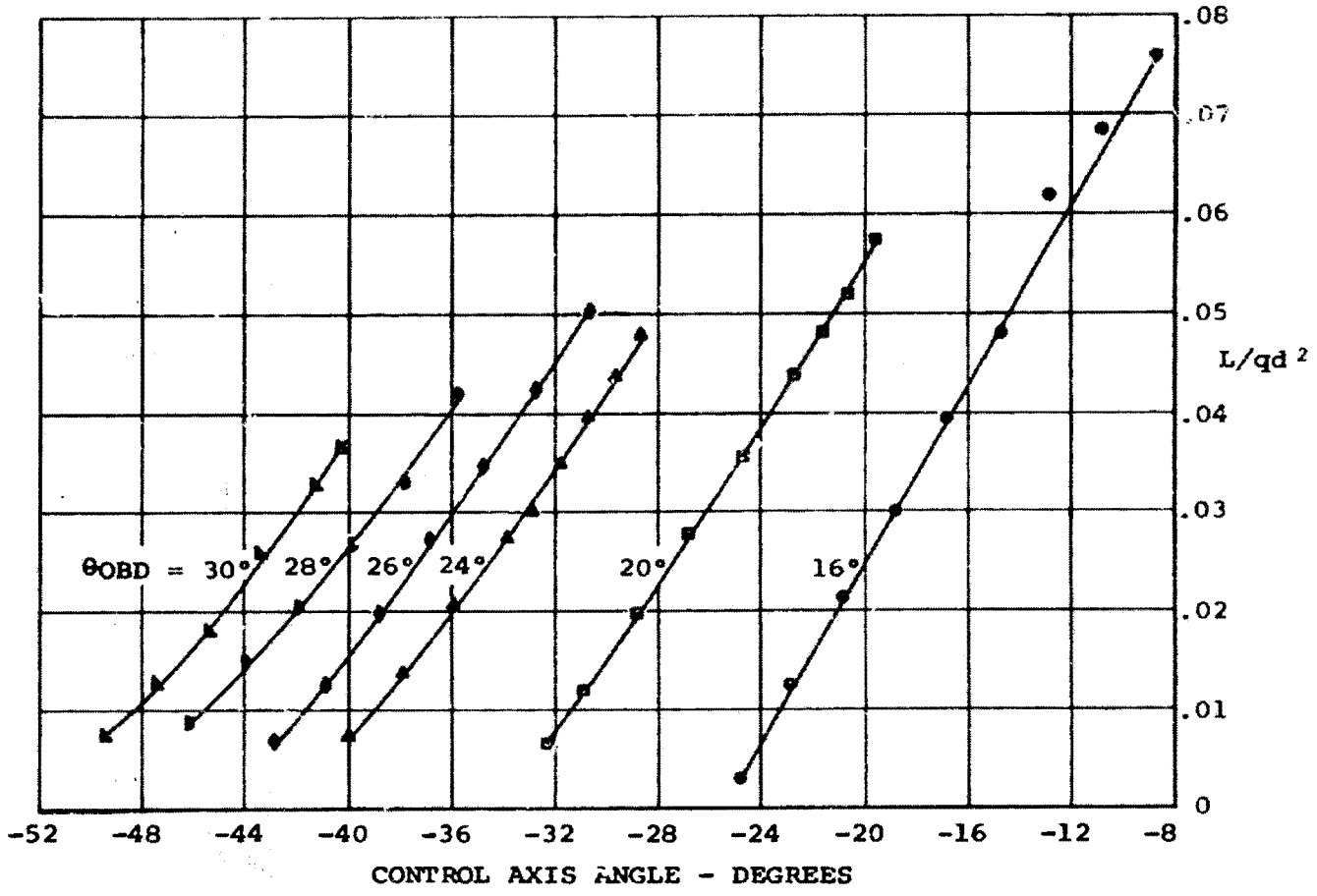

Figure 33. Conventional Rotor Nondimensionalized Lift ($\mu' = 0.60$, $M_{(1)(90)} = 0.36$).

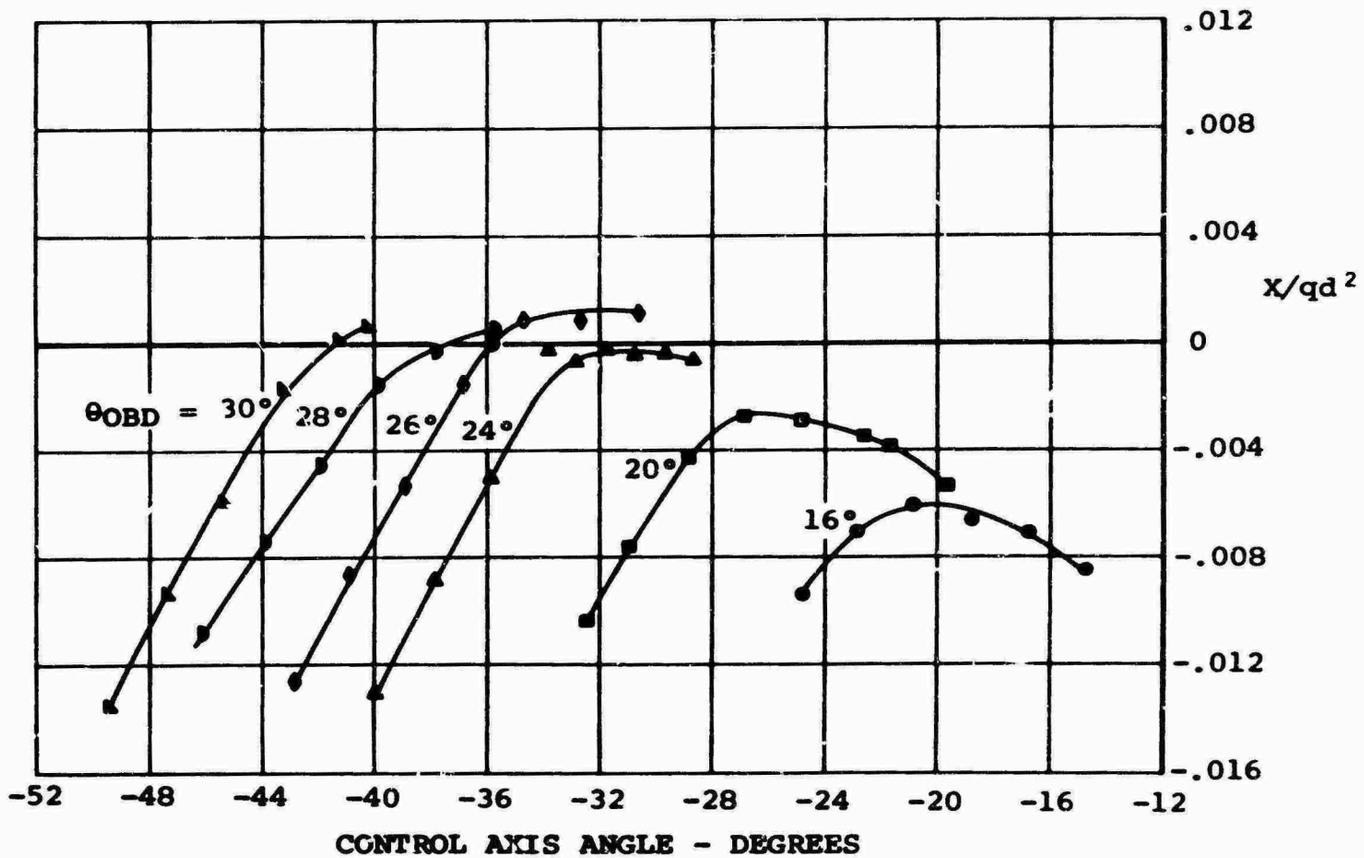

Figure 34. Conventional Rotor Nondimensionalized Propulsive Force ($\mu' = 0.60$, $M_{(1)(90)} = 0.36$).

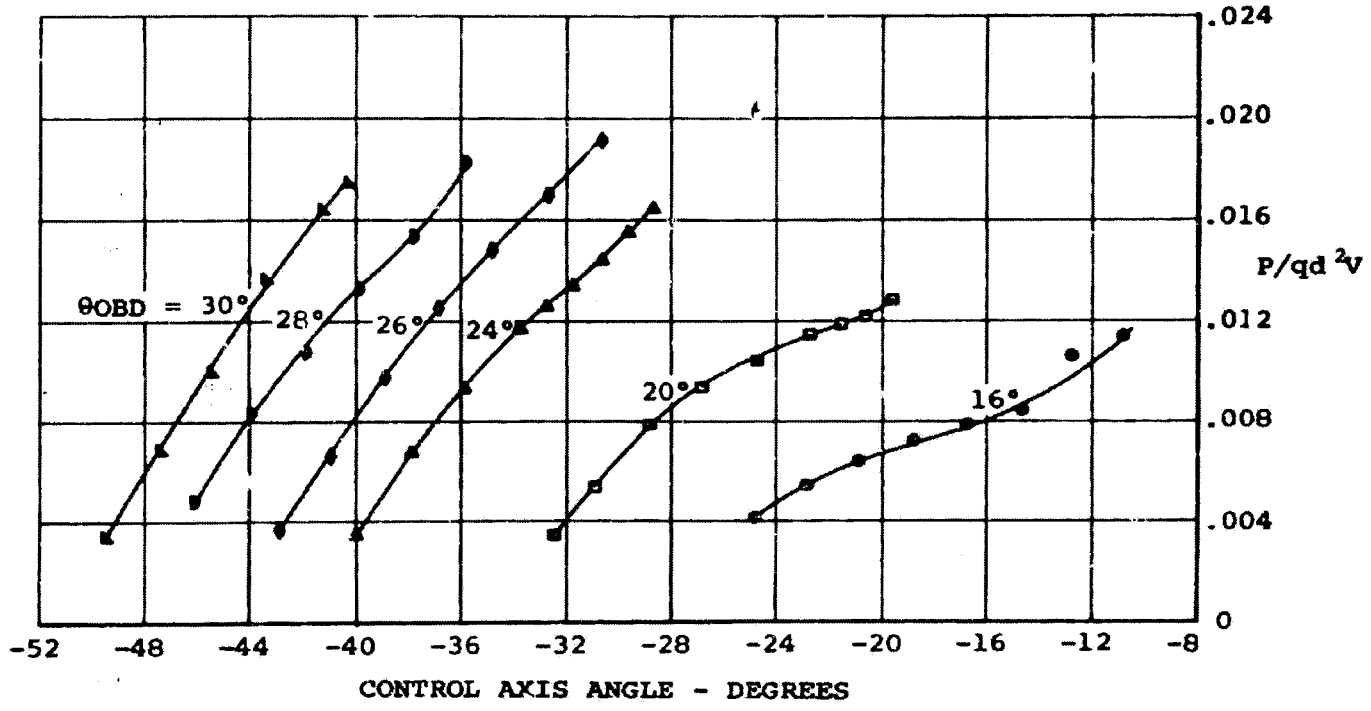

Figure 35. Conventional Rotor Nondimensionalized Power ($\mu' = 0.60$, $M_{(1)(90)} = 0.36$).

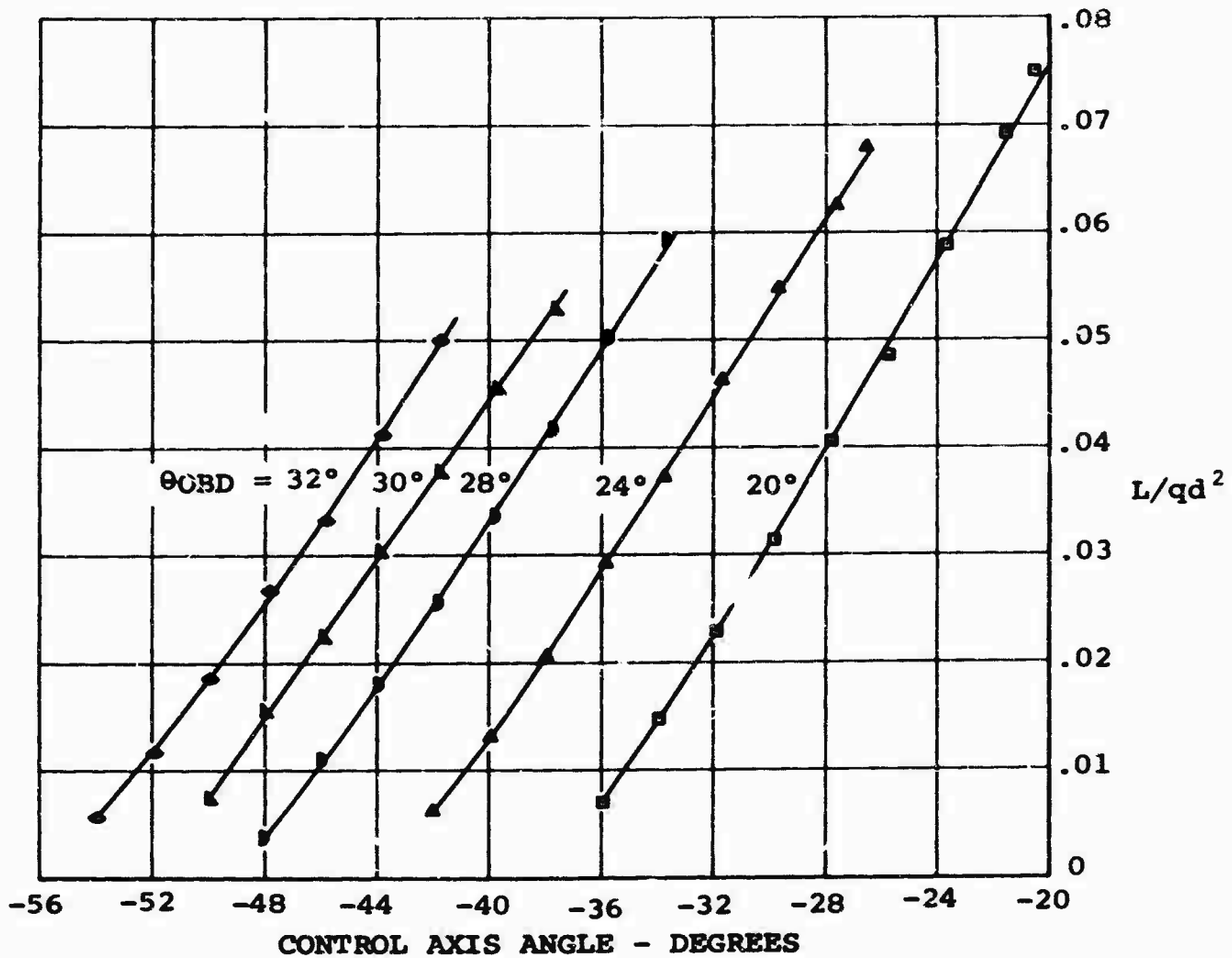

Figure 36. Segmented Rotor Nondimensionalized Lift for Pitch Schedule 4 Where $\Delta\theta_{INBD} = 0°$, $\Delta\psi = 0°$, $\mu' = 0.60$, $M_{(1)(90)} = 0.36$.

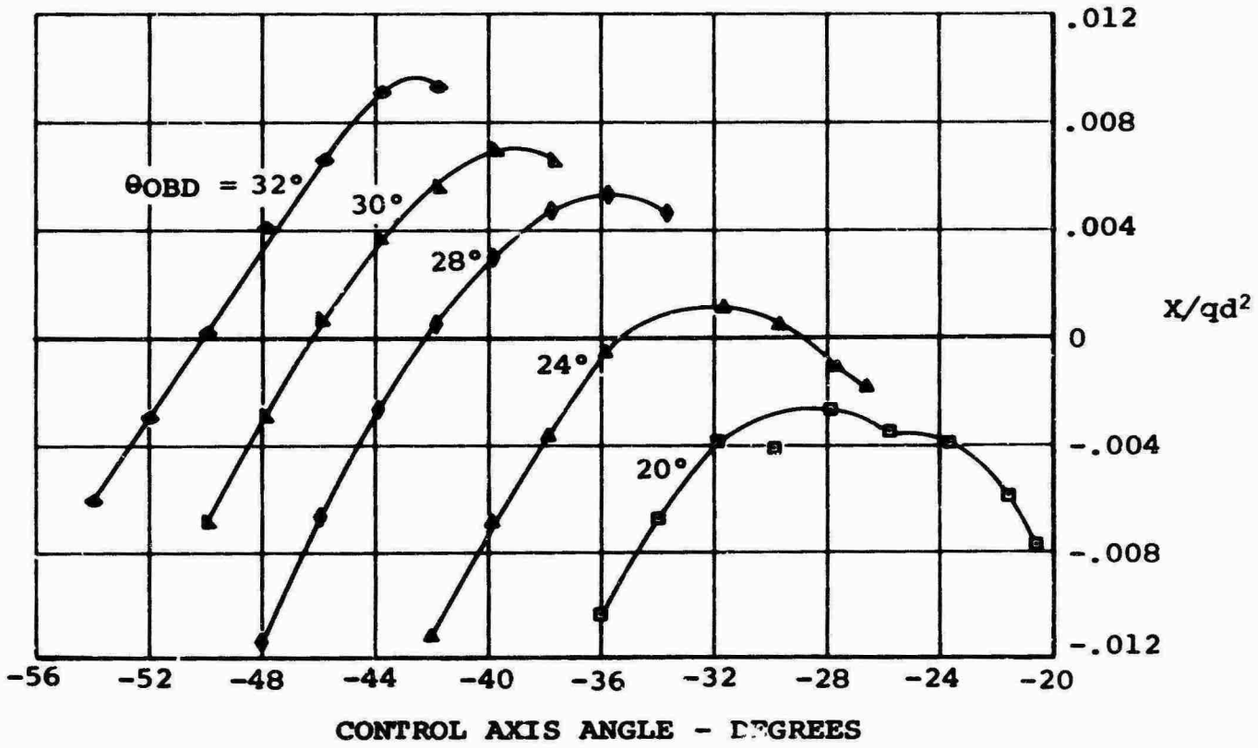

Figure 37. Segmented Rotor Nondimensionalized Propulsive Force for Pitch Schedule 4 Where $\Delta\theta_{INBD} = 0°$, $\Delta\psi = 0°$, $\mu' = 0.60$, $M_{(1)(90)} = 0.36$.

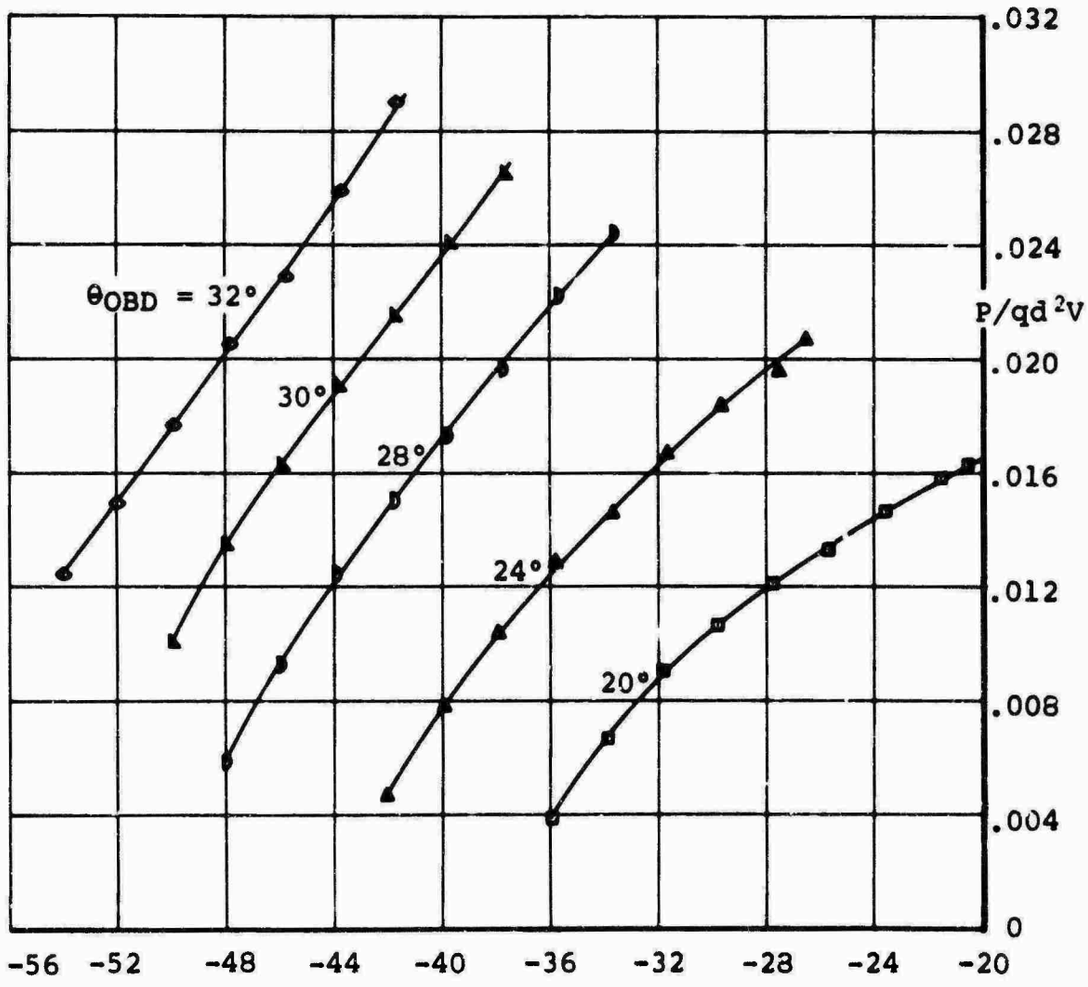

Figure 38. Segmented Rotor Nondimensionalized Power for Pitch Schedule 4 Where $\Delta\theta_{INBD} = 0°$, $\Delta\psi = 0°$, $\mu' = 0.60$, $M_{(1)(90)} = 0.36$.

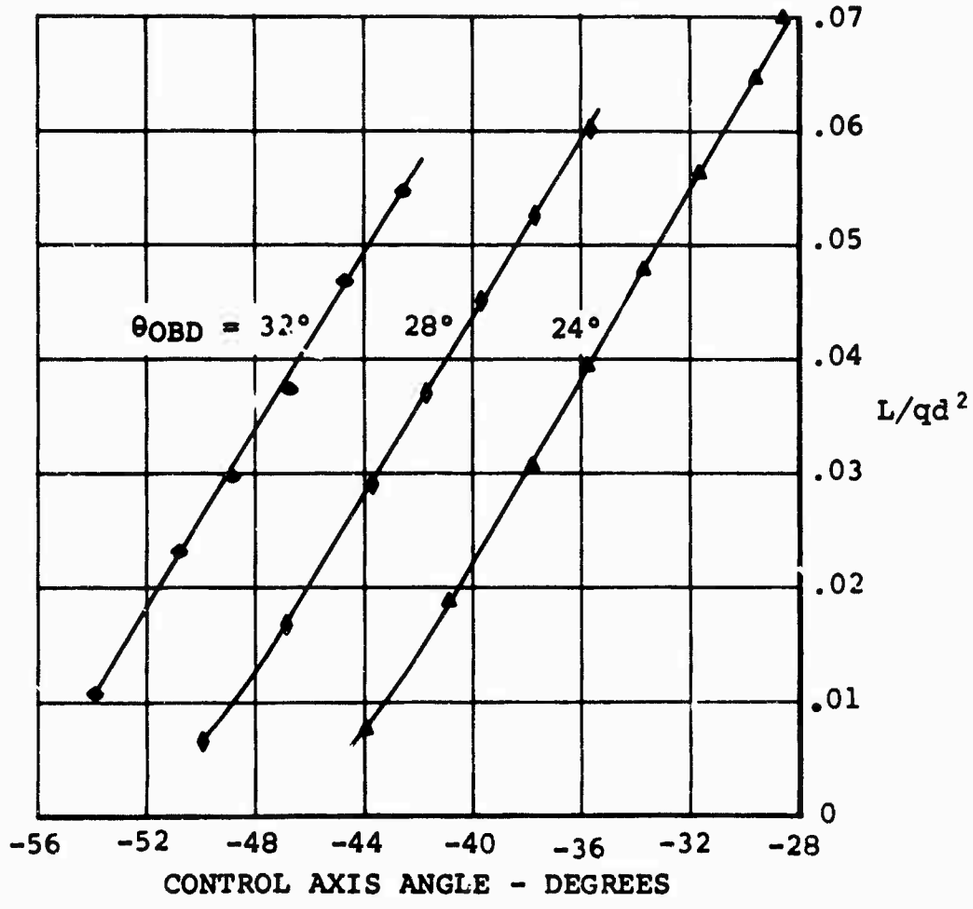

Figure 39. Segmented Rotor Nondimensionalized Lift for Pitch Schedule 3 Where $\Delta\theta_{INBD} = 4°$, $\Delta\psi = 0°$, $\mu' = 0.60$, $M_{(1)(90)} = 0.36$.

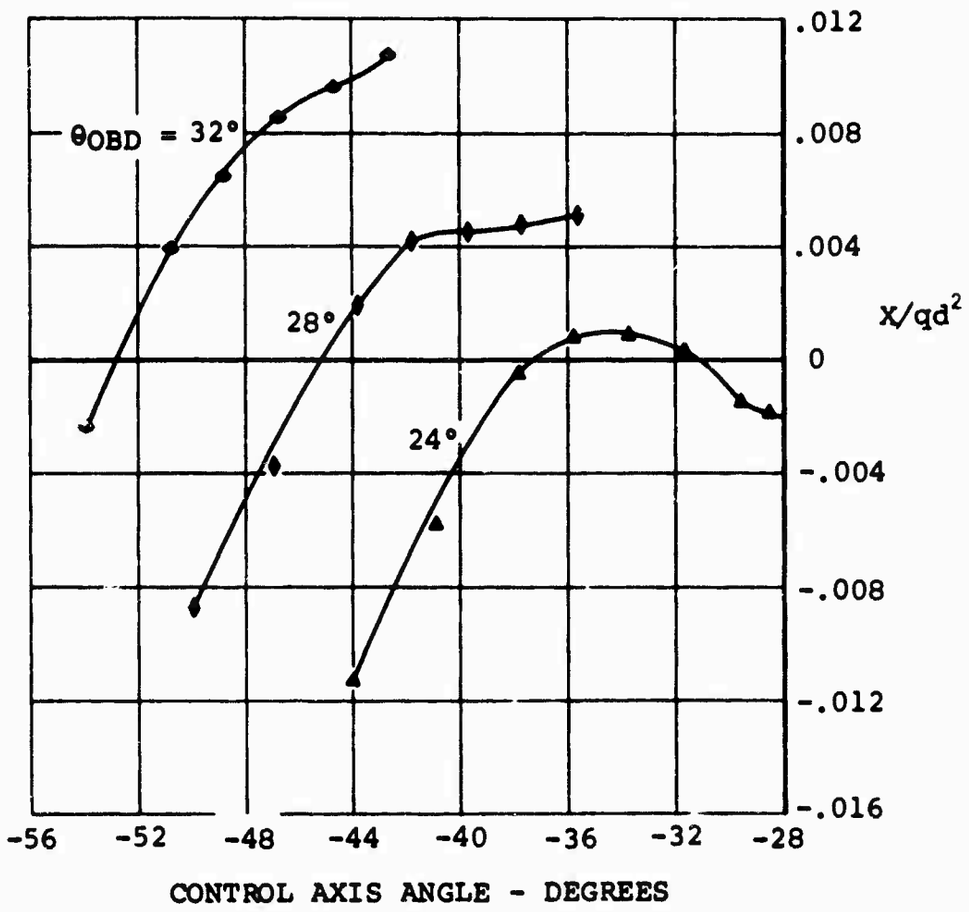

Figure 40. Segmented Rotor Nondimensionalized Propulsive Force for Pitch Schedule 3 Where $\theta_{INBD} = 4°$, $\Delta\psi = 0°$, $\mu' = 0.60$, $M_{(1)(90)} = 0.36$.

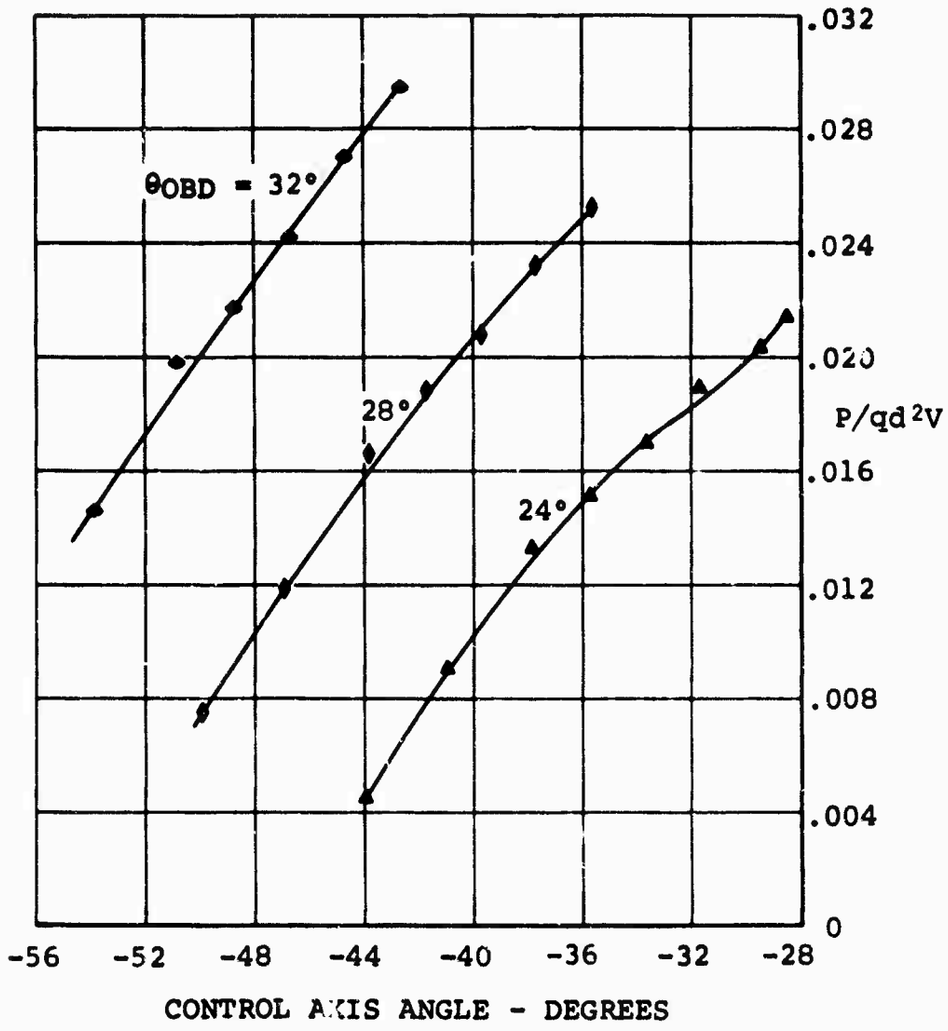

Figure 41. Segmented Rotor Nondimensionalized Power for Pitch Schedule 3 Where $\Delta\,\theta_{INBD} = 4°$, $\Delta\psi = 0°$, $\mu' = 0.60$, $M(1)(90) = 0.36$.

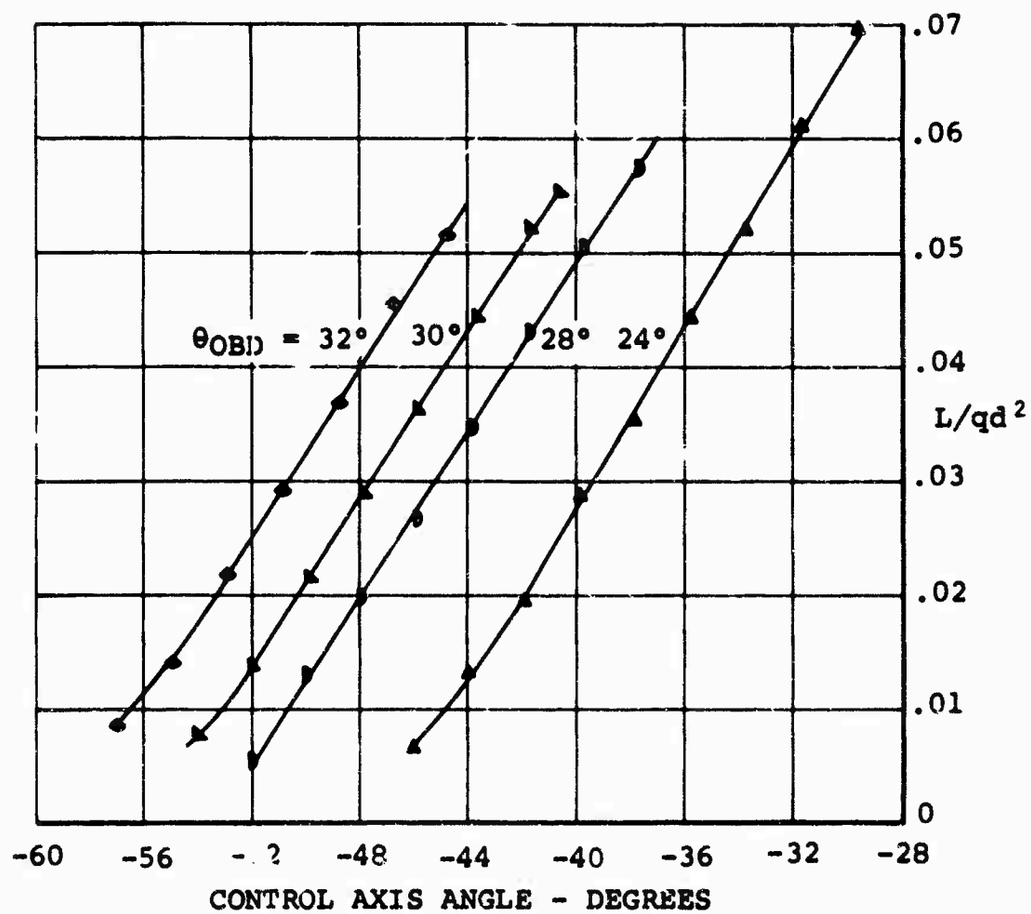

Figure 42. Segmented Rotor Nondimensionalized Lift for Pitch Schedule 3 Where $\Delta\theta_{INBD} = 8°$, $\Delta\psi = 0°$, $\mu' = 0.60$, $M_{(1)(90)} = 0.36$.

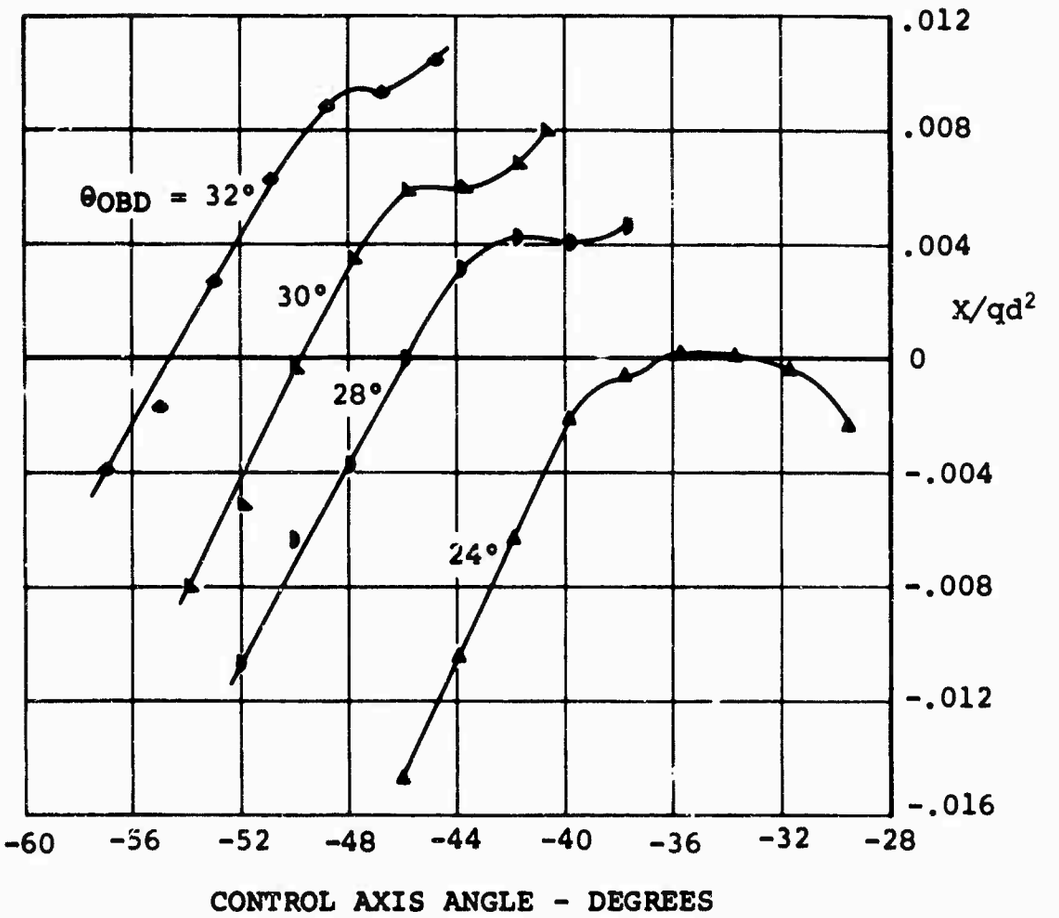

Figure 43. Segmented Rotor Nondimensionalized Propulsive Force for Pitch Schedule 3 Where $\Delta\theta_{INBD} = 8°$, $\Delta\psi = 0°$, $\mu' = 0.60$, $M(1)(90) = 0.36$.

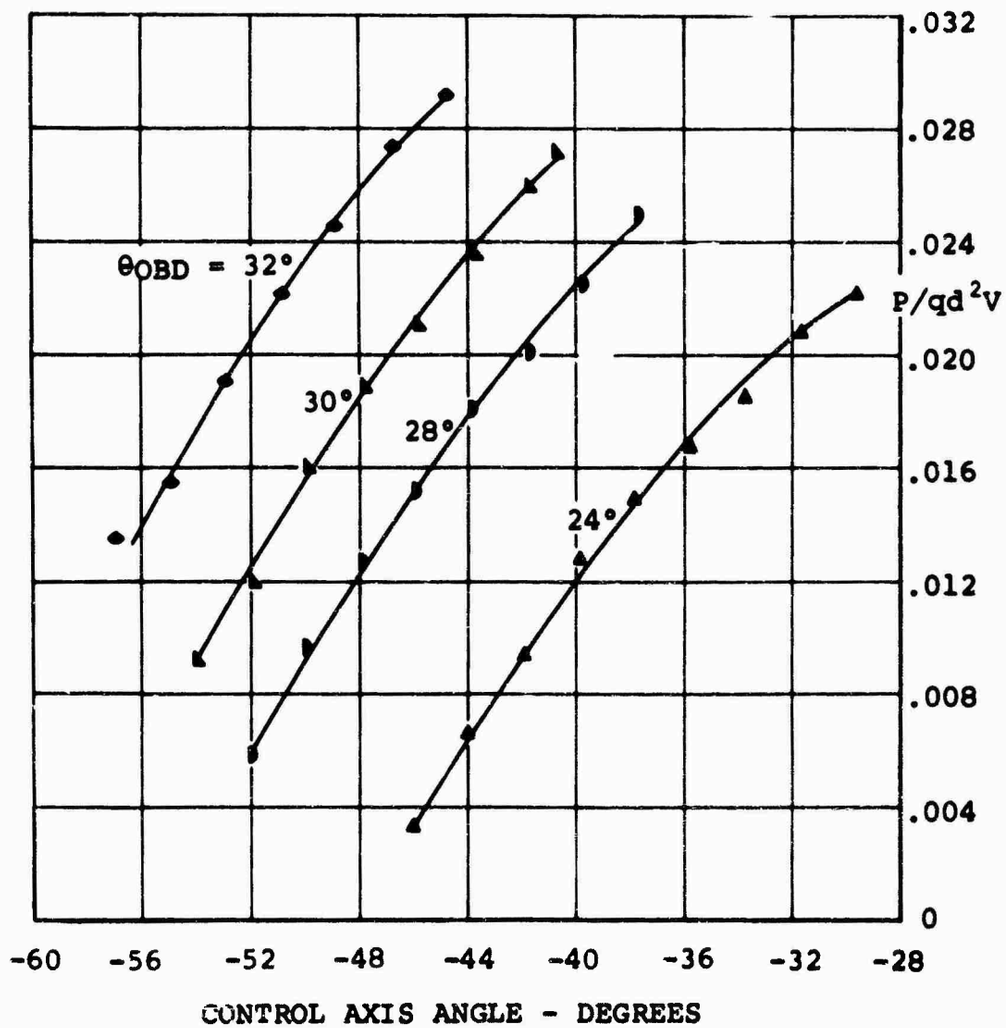

Figure 44. Segmented Rotor Nondimensionalized Power for Pitch Schedule 3 Where $\Delta\theta_{INBD} = 8°$, $\Delta\psi = 0°$, $\mu' = 0.60$, $M_{(1)(90)} = 0.36$.

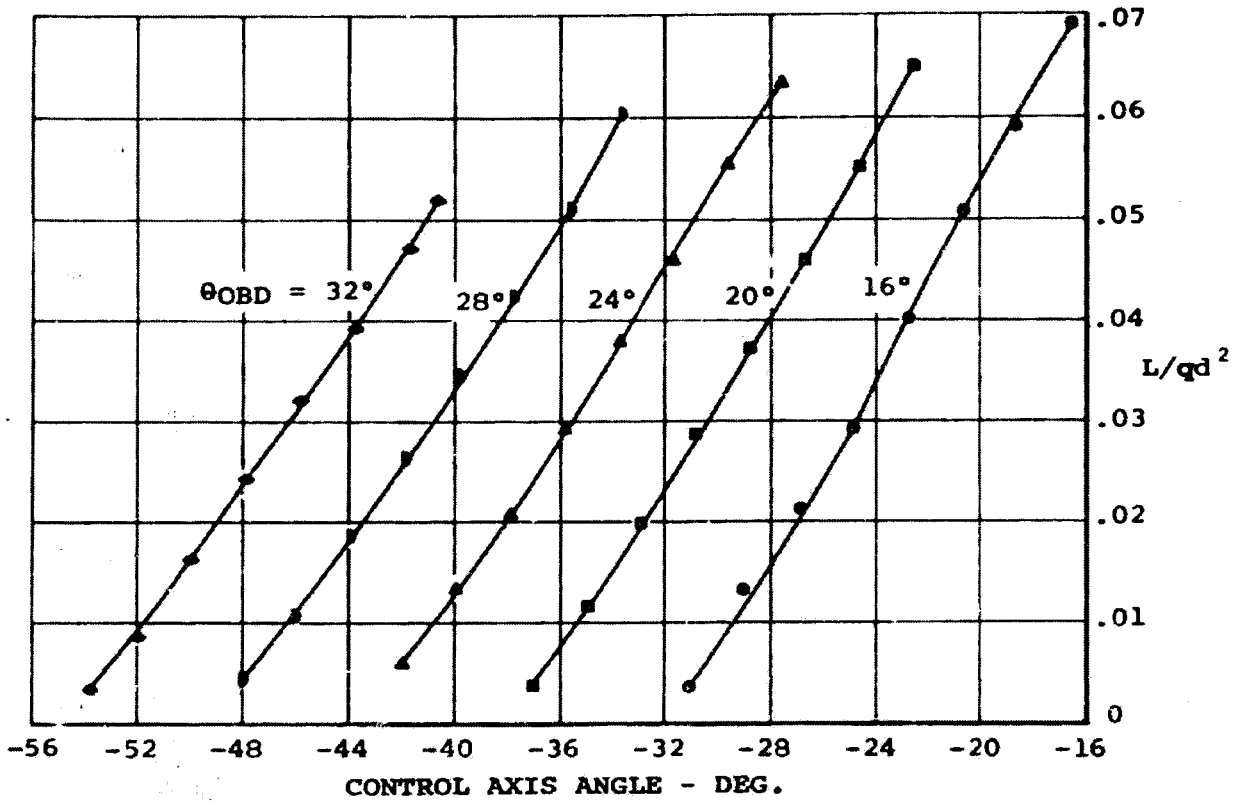

Figure 45. Segmented Rotor Nondimensionalized Lift for Pitch Schedule 3 Where $\Delta\theta_{INBD} = 0°$, $\Delta\psi = -20°$, $\mu' = 0.60$, $M(1)(90) = 0.36$.

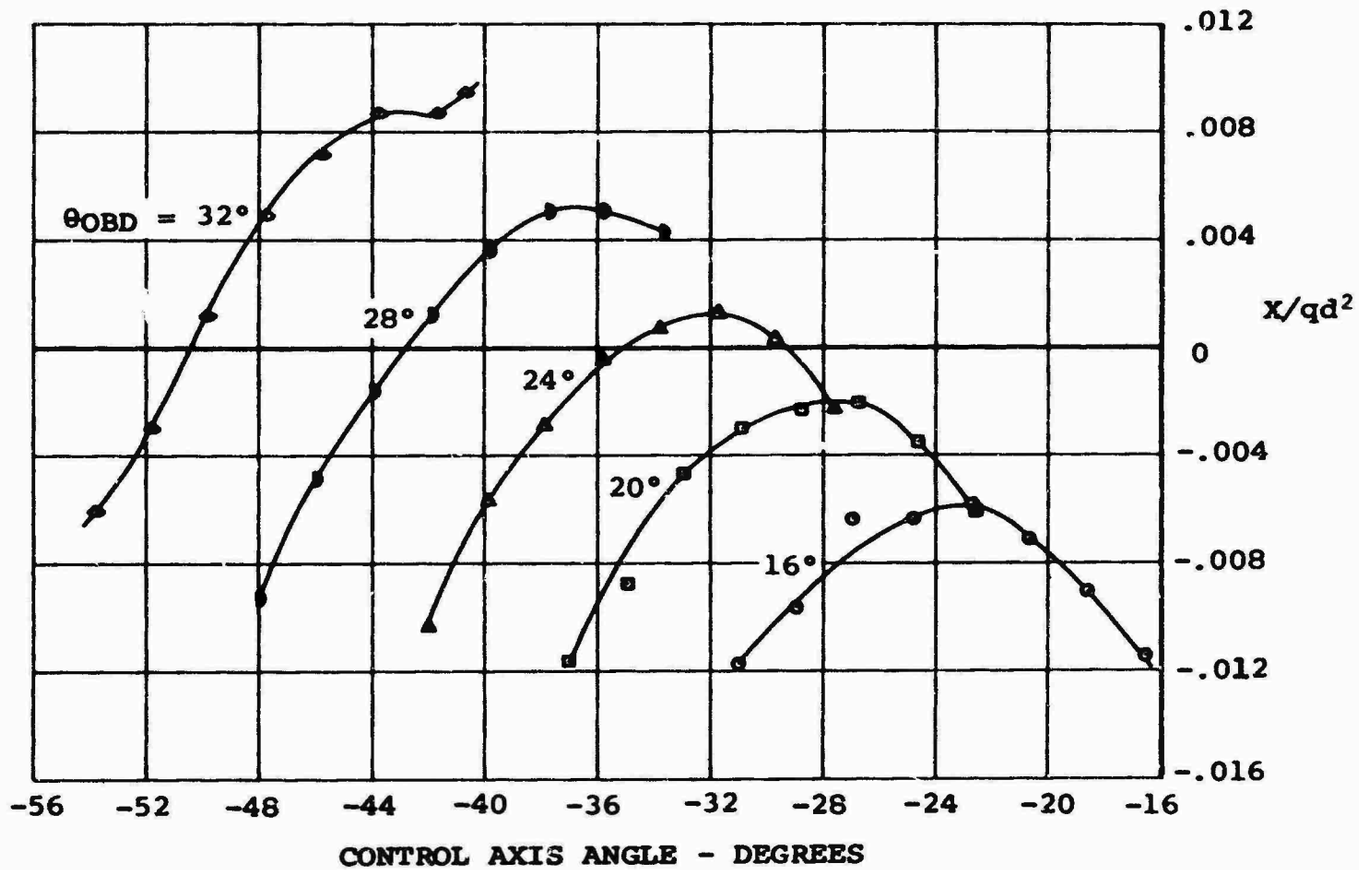

Figure 46. Segmented Rotor Nondimensionalized Propulsive Force for Pitch Schedule 3 Where $\Delta\theta_{INBD} = 0°$, $\Delta\psi = -20°$, $\mu' = 0.60$, $M_{(1)(90)} = 0.36$.

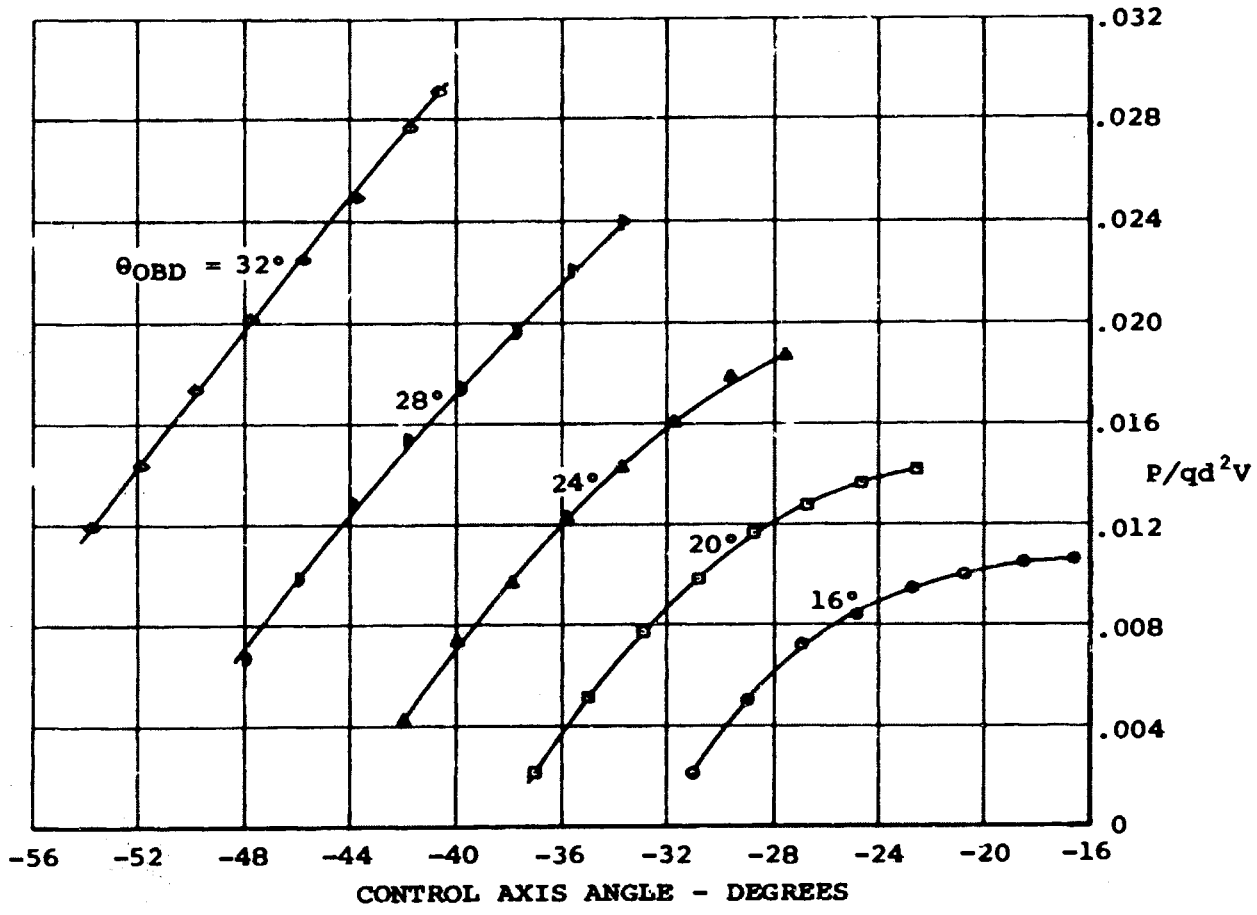

Figure 47. Segmented Rotor Nondimensionalized Power for Pitch Schedule 3 Where $\Delta\theta_{INBD} = 0°$, $\Delta\psi = -20°$, $\mu' = 0.60$, $M_{(1)(90)} = 0.36$.

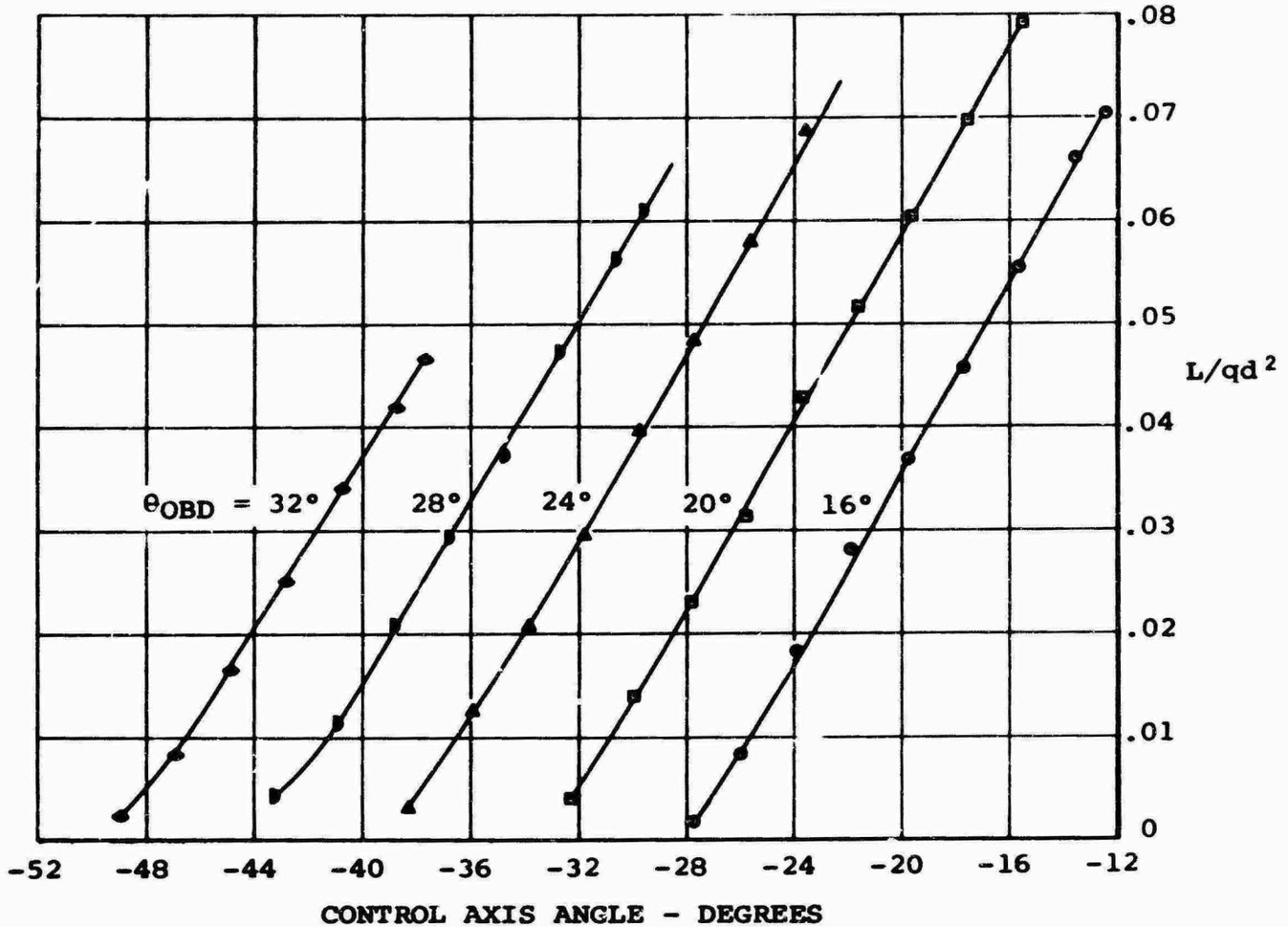

Figure 48. Segmented Rotor Nondimensionalized Lift for Pitch Schedule 3 Where $\Delta\theta_{INBD} = -15.9°$, $\Delta\psi = 20°$, $\mu' = 0.60$, $M(1)(90) = 0.36$.

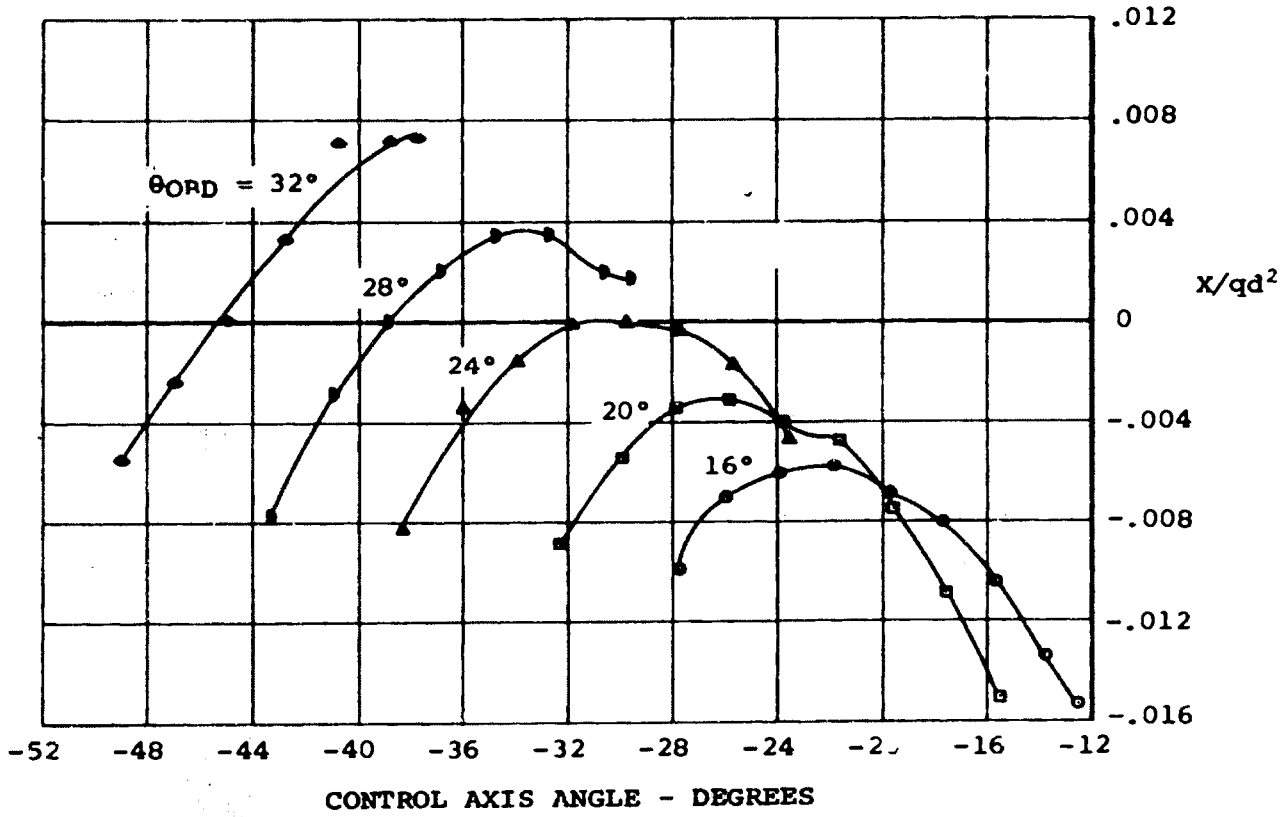

Figure 49. Segmented Rotor Nondimensionalized Propulsive Force for Pitch Schedule 3 Where $\Delta\theta_{INBD}$ = -15.9°, $\Delta\psi$ = 20°, μ' = 0.60, M(1)(90) = 0.36.

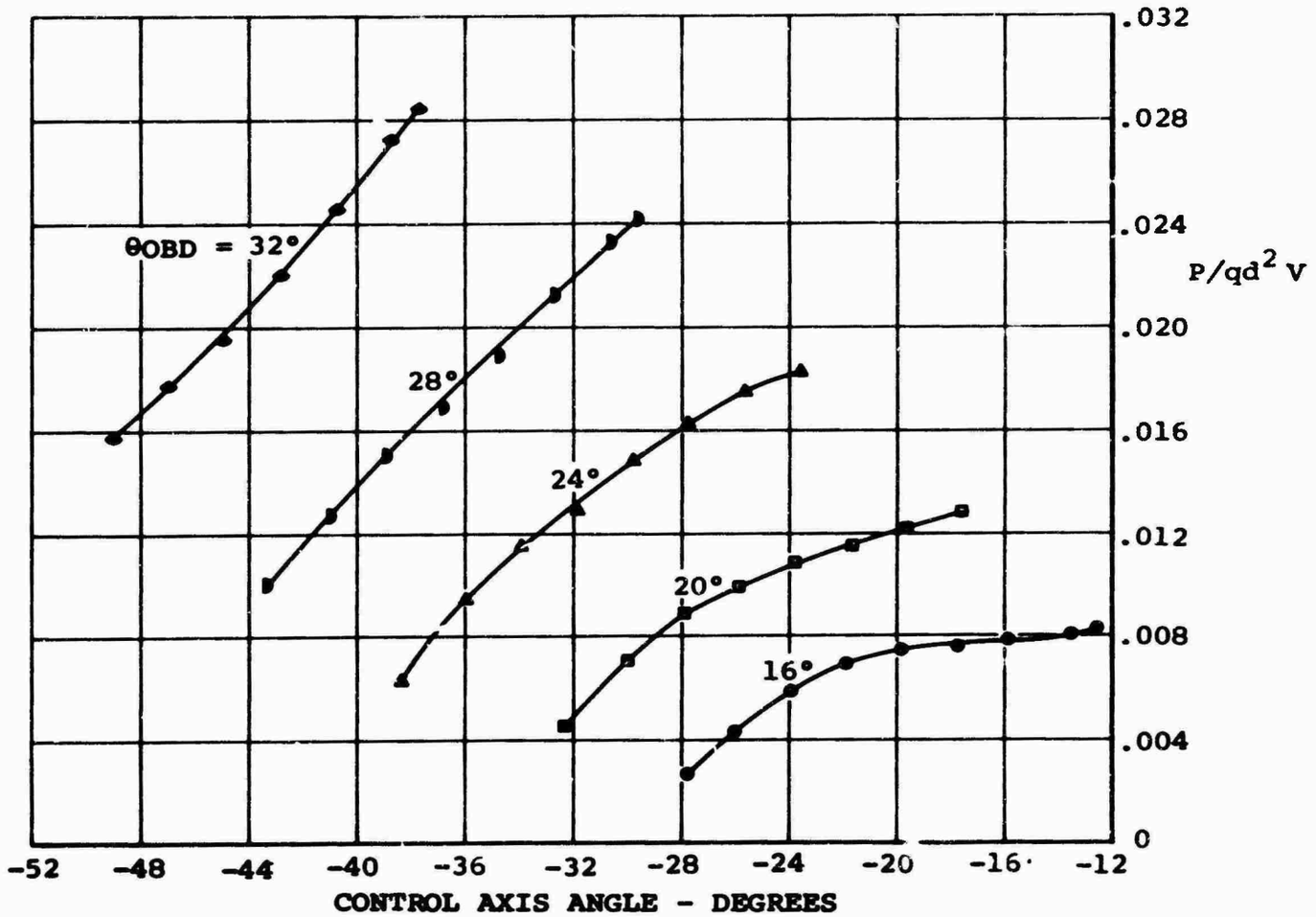

Figure 50. Segmented Rotor Nondimensionalized Power for Pitch Schedule 3 Where $\Delta\theta_{INBD} = -15.9°$, $\Delta\psi = 20°$, $\mu' = 0.60$, $M(1)(90) = 0.36$.

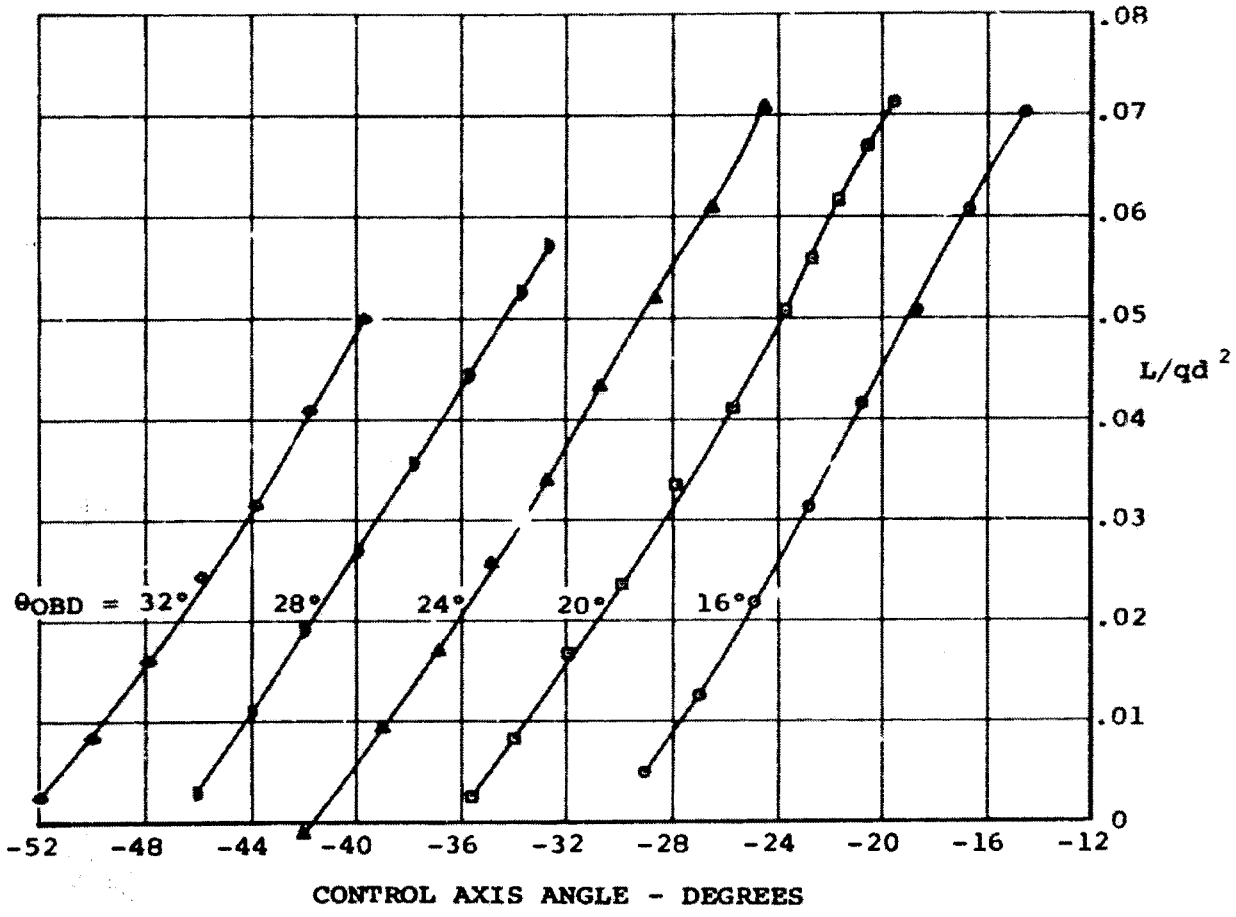

Figure 51. Segmented Rotor Nondimensionalized Lift for Pitch Schedule 3 Where $\Delta\theta_{INBD} = -10°$, $\Delta\psi = 20°$, $\mu' = 0.60$, $M(1)(90) = 0.36$.

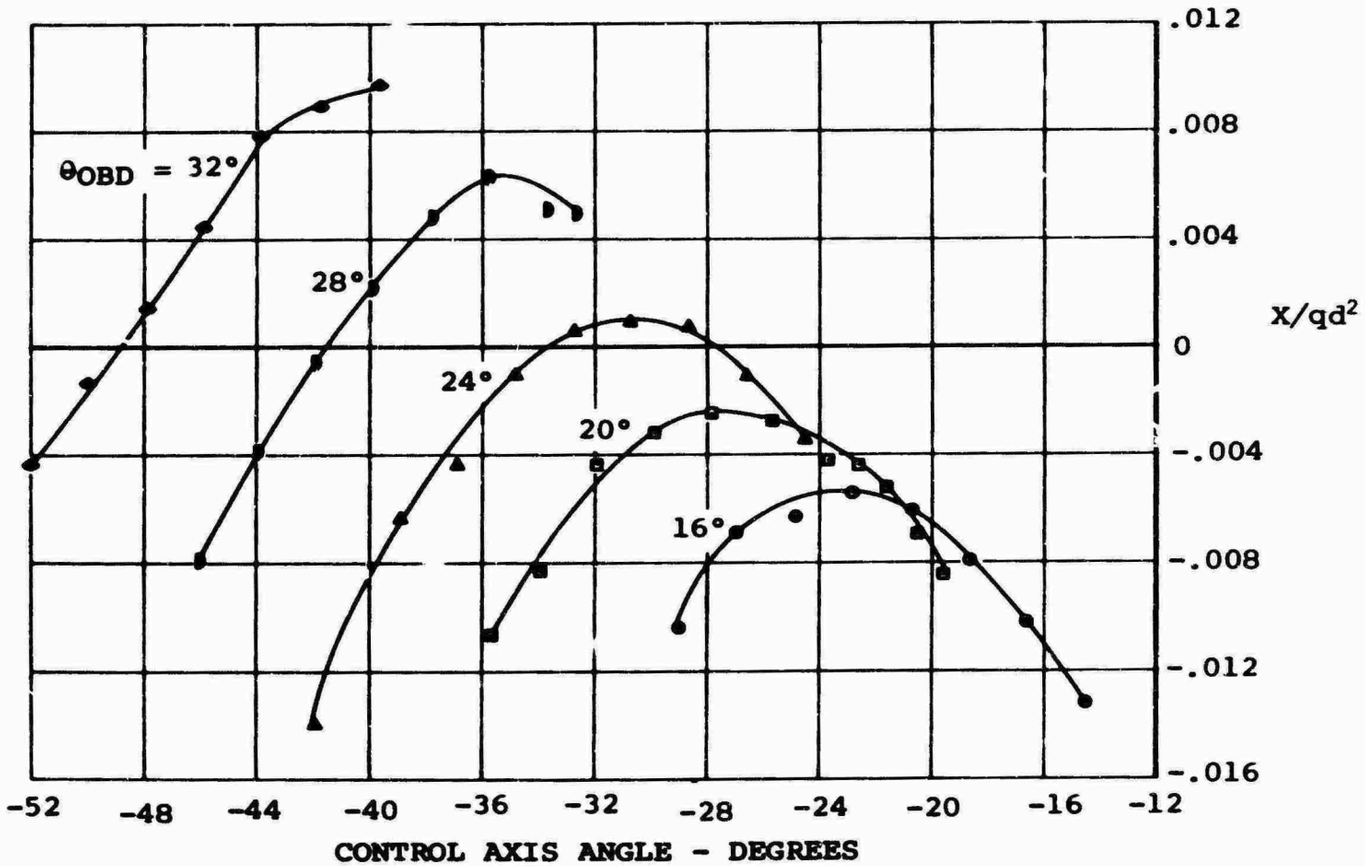

Figure 52. Segmented Rotor Nondimensionalized Propulsive Force for Pitch Schedule 3 Where $\Delta\theta_{INBD} = -10°$, $\Delta\psi = 20°$, $\mu' = 0.60$, $M(1)(90) = 0.36$.

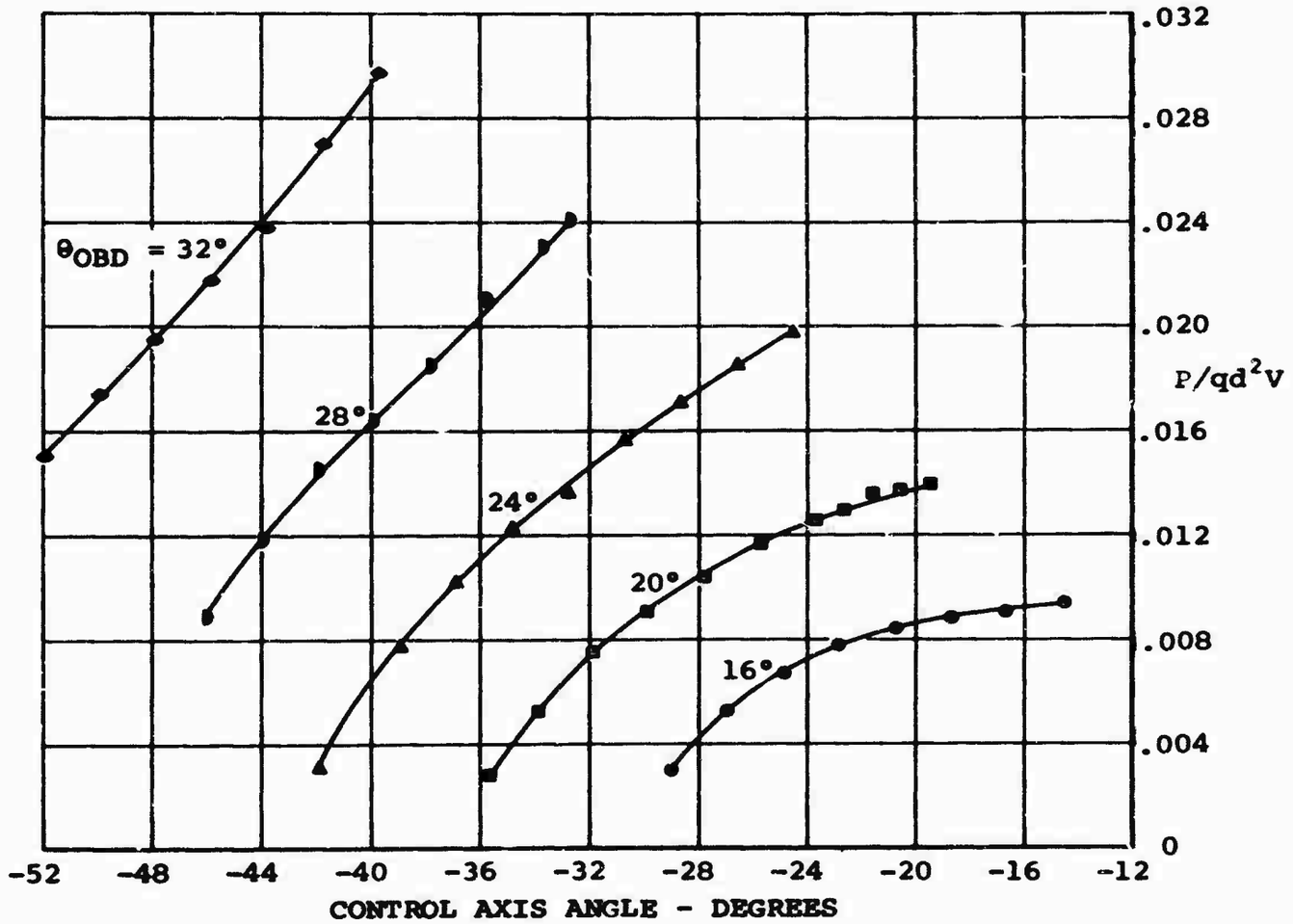

Figure 53. Segmented Rotor Nondimensionalized Power for Pitch Schedule 3 Where $\Delta\theta_{INBD} = -10°$, $\Delta\psi = 20°$, $\mu' = 0.60$, $M(1)(90) = 0.36$.

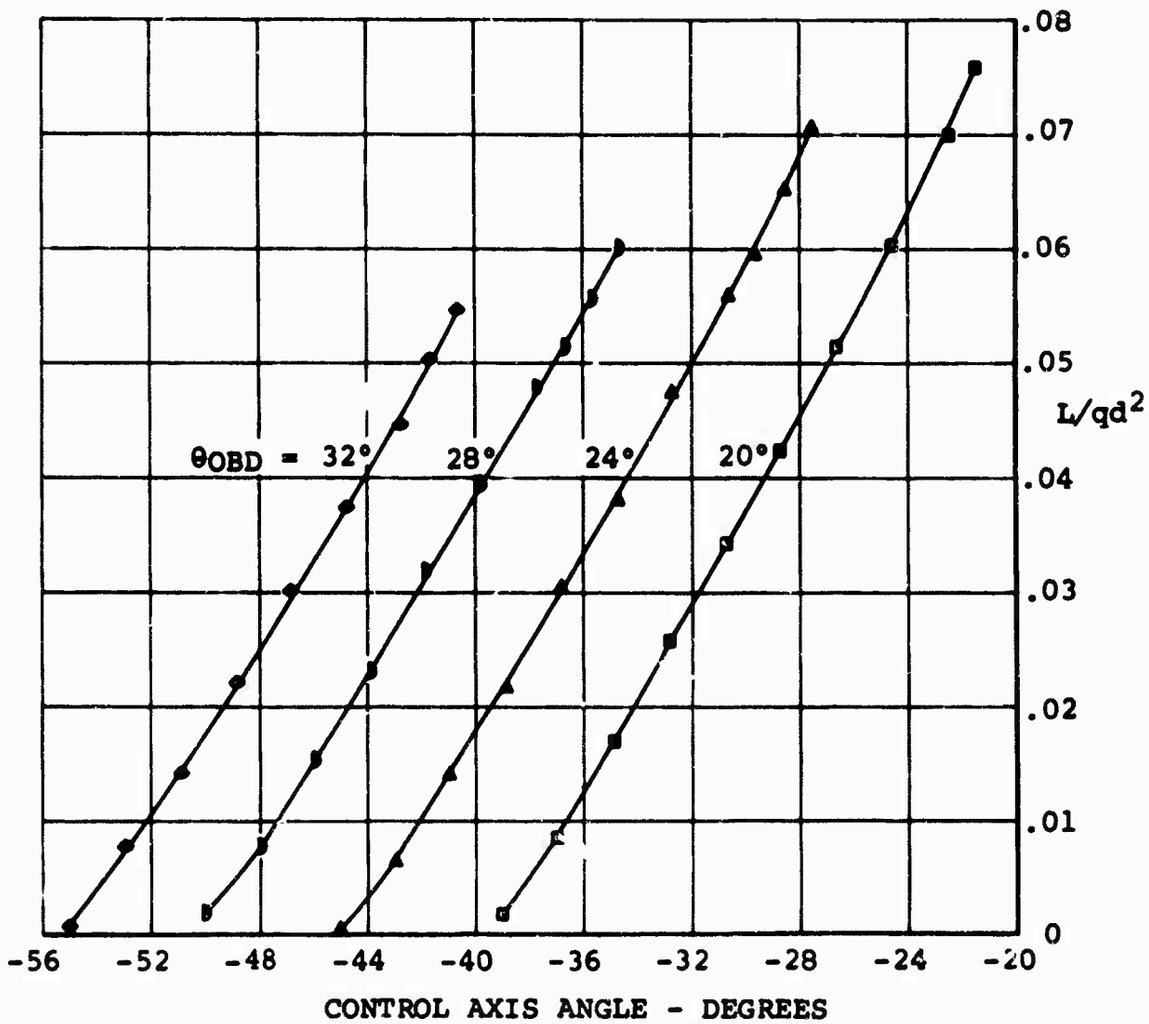

Figure 54. Segmented Rotor Nondimensionalized Lift for Pitch Schedule 3 Where $\Delta\theta_{INBD} = 0°$, $\Delta\psi = 20°$, $\mu' = 0.60$, $M_{(1)(90)} = 0.36$.

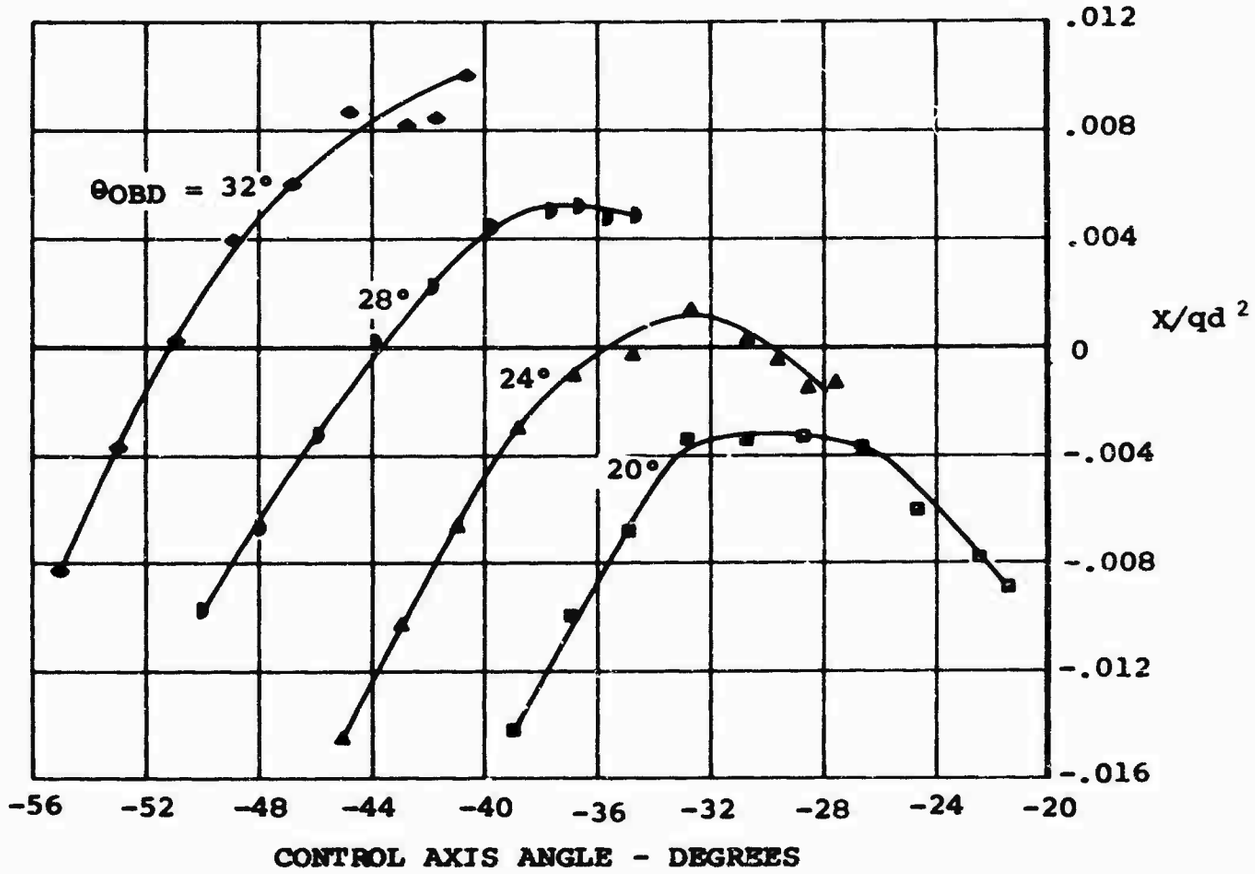

Figure 55. Segmented Rotor Nondimensionalized Propulsive Force for Pitch Schedule 3 Where $\Delta\theta_{INBD} = 0°$, $\Delta\psi = 20°$, $\mu' = 0.60$, $M(1)(90) = 0.36$.

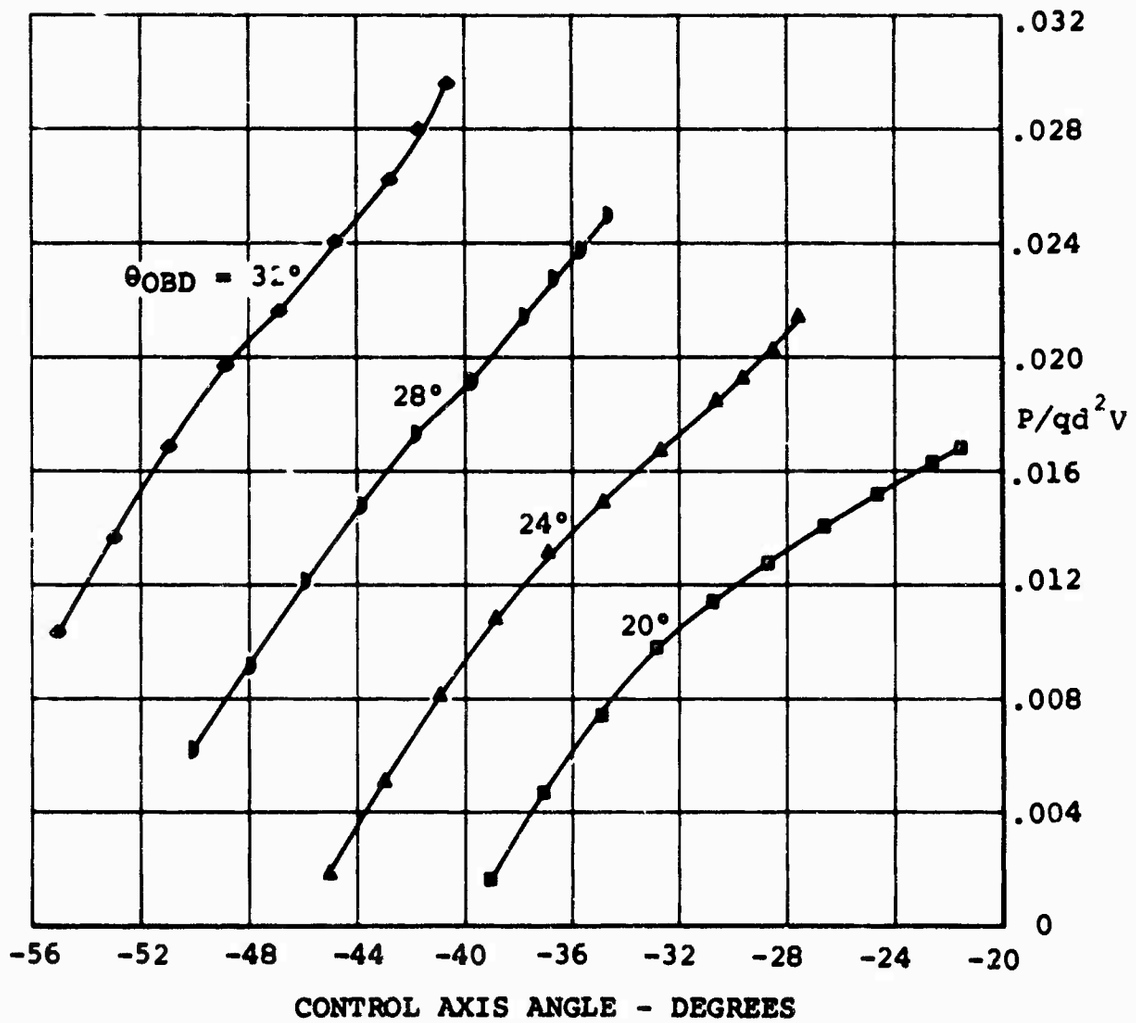

Figure 56. Segmented Rotor Nondimensionalized Power for Pitch Schedule 3 Where $\Delta\theta_{INBD} = 0°$, $\psi = 20°$, $\mu' = 0.60$, $M_{(1)(90)} = 0.36$.

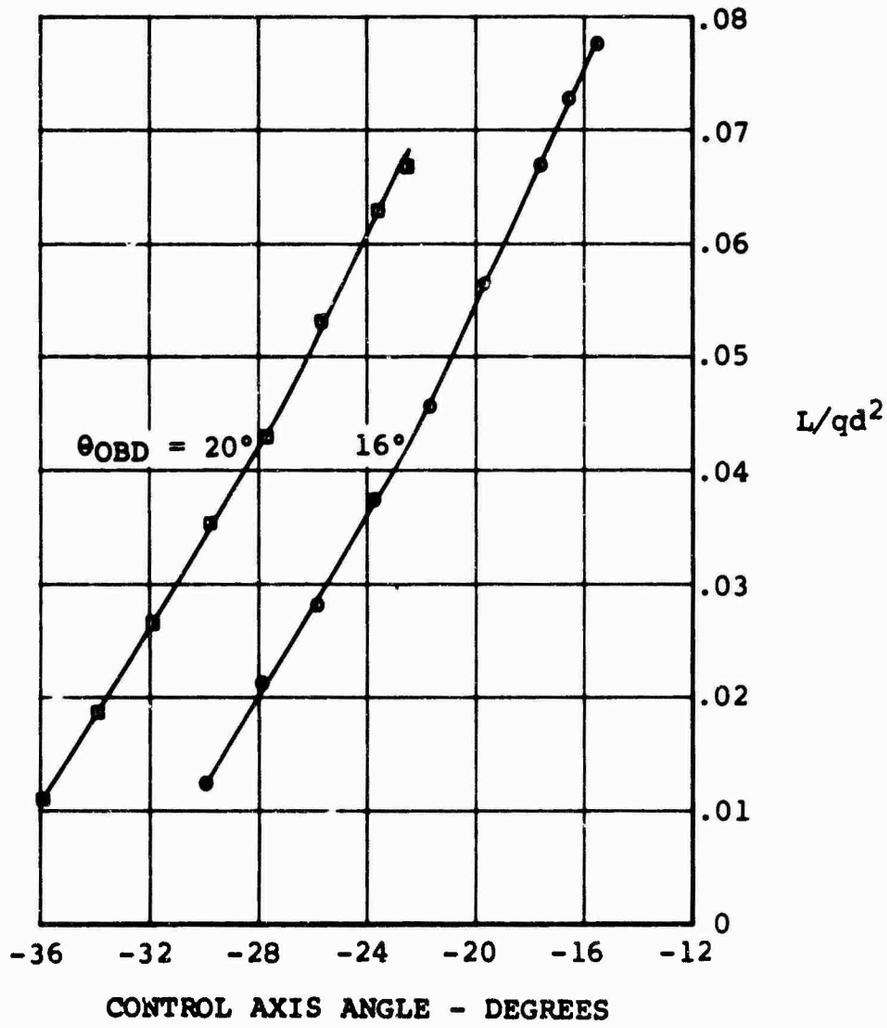

Figure 57. Segmented Rotor Nondimensionalized Lift for Pitch Schedule 3 Where $\Delta\theta_{INBD} = 0°$, $\Delta\psi = 7.5°$, $\mu' = 0.60$, $M_{(1)(90)} = 0.36$.

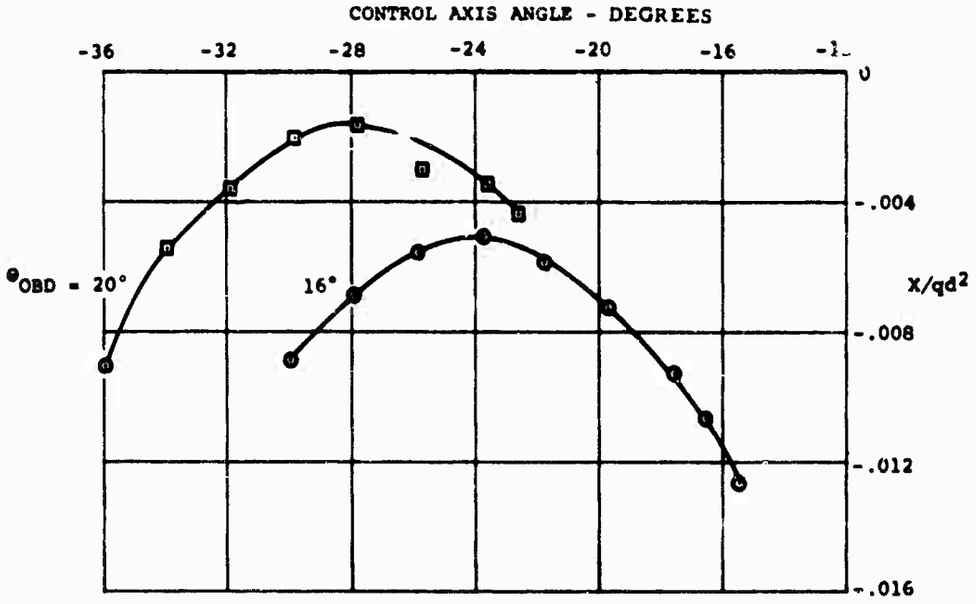

Figure 58. Segmented Rotor Nondimensionalized Propulsive Force for Pitch Schedule 3 Where $\Delta\Theta_{INBD} = 0°$, $\Delta\psi = -7.5°$, $\mu' = 0.60$, $M_{(1)(90)} = 0.36$.

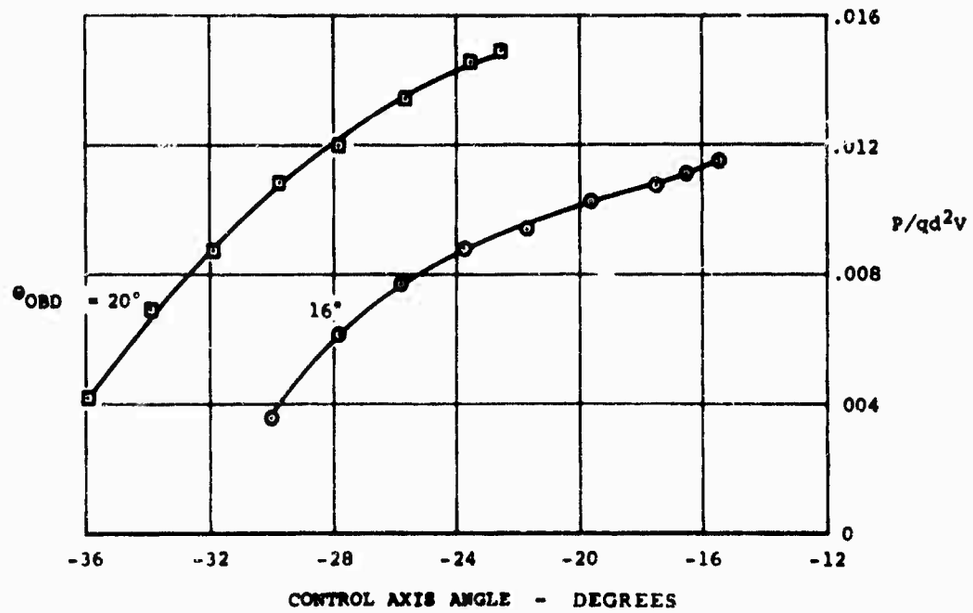

Figure 59. Segmented Rotor Nondimensionalized Power for Pitch Schedule 3 Where $\Delta\Theta_{INBD} = 0°$, $\Delta\psi = -7.5°$, $\mu' = 0.60$, $M_{(1)(90)} = 0.36$.

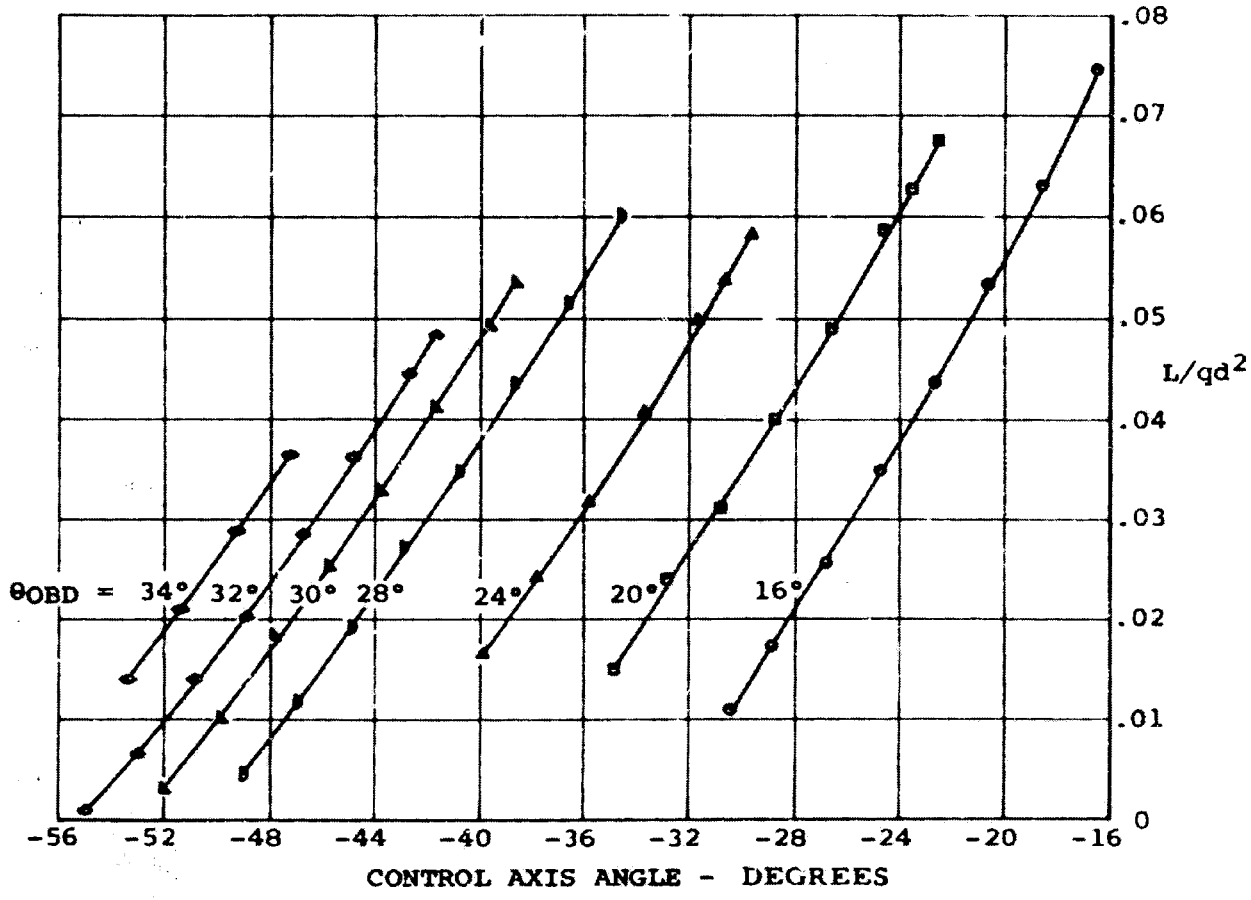

Figure 60. Segmented Rotor Nondimensionalized Lift for Pitch Schedule 3 Where $\Delta\theta_{INBD} = 0°$, $\Delta\psi = 0°$, $\mu' = 0.60$, $M_{(1)(90)} = 0.36$.

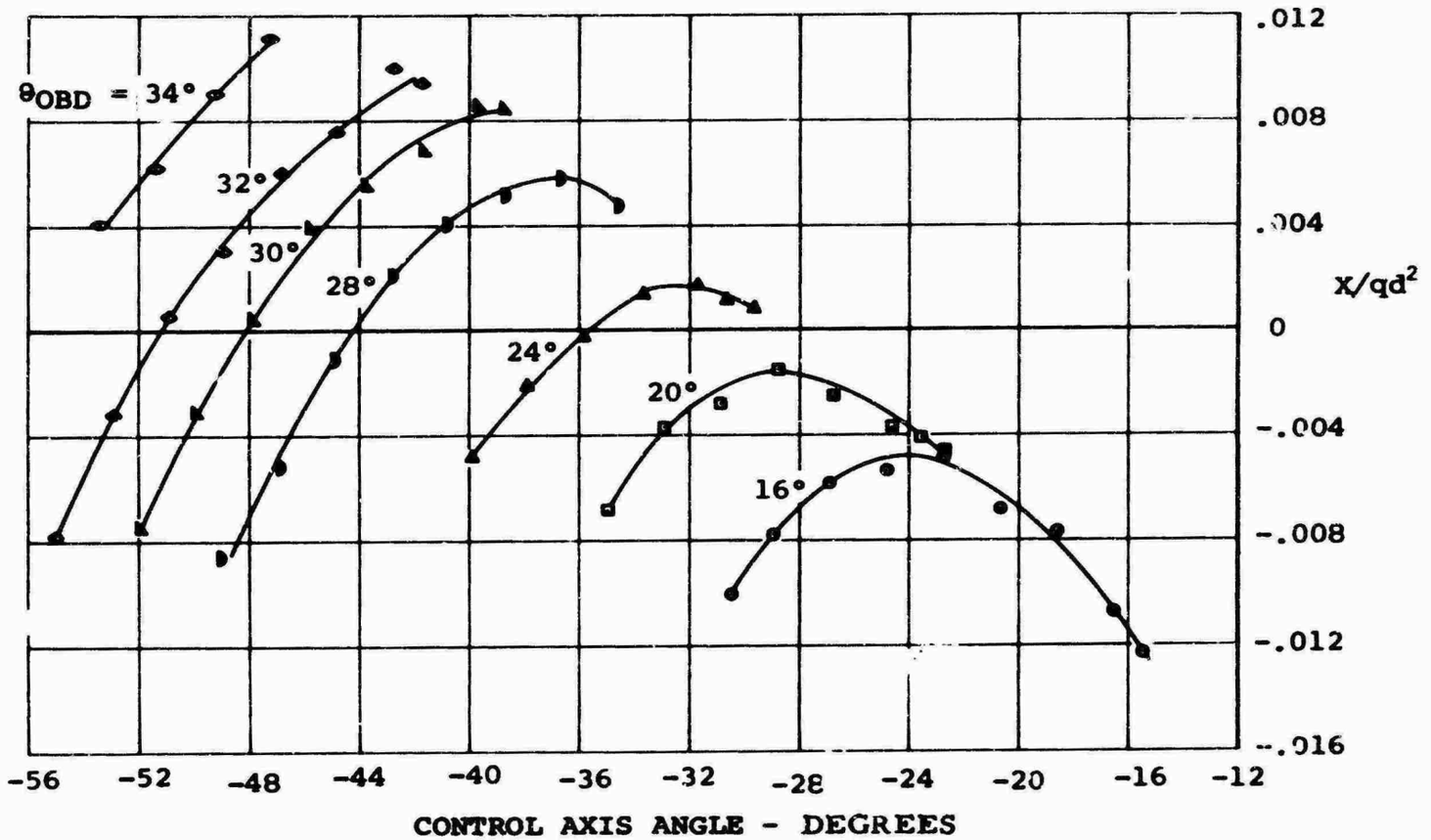

Figure 61. Segmented Rotor Nondimensionalized Propulsive Force for Pitch Schedule 3 Where $\Delta\theta_{INBD} = 0°$, $\Delta\psi = 0°$, $\mu' = 0.60$, $M(1)(90) = 0.36$.

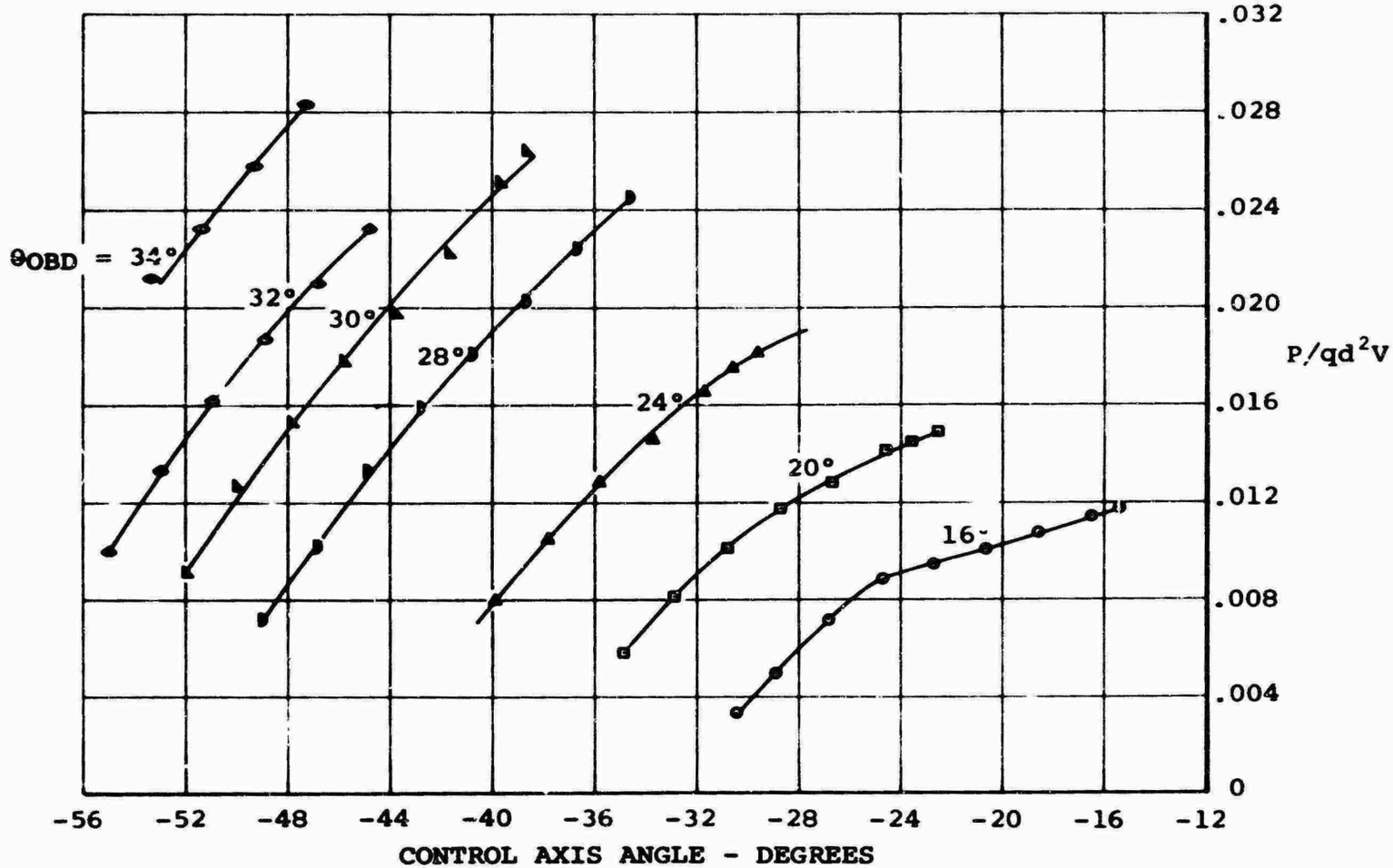

Figure 62. Segmented Rotor Nondimensionalized Power for Pitch Schedule 3 Where $\Delta\theta_{INBD} = 0°$, $\Delta\psi = 0°$, $\mu = 0.60$, $M_{(1)(90)} = 0.36$.

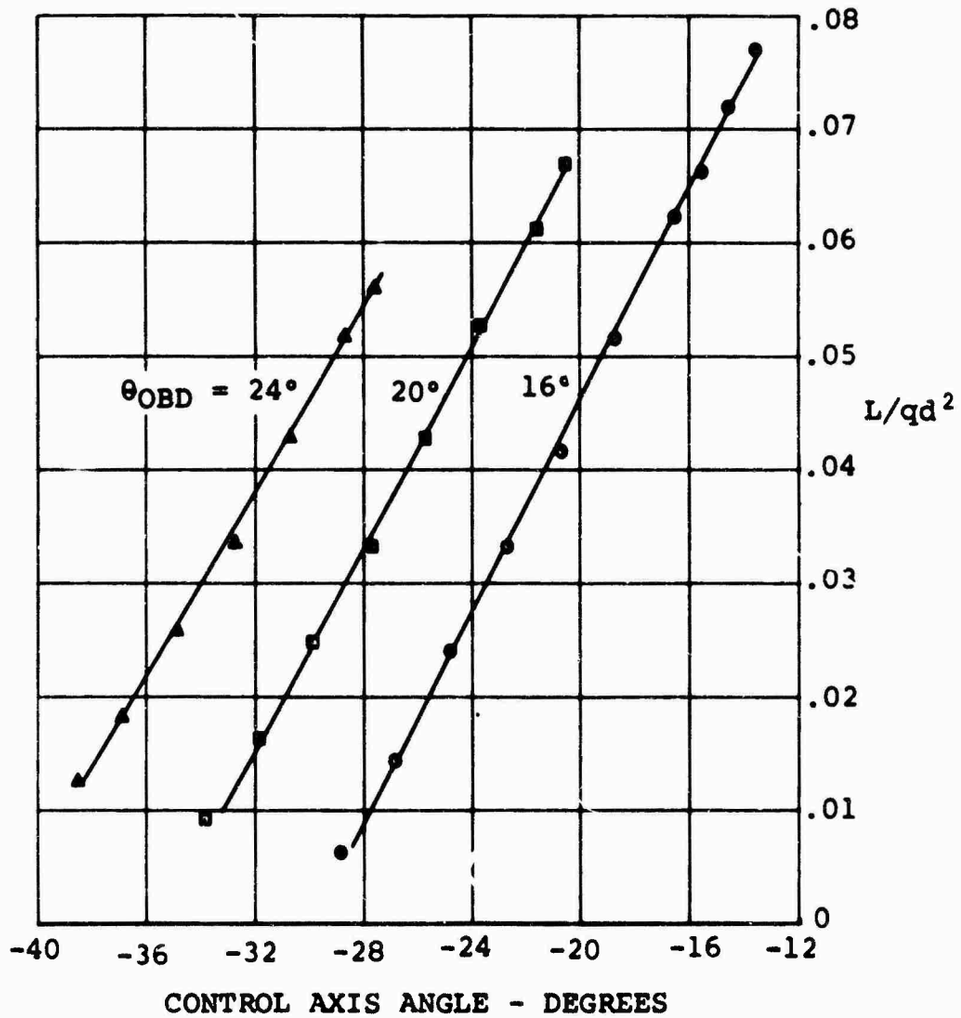

Figure 63. Segmented Rotor Nondimensionalized Lift for Pitch Schedule 3 Where $\Delta\theta_{INBD} = -10°$, $\Delta\psi = 0°$, $\mu' = 0.60$, $M_{(1)(90)} = 0.36$.

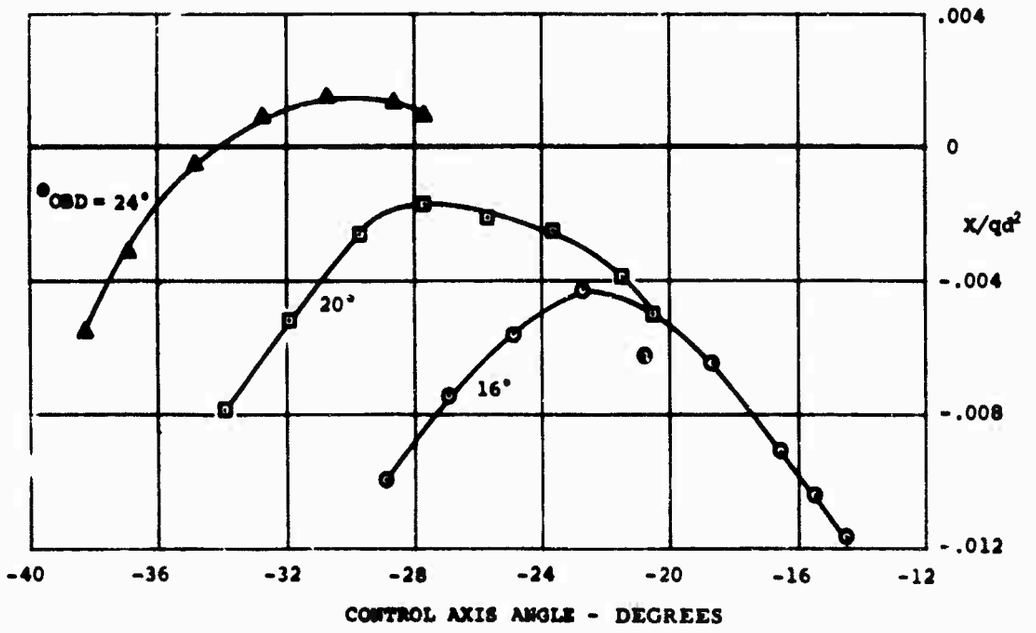

Figure 64. Segmented Rotor Nondimensionalized Propulsive Force for Pitch Schedule 3 Where $\Delta\theta_{INBD} = -10°$, $\Delta\psi = 0°$, $\mu' = 0.60$, $M_{(1)(90)} = 0.36$.

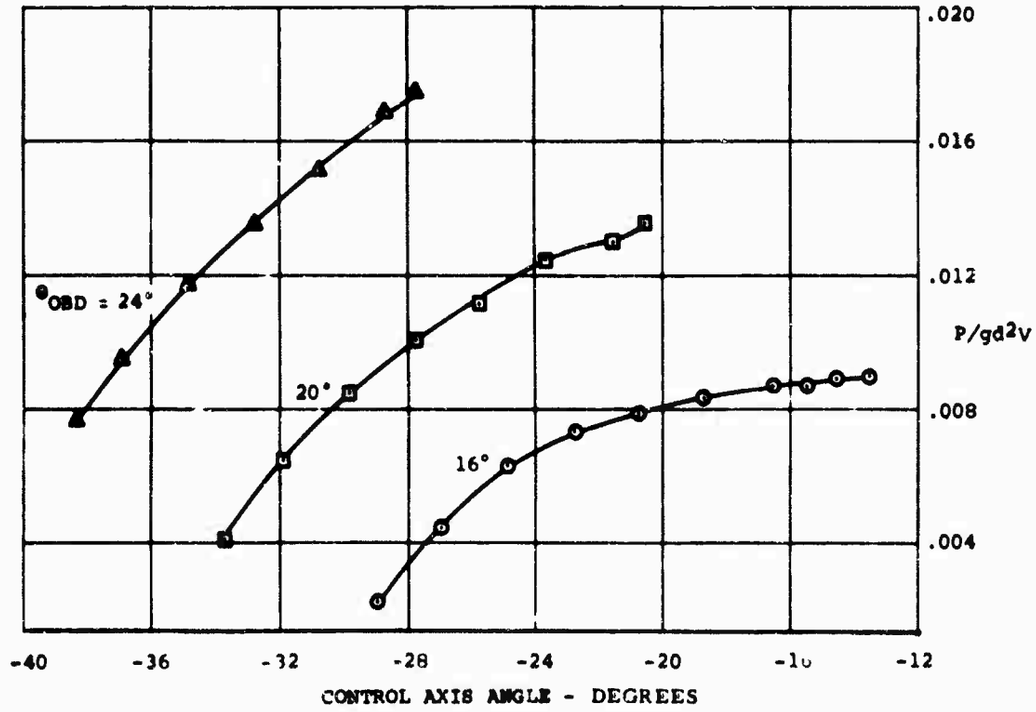

Figure 65. Segmented Rotor Nondimensionalized Power for Pitch Schedules Where $\Delta\theta_{INBD} = -10°, \Delta\psi = 0°$ $\mu' = 0.60$, $M_{(1)(90)} = 0.36$.

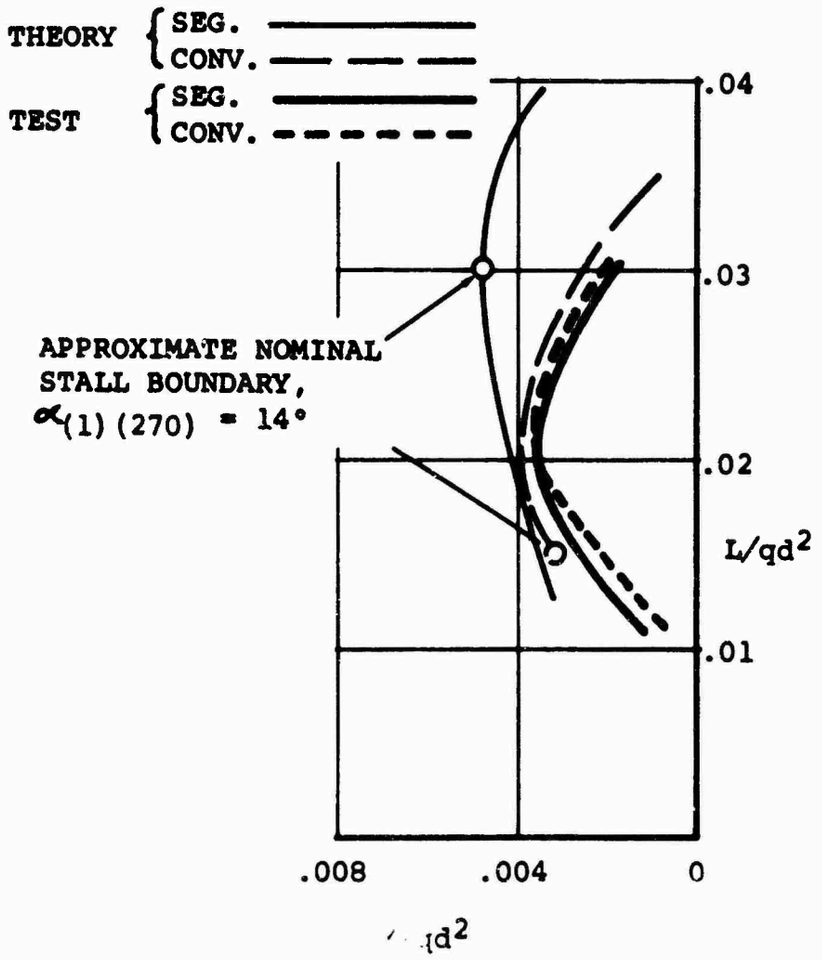

Figure 66. Comparison of Test and Theory Where $\Delta\theta_{INBD}$ = 0°, $\Delta\psi$ = 0°, P/qd^2V = 0.008, μ' = 0.60, $M_{(1)(90)}$ = 0.36, Hub and Shank Tares Removed.

BIBLIOGRAPHY

Ekquist, D., Generalized Data-Reduction Program for Powered Rotor and Propeller Wind-Tunnel Whirl Test, Aeronautical Investigation III-224, The Vertol Division of Boeing.

Harris, F. D., Preliminary Study of Radial-Flow Effects on Rotor Blades, Technical Report R-382, The Vertol Division of Boeing, 19 January 1965.

Helmbold, H. B., "Limitations of Circulation Lift," Journal of the Aeronautical Sciences, Vol. 24, No. 3, March 1957, page 237.

Heyson, H. H., Linearized Theory of Wind-Tunnel Jet-Boundary Corrections and Ground Effect for VTOL-STOL Aircraft, Technical Report R-124, National Aeronautics and Space Administration.

Schairer, G. S., Looking Ahead in V/Stol, presented at the joint IAS-RAES meeting, London, September 1961.

APPENDIX

NONDIMENSIONAL PARAMETERS FOR V/STOL AIRCRAFT PERFORMANCE ANALYSIS

Lifting systems which operate at very low airspeeds show strong interaction between lifting and propulsive characteristics. A convenient method of treating the performance problem under these circumstances is to plot the locus of lift and propulsive force (or drag) combinations for a given level of power or jet thrust, and, from such a locus, establish the maneuvering capability at a given weight by constructing a vector diagram. (See Figure 67.)

To make such plots convenient for comparison of different systems over a range of airspeeds, it is necessary to nondimensionalize the quantities. Normally, the low-speed flight regime is dominated by considerations of induced drag and power. The induced-drag coefficient of a wing, according to Prandtl's classical formula, is:

$$C_{D_i} = \frac{C_L{}^2}{\pi (AR)} \tag{17}$$

where

AR is wing aspect ratio, b^2/S.

If both sides of the equation are divided again by AR, a relation involving the span (b) but not the area (S) is obtained:

$$\frac{C_{D_i}}{(AR)} = \frac{1}{\pi}\left(\frac{C_L}{(AR)}\right)^2 \tag{18}$$

Since

$$C_{D_i} = \frac{D_i}{qS} \tag{19}$$

$$\frac{C_{D_i}}{(AR)} = \frac{D_i}{(qS)(b^2/S)} = \frac{D_i}{qb^2} \tag{20}$$

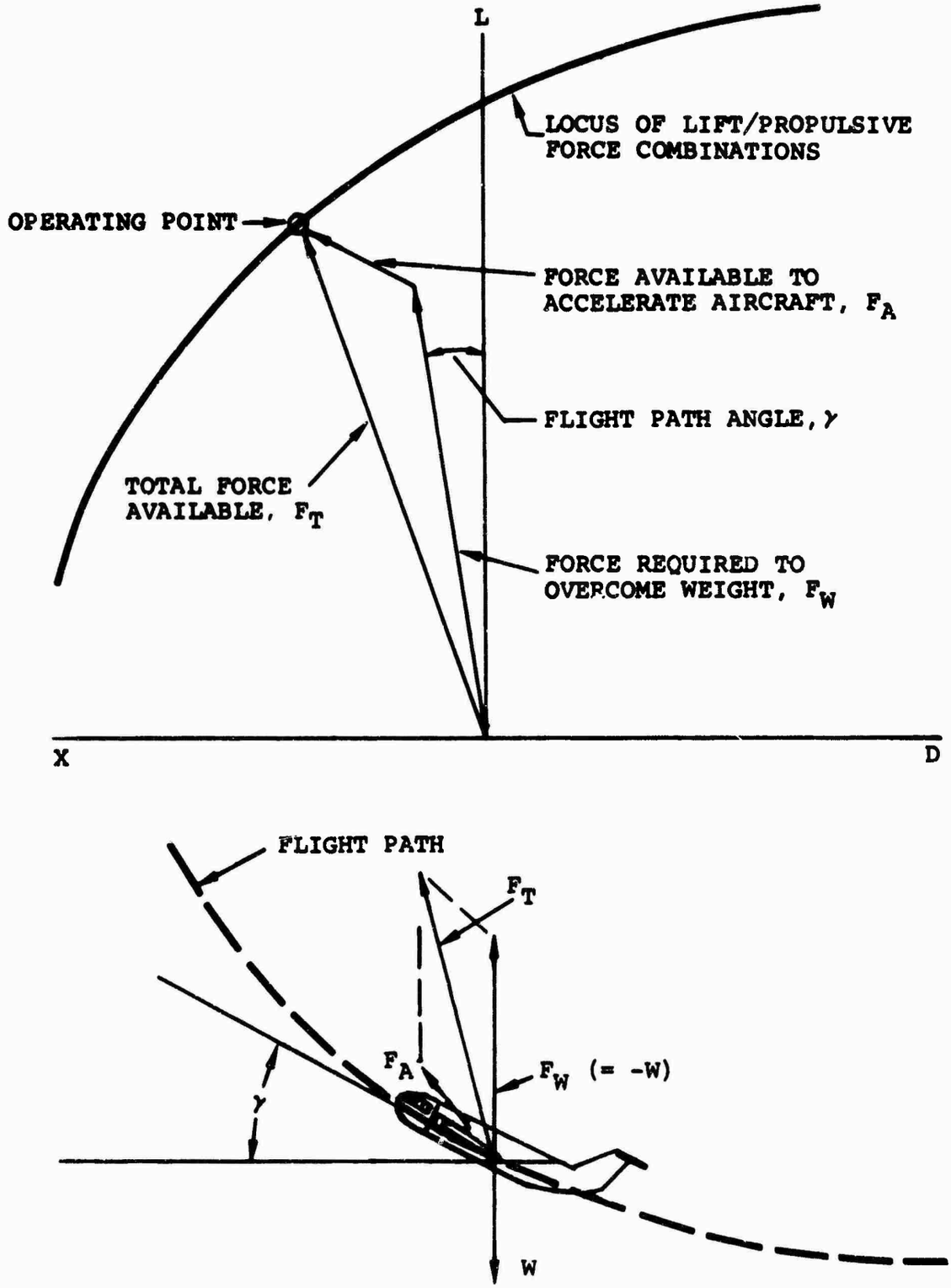

Figure 67. Determination of Aircraft Maneuver Capability.

Similarly,

$$\frac{C_L}{(AR)} = \frac{L}{qb^2} \tag{21}$$

Hence,

$$\frac{D_i}{qb^2} = \frac{1}{\pi}\left(\frac{L}{qb^2}\right)^2 \tag{22}$$

This relation can now be applied to systems having different reference areas, but equal spans.

Helmbold* extended the theory of induced drag to very high values of L/qb^2. He obtained a new universal relation between L/qb^2 and D_i/qb^2 in which the maximum possible L/qb^2 is 1.92 (see Figure 68).

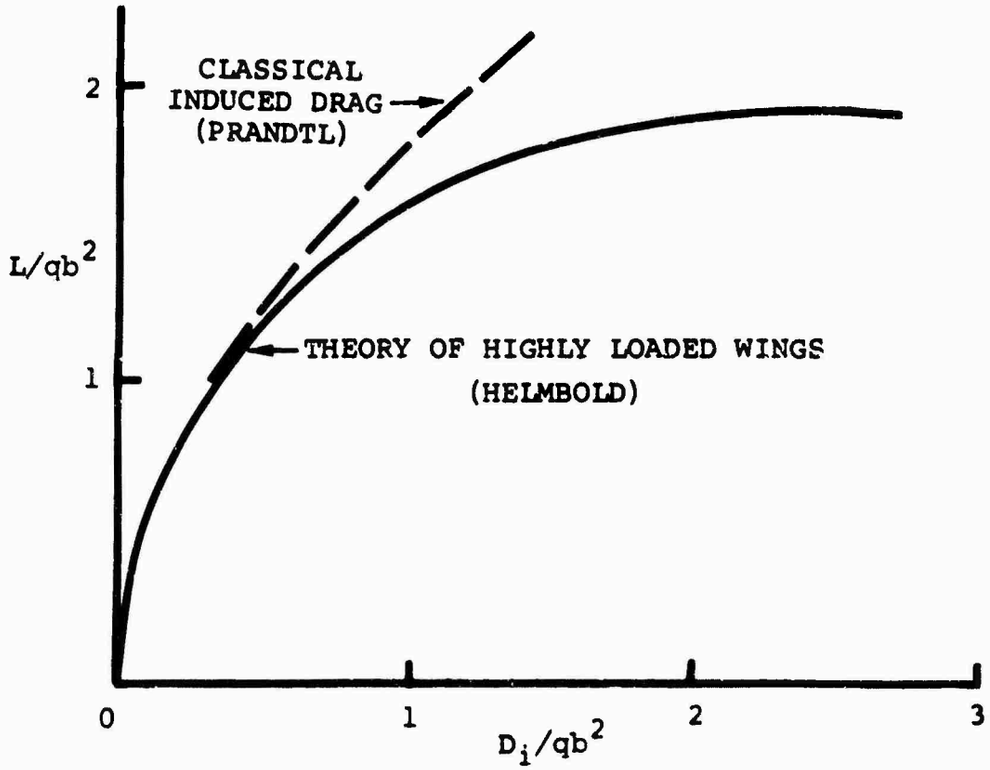

Figure 68. Universal Induced-Drag Relationship

*H. B. Helmbold, "Limitations of Circulation Lift", Journal of the Aeronautical Sciences, Vol. 24, No. 3, March 1957, page 237.

Schairer* showed that this relation could be applied to a wide variety of lift/propulsion systems, including jet-flapped wings, tilted propellers, ducted fans, rotors, and others. For rotors, the span (b) is taken to equal the diameter (d). Helmbold's curve is used as a base line, from which a vector having a length corresponding to the thrust available is used to construct an envelope (see Figure 69). If a rotor or propeller is involved, momentum theory is used to establish a thrust-power relation.

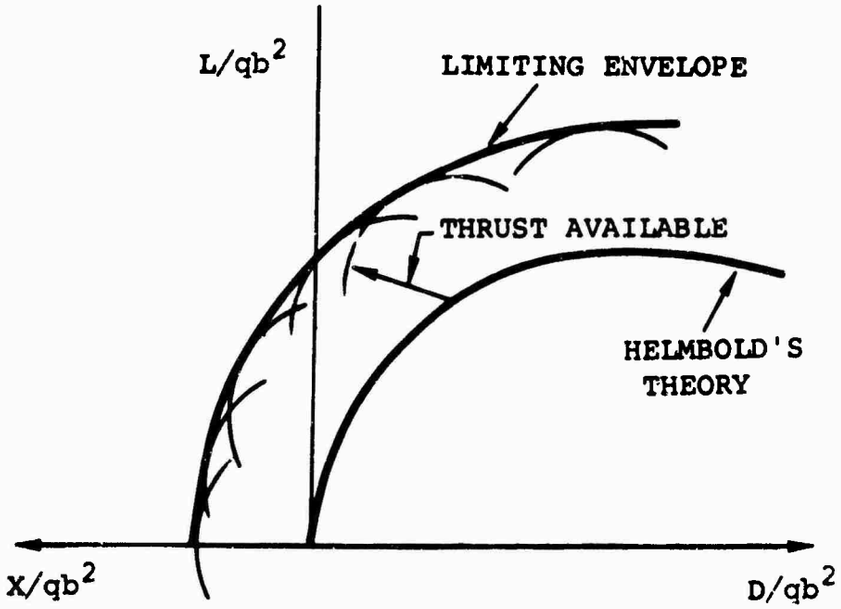

Figure 69. Construction of Force Polar Envelope for Powered Lift/Propulsion Systems.

This procedure established a limiting envelope for the force polars, and Schairer showed that it was valid for all the systems he investigated. Furthermore, most systems he investigated operated not merely within, but very close to, this envelope.

This method was adopted by Vertol Division because of its wide relevance to V/STOL performance problems.

---

*G. S. Schairer, Looking Ahead in V/STOL, presented at the joint IAS-RAES meeting, London, September 1961.

UNCLASSIFIED
Security Classification

DOCUMENT CONTROL DATA - R&D

(Security classification of title, body of abstract and indexing annotation must be entered when the overall report is classified)

1 ORIGINATING ACTIVITY (Corporate author) Vertol Division The Boeing Company Morton, Pennsylvania	2a REPORT SECURITY CLASSIFICATION UNCLASSIFIED 2b GROUP N/A

3 REPORT TITLE
DESIGN AND WIND TUNNEL TEST OF A MODEL HELICOPTER ROTOR HAVING AN INDEPENDENTLY MOVABLE INBOARD BLADE PANEL

4 DESCRIPTIVE NOTES (Type of report and inclusive dates)
Final

5 AUTHOR(S) (Last name, first name, initial)
Ekquist, Donald G.

6 REPORT DATE	7a TOTAL NO OF PAGES	7b NO OF REFS
October 1965	86	Five

8a CONTRACT OR GRANT NO.	9a ORIGINATOR'S REPORT NUMBER(S)
DA44-177-AMC-129 (T) b PROJECT NO. c. Task 1P125901A13903 d.	USAAVLABS Technical Report 65-63 9b OTHER REPORT NO(S) (Any other numbers that may be assigned this report) R-420

10 AVAILABILITY/LIMITATION NOTICES
Qualified requesters may obtain copies of this report from DDC.
This report has been furnished to the Department of Commerce for sale to the public.

11 SUPPLEMENTARY NOTES	12 SPONSORING MILITARY ACTIVITY
	U.S. Army Aviation Material Laboratories Fort Eustis, Virginia 23604

13 ABSTRACT

Wind tunnel tests of a rotor having an independently-movable inboard blade panel were conducted at an advance ratio of 0.6. It was demonstrated that this design resulted in a major advance in propulsive capability over the conventional type of rotor. Test results are presented in nondimensional plots of lift, power, and propulsive force versus control axis angle, and in cross-plotted contours of constant power of lift versus propulsive force axes.

DD FORM 1 JAN 64 1473

UNCLASSIFIED
Security Classification

14 KEY WORDS	LINK A		LINK B		LINK C	
	ROLE	WT	ROLE	WT	ROLE	WT
Helicopter Rotor Movable Inboard Segment Rotor Design Blade Panel Rotor Wind Tunnel Tests						

INSTRUCTIONS

1. ORIGINATING ACTIVITY: Enter the name end address of the contractor, subcontractor, grantee, Department of Defense activity or other organization *(corporate author)* issuing the report.

2a. REPORT SECURITY CLASSIFICATION: Enter the overall security classification of the report. Indicate whether "Restricted Data" is included. Marking is to be in accordance with appropriate security regulations.

2b. GROUP: Automatic downgrading is specified in DoD Directive 5200.10 and Armed Forces Industrial Manual. Enter the group number. Also, when applicable, show that optional markings have been used for Group 3 and Group 4 as authorized.

3. REPORT TITLE: Enter the complete report title in all capital letters. Titles in all cases should be unclassified. If a meaningful title cannot be selected without classification, show title classification in all capitals in parenthesis immediately following the title.

4. DESCRIPTIVE NOTES: If appropriate, enter the type of report, e.g., interim, progress, summary, annual, or final. Give the inclusive dates when a specific reporting period is covered.

5. AUTHOR(S): Enter the name(s) of author(s) as shown on or in the report. Enter last name, first name, middle initial. If military, show rank and branch of service. The name of the principal author is an absolute minimum requirement.

6. REPORT DATE: Enter the date of the report as day, month, year, or month, year. If more than one date appears on the report, use date of publication.

7. TOTAL NUMBER OF PAGES: The total page count should follow normal pagination procedures, i.e., enter the number of pages containing information.

7b. NUMBER OF REFERENCES: Enter the total number of references cited in the report.

8a. CONTRACT OR GRANT NUMBER: If appropriate, enter the applicable number of the contract or grant under which the report was written.

8b, 8c, & 8d. PROJECT NUMBER: Enter the appropriate military department identification, such as project number, subproject number, system numbers, task number, etc.

9a. ORIGINATOR'S REPORT NUMBER(S): Enter the official report number by which the document will be identified and controlled by the originating activity. This number must be unique to this report.

9b. OTHER REPORT NUMBER(S): If the report has been assigned any other report numbers *(either by the originator or by the sponsor)*, also enter this number(s).

10. AVAILABILITY/LIMITATION NOTICES: Enter any limitations on further dissemination of the report, other than those imposed by security classification, using standard statements such as:

(1) "Qualified requesters may obtain copies of this report from DDC."

(2) "Foreign announcement and dissemination of this report by DDC is not authorized."

(3) "U. S. Government agencies may obtain copies of this report directly from DDC. Other qualified DDC users shall request through _____."

(4) "U. S. military agencies may obtain copies of this report directly from DDC. Other qualified users shall request through _____."

(5) "All distribution of this report is controlled. Qualified DDC users shall request through _____."

If the report has been furnished to the Office of Technical Services, Department of Commerce, for sale to the public, indicate this fact and enter the price, if known.

11. SUPPLEMENTARY NOTES: Use for additional explanatory notes.

12. SPONSORING MILITARY ACTIVITY: Enter the name of the departmental project office or laboratory sponsoring *(paying for)* the research and development. Include address.

13. ABSTRACT: Enter an abstract giving a brief and factual summary of the document indicative of the report, even though it may also appear elsewhere in the body of the technical report. If additional space is required, a continuation sheet shall be attached.

It is highly desirable that the abstract of classified reports be unclassified. Each paragraph of the abstract shall end with an indication of the military security classification of the information in the paragraph, represented as *(TS)*, *(S)*, *(C)*, or *(U)*

There is no limitation on the length of the abstract. However, the suggested length is from 150 to 225 words.

14. KEY WORDS: Key words are technically meaningful terms or short phrases that characterize a report and may be used as index entries for cataloging the report. Key words must be selected so that no security classification is required. Identifiers, such as equipment model designation, trade name, military project code name, geographic location, may be used as key words but will be followed by an indication of technical context. The assignment of links, rules, and weights is optional.